Jack-up vessel preload reliability study

Optimizing the preload safety factor of a jack-up vessel with regards to lifting operations in various soil types

Master Thesis

S. Wouters

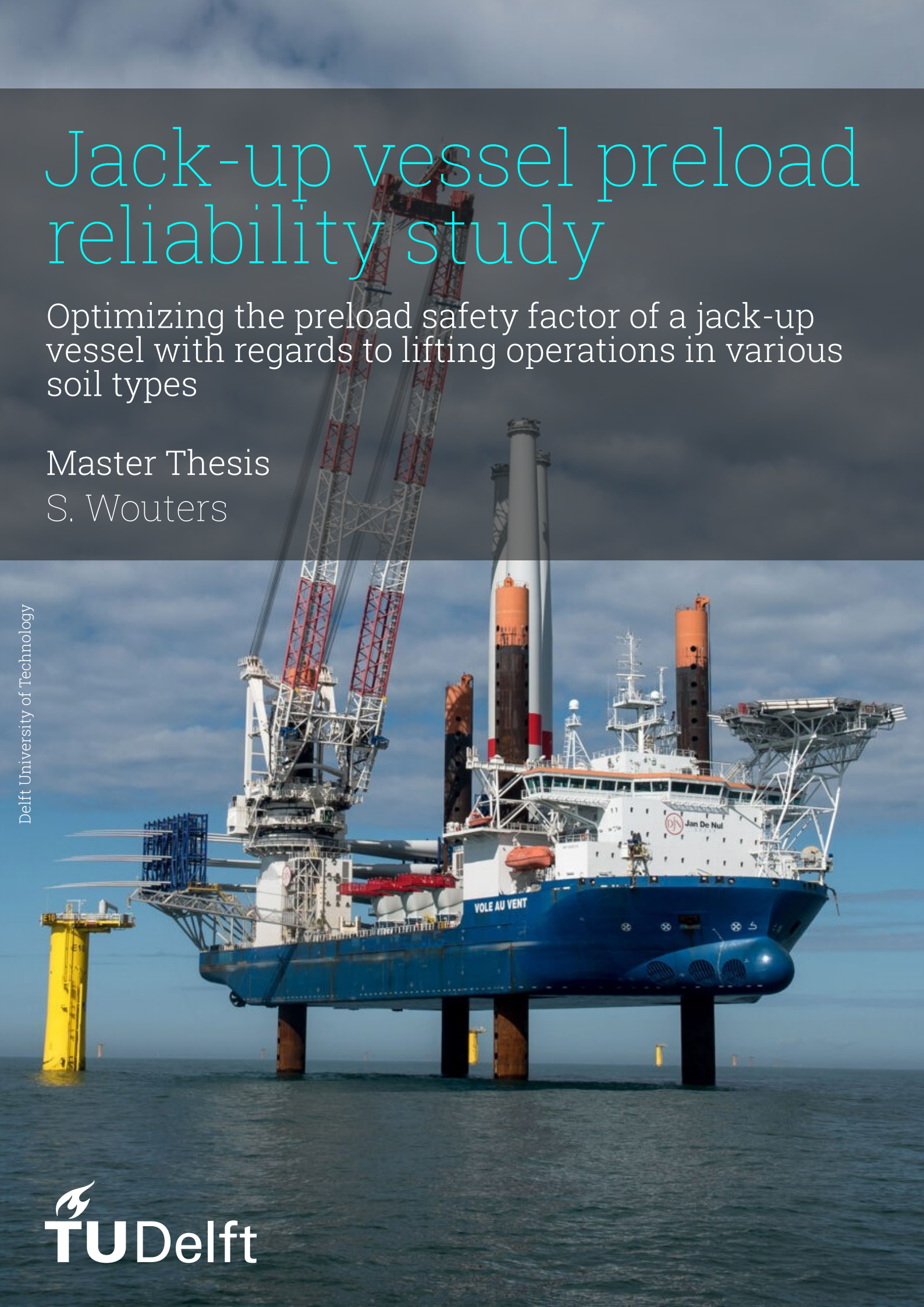

Delft University of Technology

TU Delft

Jack-up vessel preload reliability study

Optimizing the preload safety factor of a jack-up vessel with regards to lifting operations in various soil types

by

S. Wouters

at

Jan De Nul

Graduation committee:	Dr. E. Kementzetzidis	TU Delft, chairman
	Dr. H.C. Seyffert	TU Delft
	Dr. G. Lavidas	TU Delft
	Ir. G. Weymeis	Jan De Nul
Project Duration:	January, 2024 - December, 2024	
Faculty:	Faculty of Mechanical Engineering, Delft	
Student number:	4693612	

TU Delft

Jan De Nul GROUP

Preface

This thesis on ”Jack-up vessel preload reliability” marks the end of my Offshore and Dredging Engineering master at the Delft University of Technology. This research was conducted at Jan De Nul, where I enjoyed collaborating with Geert Weymeis and his team. Thank you for mentoring me and the time you invested in this thesis.
I also want to thank Tom Vermeersch from Jan De Nul for allowing me to carry out a voluntary internship at Jan De Nul at the beginning of my master and afterwards linking me with Geert, which was the start of this thesis project.

Apart from this thesis's first and most obvious goal: to obtain my diploma, my second goal was to learn a lot and increase my toolbox as an engineer. Which I most certainly did, both the hard and soft skills. The problem solving mindset you acquire as an engineer is something I am very grateful for. This thesis also emphasises the importance of not blindly trusting the established guidelines but verifying them for yourself. Which is a general lesson I will take home as well.

I would like to thank my supervising committee from the TU Delft, namely Vagelis Kementzetzidis and Harleigh Seyffert. The freedom they granted me allowed me to tackle certain problems creatively, while their feedback ensured I could see the academic forest from the trees.

The obstacle is the way. I'm proud to have accomplished this master thesis at the TU Delft because it is not easy. It requires your full focus and commitment for almost a year. Therefore, I would like to thank my family, friends and girlfriend for supporting me the past year. When I have a goal in mind, it gets my full attention. Therefore, I need to cut attention elsewhere.
In addition, my friends who have already graduated from the TU Delft. The early bird gets the worm, but the second mouse gets the cheese, so I could learn from my friend's successes and mistakes.
My parents, more specifically, for unconditionally supporting me through all these years and allowing me to study what I'm most passionate about, even if it meant studying abroad, which was definitely not the easiest option.

I look back on an incredible journey in the past years as a student, but I am also eager to discover what the future holds and grow even more, one step at a time.

S. Wouters
Delft, December 2024

Abstract

The offshore wind market has become a substantially growing industry to meet the worldwide increasing energy demands. This results in heavier crane operations on offshore jack-up vessels due to the increasing size of wind turbine components. To ensure the seabed can support the loads on the jack-up legs, a temporary foundation for the leg's footings is established before crane operations through a process known as preloading. Where the two diagonal opposing leg pairs are loaded alternatively by the weight of the vessel until a stable condition is reached. Traditionally, the capacity of those foundations is determined based on storm loads adopted from offshore oil and gas jack-up guidelines.

The main objective of this thesis is to develop a robust method for analysing the applied preload in past jack-up crane operations conducted by Jan de Nul's Vole au vent. This analysis aims to provide a better understanding of the effectiveness of traditional offshore jack-up guidelines within the rapidly growing offshore wind industry, where heavy crane operations are now performed on a daily basis. Such understanding is crucial, as these guidelines were not originally intended for the advanced state of the current offshore wind sector and are not specifically calibrated for its unique demands.

To accomplish this objective, a method is designed to assess the preload safety factors of past jacking operations and determine their optimal value for heavy lifting operations. This safety factor provides the ratio between operational leg reactions and applied preload. The developed models are then applied to a case study using measuring data from jacking operations of the Vole au vent to validate their effectiveness.
This method is based on reliability analyses which evaluate the probability of failure by assessing if a certain limit state is exceeded. Failure for jacking operations can occur when the leg reactions during crane operations become larger than the applied preload. From the acquired measuring data, certain probability distributions of the leg reactions can be obtained, which are used by a Monte Carlo Simulation to assess the probability of preload exceedance through the defined limit states. This probability of preload exceedance quantifies the reliability of the applied preload in different soil types at three offshore wind farm sites.
This research then defines optimal targets for the annual probability of preload exceedance based on the consequences of failure of operations in both low-risk and high-risk soil profiles. These targets provide a balance between operational efficiency and safety. From those targets, an optimal preload safety factor is obtained and compared to what was originally applied during the jack-up operations.

The findings of this thesis indicate the need to evaluate and improve the standards to better align with the industry's evolving requirements.
It is shown that the currently used preload safety factor from traditional offshore jack-up guidelines is not yet correctly calibrated for heavy crane operations on jack-up vessels. To achieve an optimal balance between operational efficiency and safety, the applied preload, with respect to the experienced loads from heavy crane operations, should be slightly lowered compared to what is currently applied.
In addition, this research observed that the measured conditions during jack-up operations are not correctly estimated, leading to operational and preload uncertainties.

Contents

Nomenclature

Abbreviations

Abbreviation	Definition
CDF	Cumulative Distribution Function
COV	Coefficient of Variation
DKF	Danish Kriegers Flak
EMA	Exponential Moving Average
FOSM	First-order Second Moment
ISO	International Organization for Standardization
MCS	Monte Carlo Simulation
PDF	Probability Density Function
SSA	Site Specific Assessment

This page is intentionally left empty.

1

Introduction

The offshore wind market has become a substantially growing industry to meet the worldwide increasing energy demands. This has resulted in the development of offshore wind technologies, leading to an evolution in offshore wind turbine sizes [4]. Increasing wind turbine sizes will result in heavier turbine components, which are generally installed by jack-up vessels for bottom-founded wind turbines. These installation vessels can jack themselves up to elevate their hull above the waterline and install the turbine components in a stabilised position. By doing so, the entire weight of the vessel and turbine components, operational loading, and metocean loading converge in the jack-up legs, which are stabilised on the seafloor by their footings (spudcans). These spudcans create the required support for the operations by preloading the jack-up legs in advance. Currently, industry standards for foundation capacity are based on the loads from a fifty-year storm event [35] [27], despite the fact that daily occurring operational loads may soon match or exceed these due to increasing turbine component weight.
Jan De Nul is a leading contractor in the offshore wind installation market with two jack-up vessels in its fleet: Vole au vent and Voltaire. This research aims to provide insights into the preload assessment methods used for Jan De Nul's Vole au vent by evaluating their reliability. To enhance the safety and efficiency of future jack-up operations.

Problem statement and research goals

Current offshore jack-up guidelines primarily base their foundation assessment on environmental storm loading, which originates from the offshore oil and gas industry, where jack-up platforms do not have large crane loads. The offshore wind installation jack-ups on the other hand experience much larger crane loads due to the installation of wind turbine components, which will only increase in size in the coming years. These operational loads also take place on a daily basis making them much more probable than storm loads.
In addition, current methods to obtain preload capacity are based on a deterministic approach described by ISO 19905-1. It deals with engineering and operational uncertainties and risks by applying partial safety factors to the estimated loads and spudcan resistance. These methods are not yet calibrated for the offshore wind industry, indicating a need for evaluation and potential improvement as the industry evolves. Methods to determine the response or resistance of a system are already greatly described in the literature for other engineering categories, such as structural engineering. The use of such reliability methods could therefore also be useful to offshore foundation engineering.
By knowing whether or not the reliability of the applied preload safety factor is consistent, future operational procedures and engineering methods could be further optimised, leading to a more reliable and more efficient method of installing offshore wind turbines. An overestimated preload safety factor might cause the preload operation to take more time and cause more strain on the jacking system then needed, which reduces the lifespan of critical components.
The main objective of this research is to develop a robust method for analysing the preload conservatism of past jack-up operations conducted by the vessel Vole au vent. This method will assess preload safety factors and determine their optimal value for heavy lifting operations. The developed models will be applied to a case study using measuring data from previous jacking operations of the Vole au vent to validate their effectiveness.

Research questions

To accomplish the research goal, the following research questions are proposed. Which are supported by sub-questions in order to help answer them.

Research question 1: *How can a framework be developed to assess preload conservatism of past offshore wind jack-up vessel lifting operations?*

- How do the estimated leg reactions compare to the observed leg reactions during past operations, specifically at maximum preload and maximum operational load?
- How can the probability of preload failure be evaluated in relation to operational loads, considering both estimated and applied preload values?
- What is an acceptable threshold for the annual probability of preload exceedance in offshore wind jack-up vessel operations?

Research question 2: *What is the optimal preload safety factor relative to the acceptable annual probability of preload exceedance?*

- How does the determined optimal safety factor compare to values applied in previous operations?

Significance and contribution

Practical

Current offshore wind jack-up standards do not explicitly specify how large crane operations should be considered in the preload assessments. While in reality, this is becoming a more prevalent load case. This research aims to provide Jan De Nul with deeper insights into how current industry safety factors affect the reliability of their jack-up crane operations. As a result, they may adjust certain operational practices or refine specific theoretical models, leading to safer and more efficient methods for installing offshore wind turbines.

Scientific

This research will combine two fields not frequently integrated in the literature. Namely, offshore wind jack-up engineering and mathematical reliability methods.

Societal and environmental

This research could lead to a better understanding of the quickly growing offshore wind industry. Resulting in an optimal balance between a safer offshore work environment and efficient installation of renewable energy, ultimately benefiting society. Additionally, the installation of offshore wind turbines contributes to a more sustainable planet by reducing the need for facilities that emit greenhouse gases.

Ethical

This research might increase the standards of safety and reliability for jack-up operations, which is the ethical obligation of engineers who design and plan such operations.

Legal

There is currently a gap between what the offshore jack-up standard was intended for, and where it is currently used for. This research could lead to a legal review of these standards to ensure that they are adequate for current applications, mitigating potential issues as the industry continues to grow.

Thesis outline

The outline of this thesis is established to answer the research questions chronologically. First, the already known information is provided; this includes a summary of the literature review in chapter 2 and the background information of the assessed case study in chapter 3. Continuing on the acquired information, a detailed description of the research framework is also discussed in chapter 3. Hereafter, the methods used to answer the first part of the research questions are provided in chapter 4. The second research question is answered through the approach from chapter 5. The developed framework is then tested on the provided case study; of which the obtained results are described in chapter 6. The thesis is finalized by concluding the answers to the research questions and providing recommendations for future research in chapter 7.

2

Literature review

This chapter outlines the literature used for this research. At first, the preloading procedure is explained in section 2.1. Hereafter, the foundation integrity assessment as established in ISO 19905-1 is presented in section 2.2. Next, section 2.3 covers the fundamentals of reliability analysis methods, followed by the description of a method to obtain reliability targets in section 2.4.
This literature review provides a summarized version of the original literature study that preceded this research. The concepts presented in this chapter serve as a theoretical foundation for the rest of the research.

2.1. Preload procedure

To install wind turbine components in a stabilized position, jack-up vessels elevate their entire hull above the waterline with their jacking legs. As a result the weight of the jack-up vessel and the loads created by crane operations and environmental conditions will converge in these jack-up legs. To ensure the seabed can support the loads on the jack-up legs, a foundation for the leg's footings is established before crane operations through a process known as preloading. This section describes the preloading procedure and the main risks such as punch-through.

2.1.1. Preload phases

After the transit stage, the vessel arrives at the location where a dynamic positioning system keeps the vessel stationary while the jacking legs are lowered [12]. When the legs are lowered and slightly penetrating the seabed the preloading operation is carried out. The goal of this operation is to install the leg footings or spudcans by vertically loading the soil beneath each jack-up leg. This is done by extending the legs and pushing them further into the soil under the vessel's weight. By doing so, the soil will get compressed which makes it stronger, until an equilibrium between the applied load and resistance of the soil is obtained [37]. Ensuring sufficient foundation capacity when maximum load is applied.

Preloading operations are carried out with the hull elevated at the lowest practicable airgap, or with the hull partially buoyant when there is a risk of rapid leg settlement. Jack-up vessels with four legs typically achieve foundation preload by carrying the entire vessel weight alternatively on the two diagonal opposing leg pairs, until a stable condition is reached [32]. If vessel weight is not enough, ballast water is pumped into the ballast tanks.
A preload cycle generally exists of a leg extension phase where the load increases, followed by a holding phase with no further leg extension where the soil settles over time which slightly lowers the leg load, as can be seen in figure 2.1 [14]. Additional load cycles might be executed to ensure that each leg can withstand the preload without excessive leg settlement. This process is then repeated for the other leg pair, while the load distribution between the four legs is continuous. The preload process is completed by actively loading both leg pairs. It is common that not all legs have equal penetration,

this is due to different soil conditions and structural asymmetry [9].

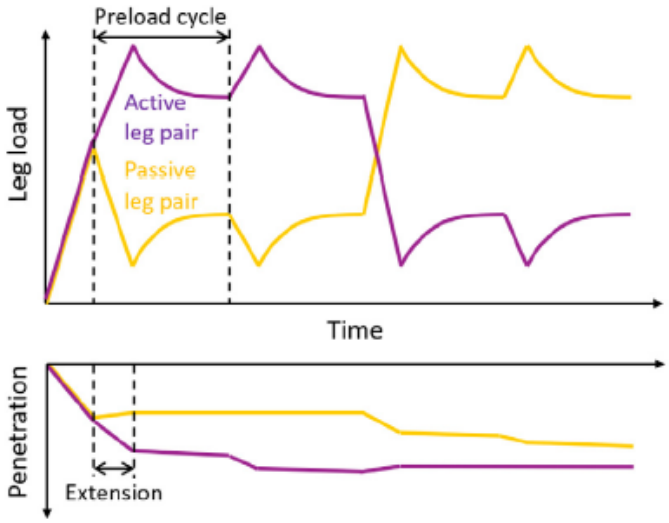

Figure 2.1: Leg load and penetration during different preloading cycles [32]

2.1.2. Punch-through

During preloading the soil beneath the spudcan is compressed until the bearing capacity of the soil is able to resist the preload. When preloading in layered soil, where a strong soil layer overlays a weaker soil layer, the compressed stronger soil might get pushed into the softer layer beneath it. When this happens, the bearing capacity of the soil, which has been built up until that point, all of a sudden drastically reduces [17]. This so-called punch-through of the soil will result in rapid uncontrolled leg penetration, which can lead to the buckling of the other leg from the active leg pair as shown in figure 2.2 [17]. This effect should not be confused with rapid footing settlement, which is allowed to happen. Punch-through is extremely costly, and unsafe and might even lead to total loss of the jack-up vessel [14] [15].

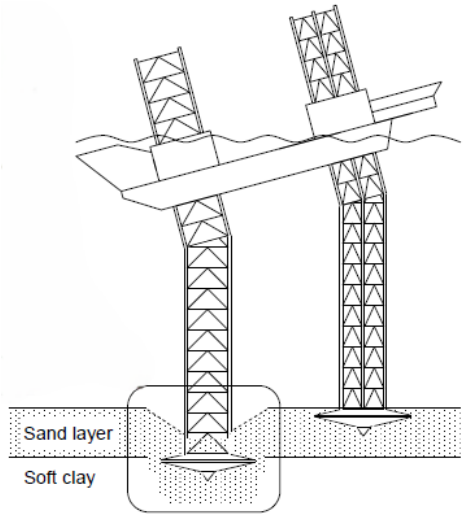

Figure 2.2: Punch-through failure on sand overlaying clay [17]

To intervene before punch-through occurs, the bearing capacity for each spudcan is carefully observed for different penetration depths during preloading [9]. Other additional mitigation techniques are used when the risk of punch-through is identified in the site specific assessment. These include preloading at the lowest practicable airgap and 'Swiss Cheesing' where holes are drilled through the

critical soil layer to decrease the soil strength before preloading, leading to a more controlled penetration[14].

2.1.3. Conclusion

The foundation of jack-up legs is established by preloading the soil underneath their spudcans. Providing the required resistance to safely execute heavy lifting operations. Preloading is a process of carrying the entire vessel weight alternatively on the two diagonal opposing leg pairs, until a stable condition is reached. A preloading cycle is characterized by two phases: a leg extension phase, followed by a holding phase. Additional preload cycles might be needed to ensure that each leg can withstand the preload without excessive leg settlement.
The literature summarized in this section is used to understand the preload cycles and phases from the obtained measuring data of the leg reactions. It also provides an explanation of the main risks involved with jacking operations, which helps to assess failure targets later on in the research.

2.2. Foundation integrity assessment

Before each jack-up operation at a specific site, it should be assessed if the operation can be executed without failure to the selected limit states. For jack-up operations, the ultimate limit states are usually only required to be checked during extreme conditions. The International Organization of Standardization has set this extreme condition for mobile jack-up vessels to be the occurrence of a fifty-year storm on the specific site [27]. All information in section 2.2 will therefore be obtained from ISO 19905-1: Site-specific assessment of mobile offshore units [27], unless specified otherwise.
This section will first provide a general formulation and requirement for the utilization in section 2.2.1. The extreme storm assessment should be conducted by checking the applicability of the jack-up vessel for several criteria including: structural strength of legs, spudcan, and holding system, hull elevation, leg length reserve, overturning stability, foundation integrity, interaction with adjacent infrastructure, and temperature. Since the integrity of the foundation is central to the site specific assessment and this research, only the foundation integrity checks will be covered in this literature review in section 2.2.2.

2.2.1. General formulation

Generally, as long as the resistance is larger than the loads certain criteria won't fail. To account for operational uncertainties and measuring and modelling inaccuracies, the assessment checks make use of partial safety factors. In this method, the partial load factors are applied to the individual loads and not to the effect of the combined loads. The partial resistance factors are applied to the foundation capacity or structural strength. Individual loads are for instance loads due to weight, crane operations, and static and dynamic metocean actions, which lead to the load effects at the footings. Resistance factors are applied to the bearing capacity of the soil at the spudcan tip created by preloading.

For each assessment criteria, a utilization U should be calculated which satisfies the requirement as seen in equation (2.1). For assessments where the loads can be expressed with a single response, the utilization can generally be obtained by equation (2.2). For assessments where the resistance is given by an interaction surface, for example the yield surface for foundations, the utilization can generally be calculated with equation (2.3).

$$U \leq 1.0 \tag{2.1}$$

$$U = \frac{\text{effect due to factored loads}}{\text{factored resistance}} \tag{2.2}$$

$$U = \frac{\text{length of the vector from a specified origin to the load effects}}{\text{length of the vector from the same origin to the factored interaction surface}} \tag{2.3}$$

2.2.2. Foundation integrity check

The foundation integrity assessment is composed of multiple checks, as seen in figure 2.3. Starting with the preload and windward leg checks as they are the most conservative. When a check is approved, the foundation is accepted; when a check is not approved, the following check should be performed which increases in complexity but reduces conservatism. The displacement check is the last check where it is accepted that the foundation will fail but it must do so within an acceptable limit. If the last check is not approved, the foundation is not acceptable and the jack-up operation can not be executed. The assessment load case will always refer to the load effect from the factored loads.

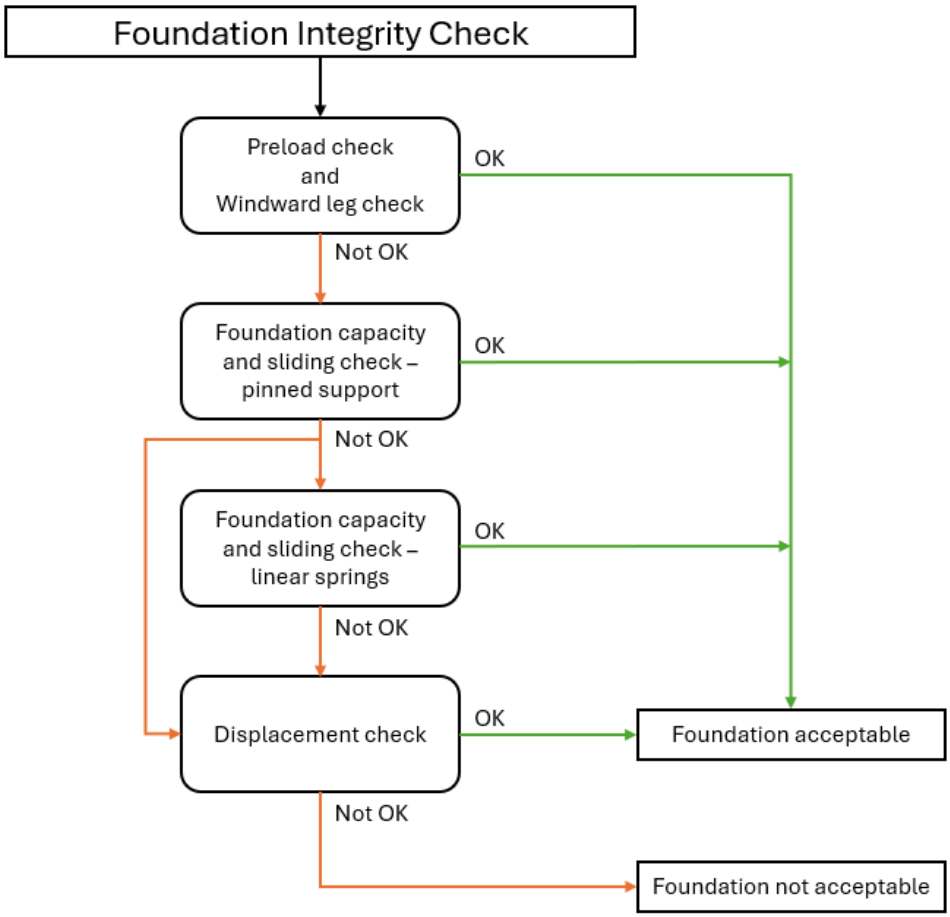

Figure 2.3: Foundation acceptance checks approach

Yield interaction

The foundation integrity checks are based on the concept of yield interaction; which is discussed here shortly before moving on to the checks.

During preloading the soil below the spudcan will deform plastically and harden the foundation until bearing capacity and preload are in equilibrium. After preloading, the soil will unload elastically, creating a certain stiffness for the foundation [8]. As long as the stresses in the soil remain within their elastic boundaries during the operation, the foundation won't fail; these stress boundaries can be presented in a yield surface. Soil stresses are not only in vertical direction but from horizontal loads and moments as well [40]. When loads with different directions take place simultaneously, for example during a storm, the stress boundaries in each direction are reached much quicker. A yield surface as presented in figure 2.4, takes account of the stress boundaries. Which depend on spudcan geometry and soil properties with maximum moment, vertical, and horizontal capacities [28].

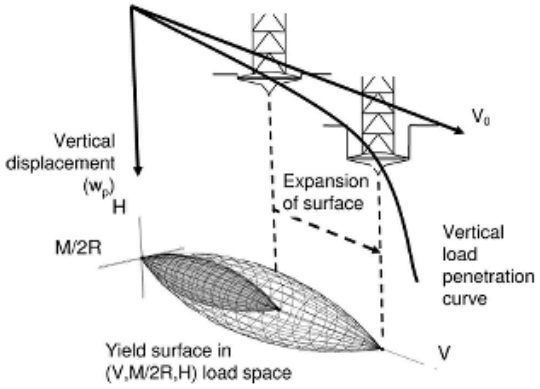

Figure 2.4: Loading yield surface [28]

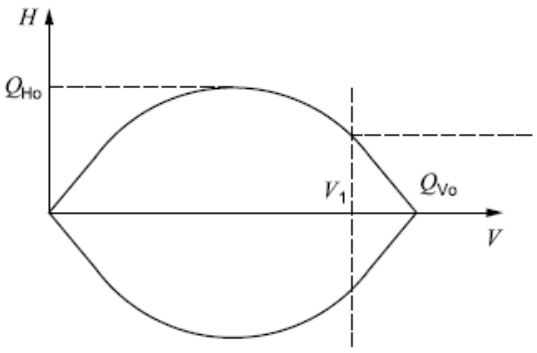

Figure 2.5: Yield surface without sustaining moment [27]

Foundation models for spudcans are generally described by a pinned support [27], which can't sustain moment. The yield surface for spudcans can therefore be described as a two dimensional vertical-horizontal foundation capacity envelope as seen in figure 2.5. This capacity envelope is described by equation (2.4) where Q_V is the gross ultimate bearing capacity established by preloading and F_H and F_V the horizontal and vertical spudcan reactions in response to the assessment load actions [36]. The horizontal bearing capacity Q_{Hs} should be determined for each soil type and account for horizontal sliding.
If the yield formula equals zero or less than zero, then the force combination lies inside the yield surface; if it is larger than zero, the force combination lies outside the yield surface and the foundation will plastically fail to these loads. In this equation, a is the penetration depth factor as described in equation (2.5), if the limit of a goes to zero for very shallow penetrations then the yield equation can be described by equation (2.6).

$$\left(\frac{F_H}{Q_{Hs}}\right)^2 - 16(1-a)\left(\frac{F_V}{Q_V}\right)^2\left(1-\frac{F_V}{Q_V}\right)^2 - 4a\left(\frac{F_V}{Q_V}\right)\left(1-\frac{F_V}{Q_V}\right) = 0 \tag{2.4}$$

$$\begin{aligned} a &= D/2.5B \qquad \text{(for } D < 2.5B\text{)} \\ a &= 1.0 \qquad\quad\ \ \text{(for } D \geq 2.5B\text{)} \end{aligned} \tag{2.5}$$

$$\left(\frac{F_H}{Q_{Hs}}\right) - 4\left(\frac{F_V}{Q_V}\right)\left(1-\frac{F_V}{Q_V}\right) = 0 \tag{2.6}$$

Preload check and windward leg check

Firstly, the ultimate bearing capacity for the vertical loading of the leeward leg is assessed in terms of the preload check for a pinned foundation. This check should only be applied when the horizontal force on the leeward leg spudcan F_H is no greater than the limiting horizontal capacity F_{H1} for a certain soil type and embedment. This limiting horizontal capacity is derived from the intersection between the unfactored vertical-horizontal bearing capacity envelope and conservatively adjusted as seen in table 2.1, where Q_{Vnet} can be determined with equation (2.7).

For a pinned support the maximum gross vertical force F_V acting on the soil beneath the spudcan due to the assessment load case should comply with the limits presented in equation (2.8) for a spudcan with no backfill and equation (2.9) for a spudcan with backfill. The gross vertical force includes the weight of the backflow and infill during $W_{BF,o}$ and after $W_{BF,A}$ preloading and the soil buoyancy of the spudcan B_S below the bearing area. In these limit checks, V_{Lo} represents the vertical preload force and $\gamma_{R,PRE}$ the preload resistance factor which is equal to 1.10 as stated by [27].

$$Q_{Vnet} = s_u \cdot N_c \cdot \pi\frac{B^2}{4} \tag{2.7}$$

$$F_V \leq \frac{V_{Lo}}{\gamma_{R,PRE}} - B_S \qquad \text{(with no backfill)} \tag{2.8}$$

$$F_V \leq \frac{V_{Lo}}{\gamma_{R,PRE}} + W_{BF,o} - B_S \qquad \text{(with backfill)} \tag{2.9}$$

Table 2.1: Limiting horizontal capacity from [27]

Soil type	Embedment	F_{H1}
Sand	Partial	$\left(0.1 - 0.07\left(B/B_{max}\right)^2\right) Q_{Vnet}$
Sand	Full	$0.03 Q_{Vnet}$
Clay	Any	$0.03 Q_{Vnet}$

Secondly, when the horizontal force on the windward leg spudcan F_H is no greater than F_{H1} the windward leg check should be applied. In this check, the sliding stability of the windward leg is assessed by ensuring that the gross vertical reaction force F_V can be safely supported by the ultimate bearing capacity Q_V as presented in equation (2.10). For sand foundations with an effective friction angle smaller than 25°, the sliding check from the next section should be used.

$$F_V > \left(1 - \frac{1}{\gamma_{R,PRE}}\right) Q_V \tag{2.10}$$

Foundation capacity and sliding check

The foundation capacity check assesses the situation where a reduction in the ultimate vertical bearing capacity occurs, when it is simultaneously subjected to vertical loads, horizontal loads, and moments. For pinned foundations, the moment is ignored and the check makes use of the factored vertical-horizontal foundation capacity envelope.

To obtain the factored capacity envelope the unfactored vertical-horizontal capacity envelope is scaled by dividing its coordinates by the resistance factor $\gamma_{R,VH}$ from the point of zero net reaction which shrinks the envelope towards its scaling origin as seen in figure 2.6 from surface 1 towards 2. The point of zero net reaction is determined as in equation (2.11) and the resistance factor $\gamma_{R,VH}$ is equal to 1.10 [27].

The application of the factored capacity envelope is presented in equation (2.12), each spudcan foundation should satisfy this capacity check in order to be labelled as satisfactory. Meaning that the assessment reaction forces from factored actions fit within the factored capacity envelope. In this equation, (F_H, F_V) is the environmental response point determined from factored loads and $(F_H, F_V)_{ORG}$ is the origin used for establishing the utilization obtained as in equation (2.13). $Q_{VH,f}$ is the point where the vector from $(F_H, F_V)_{ORG}$ through (F_H, F_V) intersects the factored vertical-horizontal capacity surface.

$$\begin{aligned} F_H &= 0 \\ F_V &= W_{BF,o} - B_S \end{aligned} \tag{2.11}$$

$$\left| (F_H, F_V) - (F_H, F_V)_{ORG} \right| \leq \left| Q_{VH,f} - (F_H, F_V)_{ORG} \right| \tag{2.12}$$

$$\begin{aligned} H &= 0 \\ V &= 0.5 \frac{Q_V}{\gamma_{R,VH}} \end{aligned} \tag{2.13}$$

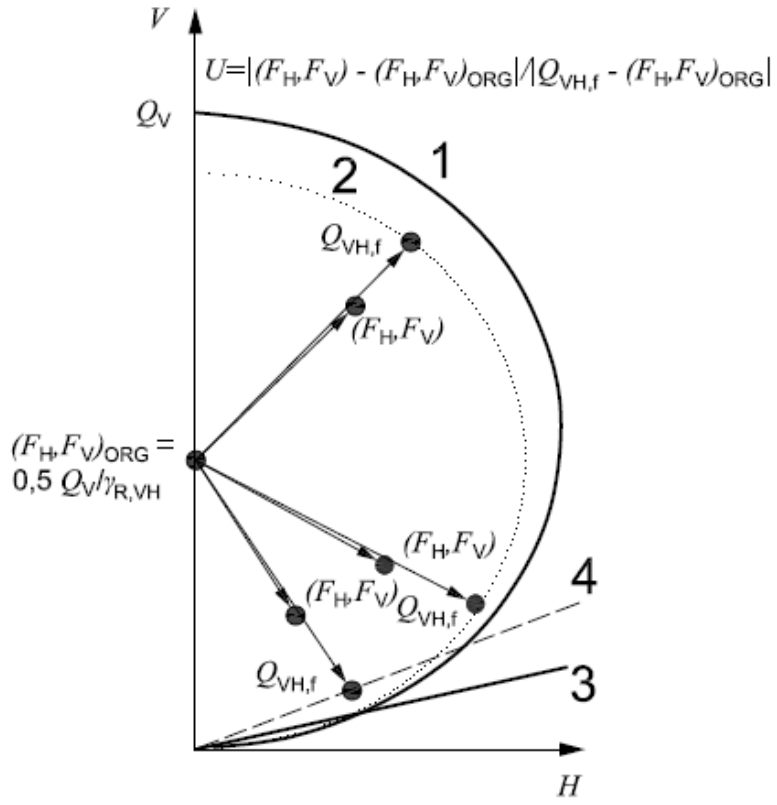

Figure 2.6: Factored vertical-horizontal capacity envelope in sand from [27]

When the foundation capacity is checked, the spudcan foundation should also be assessed on its sliding stability; since the factored sliding surface could potentially lie within the factored vertical-horizontal bearing capacity envelope. Although performing this check only for the windward leg could be sufficient, it is recommended to assess all legs and load cases.
The foundation sliding check makes use of the same utilization check as for the capacity check, see equation (2.12). Where (F_H, F_V) and $(F_H, F_V)_{ORG}$ are the same coordinates as in the capacity check but $Q_{VH,f}$ is obtained differently.
In this case, $Q_{VH,f}$ is the point where the originating vector intersects the factored sliding capacity surface, this surface is obtained by dividing the horizontal coordinates of the foundation sliding capacity Q_{Hs} by the resistance factor for horizontal foundation capacity $\gamma_{R,Hfc}$. The sliding capacity surface should be obtained depending on the soil type, with $\gamma_{R,Hfc}$ equal to 1.25 for sand and 1.56 for clay [27]. The scaling of the sliding capacity surface is presented in figure 2.6 from surface 3 to 4.

Displacement check

When the foundation capacity established by preloading is exceeded during certain operations, it results in vertical settlements of the spudcans. Which can often lead to additional foundation capacity through the expansion of the yield interaction surface, if the risk of punch-through does not exist. To assess if these settlements still result in safe operation conditions, a displacement check should be carried out. Which is the last assessment check to evaluate if the foundation is acceptable.
This check can be accomplished by identifying for which preload penetration depth the vertical-horizontal yield surface, as described in the foundation capacity check, results in a factored yield surface that exceeds the response loads on the spudcans. This additional spudcan penetration should be obtained from the predicted load-penetration curve as presented in figure 2.7. If this additional penetration is significant, the effects on the spudcan foundation and entire structure should be iterated; to establish if these consequences result in acceptable values of all previous utilization checks. A displacement check might also be needed if the foundation capacity or sliding capacity of a windward leg with pinned

foundations is not satisfied.
Consideration should be given to the operational limitations of the jack-up vessel when assessing the displacement check.

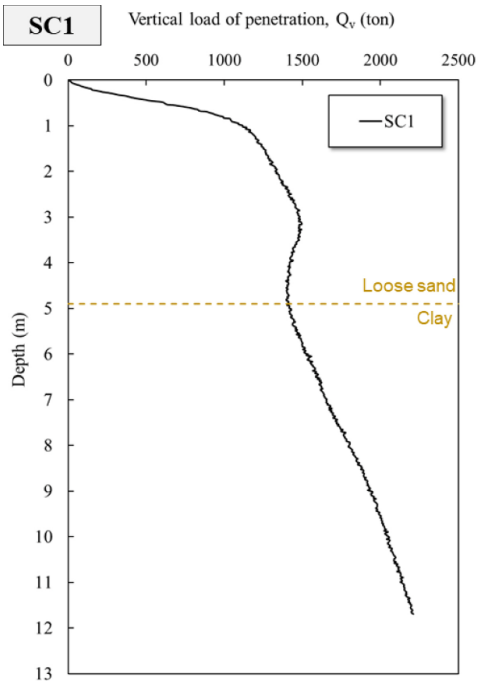

Figure 2.7: Spudcan bearing capacity versus leg penetration from [19]

2.2.3. Conclusion

The integrity of the jack-up vessel foundation should be assessed before each jack-up operation. This can be done by means of a utilization check which generally defines that the factored loads due to the relevant extreme limit state should be smaller than the factored resistance, which is established by preloading. Based on this general formulation, a foundation integrity assessment is composed, consisting of multiple checks. Each check has increasing complexity and decreasing conservatism. For assessments where the bearing capacity of the spudcans can not be determined the preload check must be satisfied in order to have an acceptable foundation.
The methods described in this literature section are used later on in this research to formulate a correct limit state function for preload failure.

2.3. Reliability analysis

Engineering problems often involve risk and uncertainties, which can lead to difficult decision making. For jack-up operations, these uncertainties can be derived from two main categories, namely loads and foundation response [41]. Load uncertainties can be linked to each load type, and can occur due to insufficient record data, mixing of different measuring approaches, and inaccuracies of the load transfer model [2]. For foundation response predictions, an analytical model is typically used. This model accounts for uncertainties arising from incomplete knowledge about the seafloor beneath the foundation and the soil's engineering properties. It also incorporates potential errors in the response and installation of the foundation [6].

To account for these uncertainties in engineering assessments, two approaches are commonly used: a deterministic approach or a stochastic approach [20]. Deterministic approaches predict the response of the system without randomness and deal with uncertainties by applying safety factors. These methods can over-design or even under-design the system and should therefore only be used when

randomness or uncertainties are small [5]. Both outcomes are not favourable since over-designing is costly and requires more time, while under-designing can result in failure of the system [3]. Although uncertainties in offshore environments are relatively high, the foundation assessment of jack-up vessels is traditionally performed with a deterministic approach as described in section 2.2 [27].
For scenarios with a relatively high level of uncertainty, a stochastic approach is more favourable since it improves the reliability of the design. A stochastic approach compares the statistical properties of the system's input and response to create a comprehensive analysis based on probability, leading to a robust system. In addition, it can also identify which areas could be further optimized [5].

Stochastic approaches treat the likelihood of a given event's occurrence and quantify uncertain actions of random events by making use of probabilistic approaches. In these approaches, the probability of certain actions can be represented by a probability density function (PDF), which describes the relative frequency of certain realizations for random variables [5].
Probabilities can be obtained for certain parameters of actions and their responses for a certain limit state. A reliability analysis then deals with the calculation and prediction of violations from these limit states during the deployment of the structure. The response or resistance to the loads is considered satisfactory when the probability of the limit state violation is within an acceptable degree of certainty. Once the probability of failure is determined, alternative designs can be made in order to improve reliability and minimize the risk of failure [5].
This section will address how data records can be described in a probabilistic manner in section 2.3.1 and will describe a few reliability methods to obtain a probability of failure for the assessed problem in section 2.3.2.

2.3.1. Probabilistic description

From a data record, a histogram can be drawn with certain intervals and fitted with a matching curve to derive the probability density function. The probability of two or more random events occurring simultaneously can be represented by a joint probability density function, which can be expressed as in equation (2.14) for the random independent variables X and Y where x and y are the values that respective random variables can have[5].

$$f_{XY}(x, y) = f_X(x) f_Y(y) \tag{2.14}$$

PDF's can be described by a couple of parameters. The mean or weighted average of the PDF is given by equation (2.15), which represents the distance from the origin to the centre of the PDF and can be referred to as the first moment. The expected mean value of a function $g(x)$ of the value of a random variable x can be calculated by equation (2.16) [5]. The second moment or variance of X measures the spread of the data around the mean and can be obtained by equation (2.17). Variability of a random variable is generally given by the standard deviation, described as in equation (2.18). By normalizing the standard deviation as in equation (2.19) the Coefficient of Variation COV δ_X is obtained, which shows the relative amount of randomness or uncertainty of a variable [5]. By combining the mean value and the standard deviation or COV, the covariance σ_{XY} can be obtained, which can be used to describe a linear association between two random variables X and Y. The covariance can be determined from equation (2.20), and a non-dimensional correlation coefficient between the two random variables can be calculated from equation (2.21). The closer the correlation coefficient is to 1 or -1, the more linear correlation exists between the two random variables [5]. Another way of describing the probability distribution is by a cumulative distribution function (CDF) $F_X(x)$, which is equal to the probability that X is less than or equal to x as seen in equation (2.22) [5].

$$\mu_X = E(X) = \int_{-\infty}^{\infty} x \cdot f_X(x)\, dx \tag{2.15}$$

$$E[g(X)] = \int_{-\infty}^{\infty} g(x) \cdot f_X(x)\, dx \tag{2.16}$$

$$V(X) = E[(X - \mu_X)^2] = E(X^2) - \mu_X^2 \tag{2.17}$$

$$\sigma_X = \sqrt{V(X)} \tag{2.18}$$

$$\delta_X = \frac{\sigma_X}{\mu_X} \tag{2.19}$$

$$\sigma_{XY} = Cov(X,Y) = E[(X-\mu_X)(Y-\mu_Y)] \tag{2.20}$$

$$\rho_{XY} = \frac{\sigma_{XY}}{\sigma_X \sigma_Y} \tag{2.21}$$

$$F_X(x) = \int_{-\infty}^{x} f_X(S)\, dS \tag{2.22}$$

Probability distributions

The right selection of the probability distribution function is crucial for further reliability analysis. To model the design parameters or random variables of the assessed problem, several types of standardized probability distributions are used; which all depend on the nature of the problem [5]. This section will describe the Gaussian or normal distribution and the lognormal distribution.

The Gaussian or normal distribution is often used for material or soil properties and normal distributed loads, and is given by equation (2.23) for distributions with zero skew, which means the distribution is symmetrical. As seen in figure 2.8 the Gaussian distribution is symmetric with respect to the mean [5].

$$f_X(x) = \frac{1}{\sigma_X \sqrt{2\pi}} \exp\left[-\frac{1}{2}\left(\frac{x-\mu_X}{\sigma_X}\right)^2\right] \tag{2.23}$$

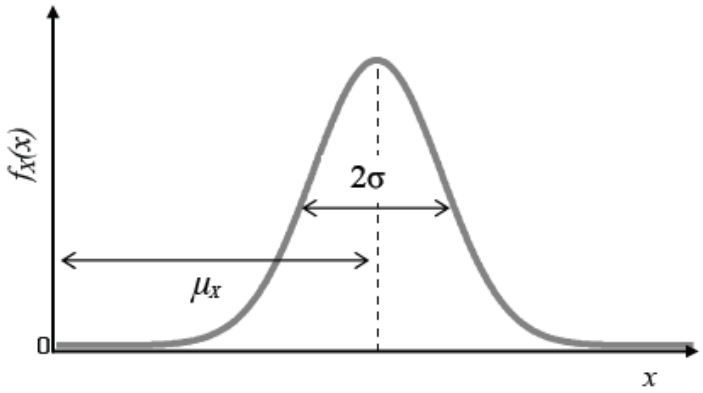

Figure 2.8: Example of a Normal Density Function

The lognormal distribution is typically found in descriptions of failure, failure rates, and phenomena with a large range of data, such as loading variables. Its probability density function can be described by equation (2.24) in terms of Y which follows a normal distribution and since $Y = lnX$ it can also be described as in equation (2.25) in terms of X which follows a lognormal distribution as presented in figure 2.9. In these equations, the standard deviation and mean of Y can be determined with equation (2.26) and equation (2.27) respectively [5].

$$f_Y(y) = \frac{1}{\sqrt{2\pi}\sigma_Y} \exp\left[-\frac{1}{2}\left(\frac{y-\mu_Y}{\sigma_Y}\right)^2\right], -\infty < y < \infty \tag{2.24}$$

$$f_X(x) = \frac{1}{\sqrt{2\pi}x\sigma_Y} \exp\left[-\frac{1}{2}\left(\frac{\ln x-\mu_Y}{\sigma_Y}\right)^2\right], 0 \leq x < \infty \tag{2.25}$$

$$\sigma_Y^2 = \ln\left[\left(\frac{\sigma_X}{\mu_X}\right)^2 + 1\right] \tag{2.26}$$

$$\mu_Y = \ln \mu_X - \frac{1}{2}\sigma_Y^2 \tag{2.27}$$

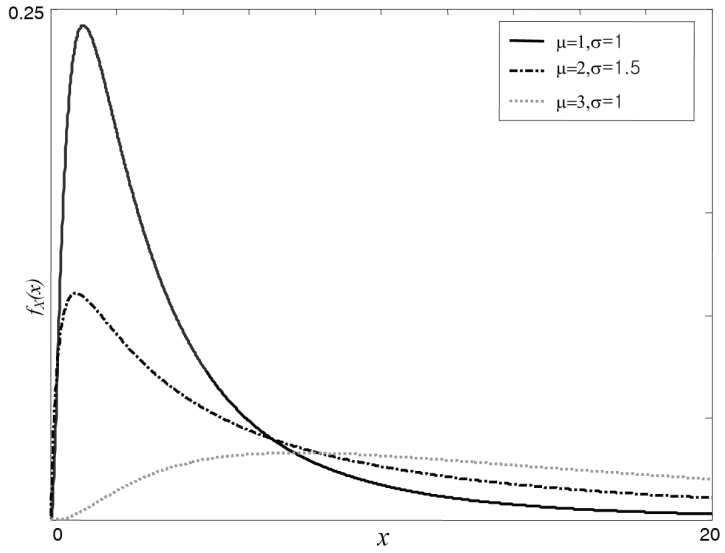

Figure 2.9: Example of a Lognormal Density Function [5]

2.3.2. Reliability methods

A reliability analysis will evaluate the probability of a failure by assessing if a certain limit state is exceeded. The limit state $g(\cdot)$ can generally be described as the difference between the resistance of the system R and the loading on the system S as described in equation (2.28). For each limit state a reliability index β can be obtained as in equation (2.29), which indicates the mean margin of safety from the failure surface. The failure surface, also known as the limit state surface, is the surface or line where the limit state function is equal to zero. If the resistance and loading are uncorrelated, the correlation coefficient ρ_{RS} becomes zero and the equation of the reliability index can be simplified [5]. When the limit state function is smaller than zero, the system fails. The probability of failure is marked in figure 2.10 and can be obtained by equation (2.30). The probability density function of the limit state function $f_g(g)$ has the same distribution as R and S if they both have the same type of distribution and are independent, and can be described as in section 2.3.1 [5].
Another way of describing reliability is by a safety factor F as seen in equation (2.31), failure will occur if F is equal to one. The reliability index for each safety factor is given as in equation (2.32) [5].

$$g(X) = R(X) - S(X) \tag{2.28}$$

$$\beta = \frac{\mu_g}{\sigma_g} = \frac{\mu_R - \mu_S}{\sqrt{\sigma_R^2 + \sigma_S^2 - 2\rho_{RS}\sigma_R\sigma_S}} \tag{2.29}$$

$$P_f = P\left[g(\cdot) < 0\right] = \int_{-\infty}^{0} f_g(g)\, dg \tag{2.30}$$

$$F = \frac{R}{S} \tag{2.31}$$

$$\beta = \frac{\mu_F - 1}{\sigma_F} \tag{2.32}$$

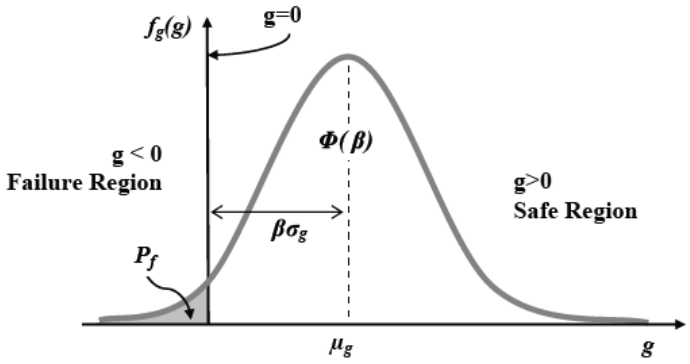

Figure 2.10: Probability Density for Limit state g(.) [5]

Solving the integration of the probability of failure for a system with multiple random variables with different distributions can become very complex. Therefore, the rest of this section will provide different methods to describe and solve limit state functions to obtain their reliability index and simplify the integration process of the probability of failure.

First-Order Second Moment

The first-order second moment (FOSM) method simplifies the complexities of the probability of failure calculation and expresses inputs and outputs as the mean and standard deviation. The limit state function is represented as the first-order Taylor series expansion at the mean value point, which makes it a linear function. At the mean, the linearized limit state function can be written as $\tilde{g}(X)$. The mean value of this approximated limit state function is equal to the original limit state function at the mean of the input variables as described by equation (2.33), its standard deviation by equation (2.34) and therefore the FOSM reliability index as in equation (2.35) [5]. The probability of failure can then be obtained from equation (2.36).
If the limit state function is linear, the reliability index from equation (2.35) is the same as in equation (2.29) [5]. If the limit state function is non-linear, the approximated limit state function can be obtained by linearizing the original limit state function at the mean value point, as described by the FOSM method.
Although the FOSM method changes the original complex problem into a simple problem it leads to inaccurate estimates for functions with a high nonlinearity and is not consistent for different expressions of the same problem [5]. Nevertheless, it can serve as a simple check for independent normal distributed linear problems of which the limit state distribution is known.

$$\mu_{\tilde{g}} \approx E\left[g\left(\mu_X\right)\right] = g\left(\mu_X\right) \tag{2.33}$$

$$\sigma_{\tilde{g}} = \sqrt{Var[\tilde{g}(X)]} = \sqrt{\left[\nabla g(\mu_X)^T\right]^2 Var(X)} = \left[\sum_{i=1}^{n}\left(\frac{\partial g(\mu_X)}{\partial x_i}\right)^2 \sigma_{x_i}^2\right]^{\frac{1}{2}} \tag{2.34}$$

$$\beta = \frac{\mu_{\tilde{g}}}{\sigma_{\tilde{g}}} \tag{2.35}$$

$$P_f = 1 - \Phi(\beta) \tag{2.36}$$

Monte Carlo Simulation

Reliability methods such as the FOSM method approximate a solution of the reliability index and therefore the probability of failure of a certain engineering problem. To be certain about the accuracy of its outcome it should be validated based on as many experiments as possible. Such validation can be done by sampling methods, which conduct simulations from a generated sampling set from the distributions of the random variables. The probability of failure or win/loss ratio of a sampling method is then accepted as the truth and compared to the probability of failure from the reliability method to validate the accuracy of the reliability index. One such sampling method is called the Monte Carlo Simulation, which is further explained in this section [5].

The Monte Carlo Simulation (MCS) is a simple random sampling method that makes realizations based on randomly generated sampling sets for uncertain variables. Firstly, a distribution type for each random variable is obtained and a PDF is determined. From this PDF a sampling set is then generated for the corresponding random variables.
The most common generation method is the inverse transform method which can graphically be summarized in figure 2.11. This method makes use of a random number generator, which generates uniform random numbers ν_i between zero and one. This number can then be situated on the corresponding uniform CDF since the numerical value of the CDF has an interval between zero and one as well. This uniform CDF value can be used as a CDF value of the target distribution. Finally, the random sample number x_i of the target PDF can be obtained by equation (2.37), which makes use of the inverse CDF $F_X^{-1}(.)$ [5].

$$F_X(x_i) = \nu_i \qquad \text{or} \qquad x_i = F_X^{-1}(\nu_i) \tag{2.37}$$

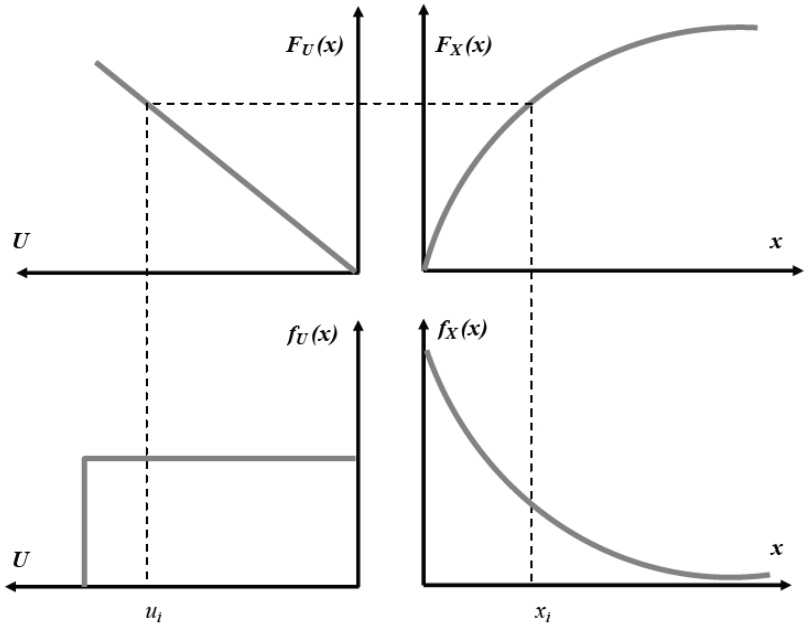

Figure 2.11: Inverse transform method for exponential distribution [5]

Hereafter, the limit state function of the system needs to be modelled to assess the failure of the drawn samples. If the limit state function is violated, the system has failed for the corresponding sample, this trial is then repeated many times to guarantee the convergence of the statistical results. The probability of failure after N trials is given as in equation (2.38) where N_f is the number of trials for which the limit state function was violated [5].

$$P_f = \frac{N_f}{N} \tag{2.38}$$

2.3.3. Conclusion

Probabilistic approaches to engineering problems might result in more reliable and efficient designs since they deal with system uncertainties by quantifying them in terms of a probability of failure. The system can then be designed in order to meet a specific target probability of failure.
Such a system or engineering problem can be described by a limit state function which generally compares the resistance of the system with the applied loads. Acquired data records for each component of the limit state function can be summarised into a histogram, from which the distribution type and probabilistic parameters can be determined. Each histogram can then be matched by a corresponding probability density function in order to solve the reliability of the system. Solving such reliability problems can be done through simple methods such as FOSM or by more accurate sampling methods such as Monte Carlo Sampling. These methods ultimately provide a probability of failure of the system, where failure is defined as the factored loads being higher than the factored resistances.
The provided methods in this section of the literature review are used later in this research to describe probability distributions of certain assessed parameters and solve limit state functions with a Monte Carlo Simulation to obtain the probability of failure of the assessed system.

2.4. Target reliability

Reliability can be a useful decision parameter for the safety assessment of a structure. Requirements for reliability can be derived from multiple socioeconomic aspects and categorized into consequence classes. To ensure a sufficient safety level the design should comply with the required reliability needed for the severity of the consequences in case of a failure [34]. This section will provide a method to obtain the required reliability-based consequence classes in section 2.4.1 and respective probability of failure targets in section 2.4.2.

2.4.1. Consequence of failure

Reliability based engineering approaches will try to search for an optimal probability of failure of the system, where optimal means reliable enough without over-designing. Therefore, the probability of failure of a structure designed with reliability methods will not be equal to zero. The amount of allowed probability of failure depends on the consequences of the respective failure. If failure of a structure has very little consequences or can easily be undone it can be designed less conservatively than a structure where failure would be catastrophic.
Consequences of failure can be divided into multiple categories such as: economic loss, human fatalities and injuries, environmental damage, loss of structure, and political impact. Models for estimating human fatalities usually consist of the quantification of the people at risk and the probability that an exposed person to the failure may actually be killed or injured [11]. A system of consequence classes for structures has been created by the International Organization of Standardization as a rule of thumb, which describes each class with its expected consequences when failure happens, as seen in table 2.2.

For each class, an appropriate failure analysis method should be used, increasing in robustness and detail with increasing consequence class. The necessary analysis for each class is summarized below [11].

- Class 1: No specific considerations.
- Class 2: Simplified analyses based on idealized load and structural performance models.
- Class 3: Identification of scenarios leading to structural collapse. Reliability analyses addressing direct and indirect consequences should be used as a basis for simplifications.
- Class 4: Extensive study and analyses of scenarios leading to structural collapse involving experts on all relevant subject matters. Detailed assessments using dynamic and non-linear structural analyses addressing direct and indirect consequences.
- Class 5: Same as class 4 with the addition of an external expert panel for quality control.

Table 2.2: Consequence classes from [11]

Consequences class	Description of expected consequences	Examples of structures
Class 1	• Predominantly insignificant material damages.	Low-rise buildings where only few people are present, minor wind turbines, stables, etc.
Class 2	• Material damages and functionality losses of significance for owners and operators but with little or no societal impact. • Damages to the qualities of the environment of an order which can be restored completely in a matter of weeks. Expected number of fatalities fewer than five.	Smaller buildings and industrial facilities, minor bridges, major wind turbines, smaller or unmanned offshore facilities, etc.
Class 3	• Material losses and functionality losses of societal significance, causing regional disruptions and delays in important societal services over several weeks. • Damages to the qualities of the environment limited to the surroundings of the failure event and which can be restored in a matter of weeks. Expected number of fatalities is fewer than fifty.	Most residential buildings, typical bridges and tunnels, typical offshore facilities, larger or hazardous industrial facilities
Class 4	• Disastrous events causing severe losses of societal services and disruptions and delays at a national scale over periods in the order of months. • Significant damages to the qualities of the environment contained at a national scale but spreading significantly beyond the surroundings of the failure event and which can only be partly restored in a matter of months. Expected number of fatalities fewer than 500.	High-rise buildings, grandstands, major bridges and tunnels, dikes, dams, smaller offshore facilities, pipelines, refineries, chemical plants, etc.
Class 5	• Catastrophic events causing losses of societal services and disruptions and delays at national and global scale over periods in the order of years. • Significant damages to the qualities of the environment of global scale and which cannot be restored. Expected number of fatalities larger than 500.	Buildings of national significance, major containments and storages of toxic materials, major offshore facilities, major dams and dikes, etc.

2.4.2. Target probability of failure

The consequence of failure for each consequence class should be reflected by the appropriate target reliability level; which is expressed as the reliability index β or annual probability of failure and can be obtained from equation (2.39) [5]. In this equation the probability of failure for a single event $P_{f,event}$ can be obtained from reliability methods as discussed in section 2.3.2.

$$P_{f,annual} = 1 - (1 - P_{f,event})^{events/year} \tag{2.39}$$

Different approaches already exist for establishing target reliability; this section will provide a method based on monetary optimization, which has been formulated by the International Organization of Standardization [11].
For each structural consequence class from section 2.4.1, a target annual probability of failure is given depending on the relative cost of the risk reduction measure; as seen in table 2.3. This cost is relative to the initial construction of the structure and reflects the required effort to reduce the probability of failure [33]. The values presented in this table can be validated by other standards as well [10] [34] but are only indicative for economic optimization and may not be acceptable for life safety risks.

Table 2.3: Tentative target reliabilities based on monetary optimization from [11]

Relative cost of safety measure	**Consequences of failure (classes from table 2.2)**		
	Class 2	**Class 3**	**Class 4**
Large	$\beta = 3.1\ (P_f \approx 10^{-3})$	$\beta = 3.3\ (P_f \approx 5 \times 10^{-4})$	$\beta = 3.7\ (P_f \approx 10^{-4})$
Medium	$\beta = 3.7\ (P_f \approx 10^{-4})$	$\beta = 4.2\ (P_f \approx 10^{-5})$	$\beta = 4.4\ (P_f \approx 5 \times 10^{-6})$
Small	$\beta = 4.2\ (P_f \approx 10^{-5})$	$\beta = 4.4\ (P_f \approx 5 \times 10^{-6})$	$\beta = 4.7\ (P_f \approx 10^{-6})$

2.4.3. Conclusion

Specific reliability targets for structures can be determined based on the severity of the consequences in case of a failure and the relative cost of measurements to decrease the probability of failure. These cost-based reliability targets are generally expressed in terms of the annual probability of failure.
Based on the established consequence classes in this literature section, an annual target probability of failure for jack-up vessel preload failure will be determined later in the research.

3

Case and research framework

A research framework is composed based on the available data and observed literature to answer the research questions and sub-questions. The available data serves as the basis of this research and is therefore discussed first in section 3.1. This section provides the general background for the site specific assessments of jacking operations and describes three different offshore wind farm sites, including the soil conditions at these sites. To complete the necessary data for the case study, Jan De Nul also provided measuring data and jacking logs of the performed jacking operations at these sites.
After the background of the research is provided, the research framework to answer the research questions is laid out in section 3.2. The research framework, by large, consists of: data processing, reliability study, and preload safety factor optimisation. For each of these research parts, different models are created. By applying the data from the case study to the designed models and analysing the results, an answer to the research questions is formulated.

3.1. Case study background

For this research, Jan De Nul has provided the necessary jacking operations data to develop a working framework around it. To make the case study sufficiently diverse, three different offshore wind farm sites are assessed. The installed wind turbines by Jan De Nul at each wind farm were deployed by the vessel Vole au vent.
Vole au vent is a jack-up vessel with a design displacement of 30000 tons and can store the components of four wind turbines on deck. These components include the wind turbine tower, nacelle and hub, and rotor blades. To lift and install these components, the vessel is equipped with a large cargo crane that can lift up to 1500 tons at a small radius. Before the lifting operation can be conducted, the vessel is jacked out of the water by the jacking system to provide stable lifting conditions. The jacking system of the Vole au vent consists of four tubular legs with rectangular spudcans, each of which is operated by two movable hydraulic jacking rings for continuous jacking operation [39].
Spudcans are upside-down cone-shaped structures attached to the bottom of the legs. Its function is to spread the load acting on the legs onto the soil in order to prevent the jack-up vessel from penetrating too deep into the seabed[21].

Site Specific Assessment

Prior to the planning of the jacking operations, a site specific assessment (SSA) is conducted based on ISO 19905-1 and preloading procedures. These SSA's contain the results of the load assessments, the preload assessments, and all necessary weight and site-specific data; the most important ones are listed on the next page [14]. For all metocean data, the fifty-year extremes are included, and the area of interest for all surveys is approximately one km^2 around the location of operation [13] [29]. The SSA's of the three sites were also provided by Jan De Nul.

- site plan with location coordinates
- tidal range and storm surge
- wind and wave, and current data
- bathymetric survey
- seabed surface survey
- geotechnical investigation

Each operation with a jack-up vessel is unique in the loads that act on the structure. It is therefore a major part of the assessment to have an analytical model of the jack-up structure, which estimates the forces and displacements in response to these applied loads [7]. This load assessment is carried out with USFOS software, of which the results are provided in the SSA's.
The considered loading conditions are storm survival and heavy lifting operations. For storm survival, the maximum seasonal metocean conditions occurring in a fifty-year time frame are considered. During storm survival, no operations take place, and the airgap between the hull of the vessel and the waterline is lowered [18].
The focus of this research is on heavy-lifting operations. Where the load assessment considers both operational environmental loads and the loads caused by lifting and installing the heaviest wind turbine component; which is usually the tower. When a component is lifted by the crane, its weight is amplified due to dynamic forces [23]. If it is then moved by the crane, the centre of gravity of the vessel will shift, resulting in an unequal distribution of the loads over the legs. The load assessment analyses the point in the lifting operation where the maximum leg reaction occurs in one of the legs at the spudcans. This analysis is conducted for both the heavy hull condition and the light hull condition, which have respectively four and one wind turbines on the vessel.

After the maximum operational leg loads are obtained, a preload assessment is conducted. This assessment provides the amount of preload necessary to obtain a foundation which can resist the applied loads.
The preload assessment in the SSA's starts by categorising each wind turbine location based on their soil profiles; since this is the most determining factor for similar spudcan penetration response. These categories might differ for each site. For each soil category, a load penetration analysis is then undertaken; which defines the spudcan penetration, foundation bearing capacity envelope and foundation stiffnesses for the specified loading conditions based on their respective optimised preload.

Finally, for each loading condition at each soil category, the required preload at the spudcan has been optimised by maximising the preload and foundation bearing capacity checks based on ISO 19905-1, as discussed in section 2.2. By excluding the buoyant leg and spudcan weight from the optimised preload at the spudcan, the optimised preload at the hull level is obtained [26].

Measurements

In addition to the SSA's of the three sites, all sorts of measurement data obtained during the jacking operation at each individual location were provided by Jan De Nul as well. These measurements include the complete time span of the jacking and lifting operations, which is different for each location. They generally start just before the onset of lowering the jacking legs up until the jacking legs are fully retracted again. Measurements include: the load on each leg measured at the jacking system, leg extension, six degrees of freedom of the vessel, draught of the vessel at fore and aft, wind speeds measured at different locations on the main crane, slewing angle of the crane, boom angle of the crane, and hook load on the crane which are all measured every 5 seconds.
The leg reactions are obtained by measuring the pressure in the hydraulic jacking system, which is created in response to the applied loads. The measured pressure is then converted to tons and saved in a database.
This data is provided in the form of a CSV-file for each jacking location. At none of the locations a storm was present, so only operational loads were measured.
Also, the jacking logs at each location were made available. In these logs, the leg loads at hull level, leg extensions, and leg penetrations of each leg are noted by a crew member at certain key phases during the upjacking of the vessel. As well as the vessel weight based on the observed hull draft.

Danish Kriegers Flak

The first site is located at the Danish Kriegers Flak (DKF) wind farm, located 15-40 kilometres offshore in the Baltic Sea, as presented in figure 3.1. Where a total of 72 Siemens Gamesa 8.4 MW bottom-fixed wind turbines have been installed by Jan De Nul [31]. Of which 22 locations have a risk category 1, 8 locations have a risk category 2 or 3 and 42 locations have a risk category 3. Based on the SSA, the foundation risk categories for DKF represent the following foundation risks.

- Category 1: general caution
- Category 2: possible leg penetration
- Category 3: possible punch-through and/or rapid leg penetration

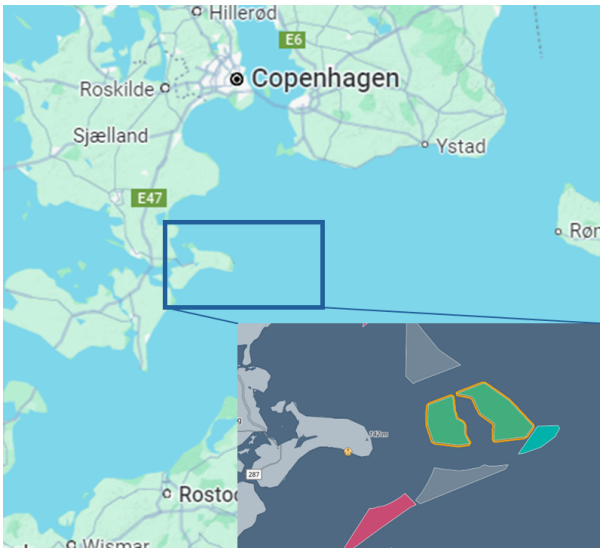

Figure 3.1: Map showing Kriegers Flak offshore wind farm [1]

Overall, Kriegers Flak presents complex and challenging ground conditions for jacking operations, but shallow water depths ranging between 17 and 31 meters, and mild environmental conditions. The total weight of one Siemens Gamesa 8.4 MW bottom-fixed wind turbine is equal to 907 ton, of which four can be carried by the Vole Au vent simultaneously. The heaviest component of the turbine is the tower, which weighs 465.3 ton [16].

Saint Nazaire

The Saint Nazaire offshore wind farm is the second site. Located in the Bay of Biscay off the West coast of France, as shown in figure 3.2, and contains 80 GE Haliade bottom-fixed wind turbines with a capacity of 6 MW [25]. The seabed at this site is mainly made out of outcropping rock which makes it difficult to jack up on. Therefore, 75 locations have been pre-cut by a cutter dredger to create a two meter deep gravel bed, which improves the jacking conditions. The other 5 locations comprise of dense sand over clay. Hence no seabed preparation was needed here. Based on these seabed conditions, two foundation risk categories are established. The maximum water depth at this site is 25 meters.

- Pre-cut seabed: general caution
- Channel deposits: severe punch-through risk

Figure 3.2: Map showing Saint Nazaire offshore wind farm [1]

Vesterhav

The third site is the Vesterhav Nord and Syd offshore wind farm in the Danish waters of the North Sea, as seen in figure 3.3. Consisting of 41 Siemens Gamesa 8.4 MW bottom-fixed wind turbines [31], which can be divided into two main categories of similar geology along with 5 individual locations with more complex soil conditions. Category 1 consists of 27 locations which are dominated by medium dense to dense sands. Category 2 has 9 locations which are dominated by medium dense sands and medium stiff to stiff clay layers. Five individual locations with dense to very dense sand overlying soft to stiff clay layers in category 3. Based on the SSA, the foundation risk categories for Vesterhav represent the following foundation risks. At Vesterhav, the water depth ranges between 20 and 26.6 meters.

- Category 1: general caution
- Category 2: general caution
- Category 3: possible punch-through and/or rapid leg penetration

Figure 3.3: Map showing Vesterhav Nord and Syd offshore wind farm [1]

The installed Siemens Gamesa 8.4 MW bottom-fixed wind turbines are the same as at the Danish Kriegers Flak, with the same weight specifications.

3.2. Research framework

This section provides an overview of the research framework used to answer the research questions. The research framework is designed around the available data from the case study as explained in section 3.1. Each individual part of the research framework is discussed further in detail in chapter 4 and chapter 5, appendix B provides an additional research into the elevated hull weight.

At first, some preparations need to be made. The parameters of interest are gathered from all the available measuring data, including the time series of the four leg reactions, crane load, and crane slewing angle. These leg reactions are then refined by an exponential moving average to reduce the noise in the measurements. The crane load and crane slewing angle are later on used to identify certain operational phases in the data. Since not all locations have qualitative measurements, the data is filtered as well; excluding operations where not all necessary data was correctly measured or saved. Hereafter, the maximum leg reactions are obtained during the preloading phase and operational phase. At last, based on the soil risk profiles as identified in the SSA, each location is categorized as a low or high risk location. The data processing is further explained in section 4.1.

In order to answer the first research sub-question the actual leg reactions from the data processing are compared to the estimated leg reactions from the SSA's in section 4.2. Here, the probability distributions of two ratios are obtained for the jacking locations at both risk categories of each site. Namely, measured maximum operational leg reaction versus estimated maximum operational leg reaction and measured preload versus prescribed preload. These distributions are obtained in the form of a histogram from which a lognormal probability density function can be obtained. These distributions represent the preload uncertainty and operational uncertainty.
Additionally, a third distribution is obtained for both risk profiles of each site, the measured maximum operational leg reaction versus measured preload.

The second research sub-question is answered in section 4.2 as well. To assess the reliability of a system by its probability of failure, a certain limit state function should be determined, which describes the failure of the respective system. This is done for both the estimated and actual operational conditions, based on the foundation integrity checks of ISO 19905-1. To obtain a result for the probability of failure of the system, a Monte Carlo Simulation is used. Which samples values from the obtained probability distributions and inserts them into the defined limit states. Resulting in an annual probability of failure, with failure referring to preload exceedance in this case.

The methods to answer the third research sub-question and second research question are explained in chapter 5. An optimal target for the annual preload exceedance is here obtained from methods described in the literature and in agreement with Jan De Nul. Section 5.2 outlines the method used to determine the ideal preload safety factor for each risk category, for the theoretical values that aim to achieve the desired actual applied preload safety factor.

An overview of the research framework is presented in figure 3.4, which also includes some additional findings as output. These findings are out of the scope of this research but give interesting insights into why estimated and measured leg reactions are so different. These findings are included in appendix B.

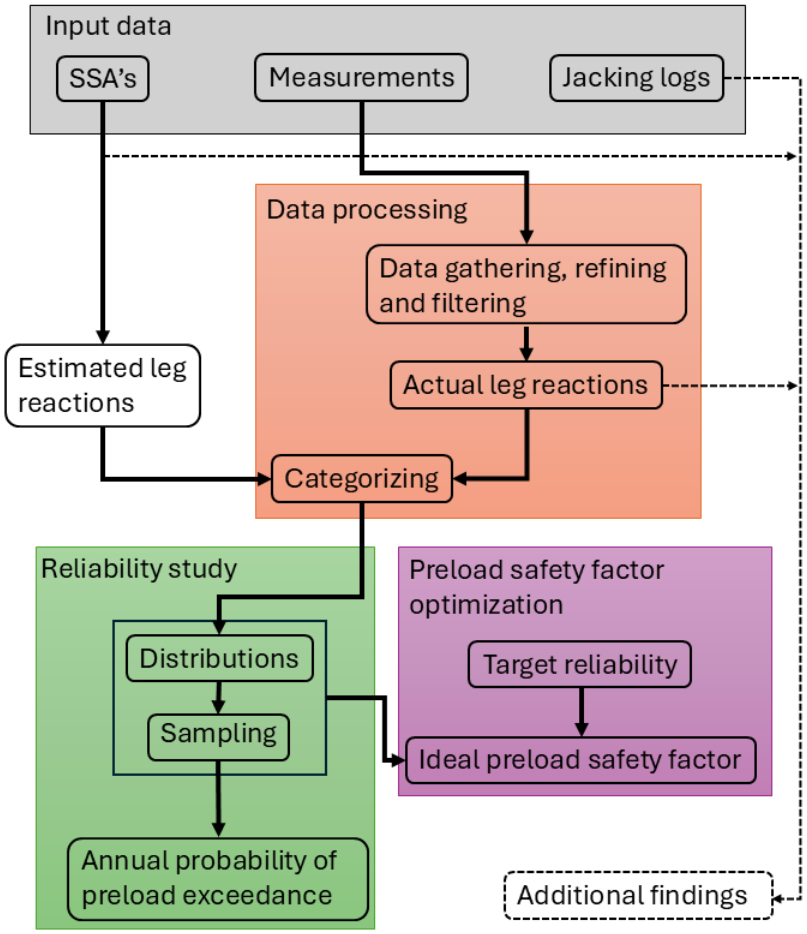

Figure 3.4: Research flowchart

4

Reliability study

This chapter begins by describing the methods used to process the acquired data in section 4.1. The data processing is carried out in several steps. First, time series data of measured leg reactions, crane loads, and crane slewing angles from past offshore jacking operations are gathered. Hereafter, the time series of leg reactions are refined and any faulty measurements are filtered out. From the cleaned time series, the maximum leg reactions during preloading and heavy lifting operations are identified. In parallel, the same leg reaction parameters are also retrieved from the site specific assessments. Both the actual and estimated values are then categorised based on soil risk profiles.
This processed data serves as a basis for the subsequent reliability study, which aims to answer the first and second research sub-questions. Section 4.2 discusses the methods used to define parameter distributions, identify failure through a limit state function, and sampling of random values using a Monte Carlo Simulation to calculate the annual probability of preload exceedance for the given scenarios.

4.1. Data processing

For each individual location where a jacking operation was conducted, a datasheet is provided with time series of all sorts of measured parameters. Over the three offshore wind farm sites from the case study, a total of 192 jacking operations were measured, each with their respective datasheet. Since the amount of measuring data is too large to manually go over each operation, a series of Python scripts are developed to extract the useful data. This section will explain how the data is processed to obtain a reliable output for the actual leg reactions.

4.1.1. Data gathering, refining and filtering

Gathering

As discussed in section 3.1, the provided data includes the time series of many different parameters. Most of which are not of interest to this research. Therefore, all useful data is first gathered from each individual data sheet and placed together in a single file.
The extracted data includes the four leg reactions measured at hull level as seen in figure 4.1, which shows an example of the leg reactions of the first part of an operation. From the literature described in section 2.1, multiple phases can be marked in the time series of the leg reactions.

These different phases are also indicated in figure 4.1 and can be explained as follows:

- A: the vessel is being positioned
- B: the legs are extended until contact with the soil
- C: the first diagonal leg pair is preloaded in multiple cycles
- D: the second diagonal leg pair is preloaded in multiple cycles
- E: both leg pairs are actively loaded, completing the preload phase
- F: operation phase, where multiple crane operations will install the wind turbine components

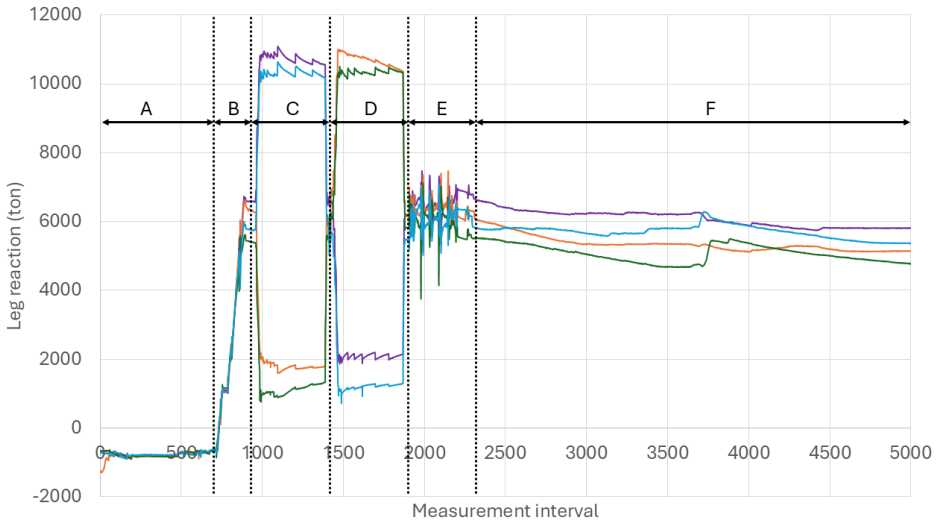

Figure 4.1: Example of measured leg reactions at hull level

To help identify certain operational phases in the leg reactions, the crane load and crane slewing angle are obtained from the data as well. In theory, the crane load provides enough information to identify when a lifting operation took place. But, during some operations the crane load was not measured or not of sufficient quality but, the crane slewing angle was, and vice versa. Therefore, the crane slewing angle was also extracted, which is the horizontal rotation of the crane.

Refining

These leg reactions are then refined to reduce the noise in the measurements and the impact of an individual outlying value, which makes the method more robust. To average out the leg reaction measurements, an exponential moving average (EMA) is applied; which is one of many different smoothing techniques for time series. The EMA method was chosen because it perfectly suits the job of refining many different large time series, as well as its simplicity. At each point in the time series, the EMA takes the weighted average of the previous N measurements with more weight on the values closer to the current point. Where N is the window length of the EMA. An EMA of length 10 will, for example, calculate the exponential average of the past 10 measurements, including the current one. A general formulation to define the EMA is presented in equation (4.1), although a built-in Python function is used to do this. In this equation, EMA_t represents the exponential moving average at time t where X_t is the value of the original time series at time t. The smoothing factor α determines how much weight is given to the most recent data point versus the previous EMA at the previous time step EMA_{t-1} [30].

$$\begin{aligned} EMA_t &= \alpha \cdot X_t + (1-\alpha) \cdot EMA_{t-1} \\ \alpha &= \frac{2}{N+1} \end{aligned} \tag{4.1}$$

The effect of different EMA lengths is shown in figure 4.2, where a 500-second sample of a leg reaction is taken around its maximum preload and shown in blue. The sample is taken from the measurements of leg 1 in phase C, from data point 1050 till 1150 in figure 4.1, shown in purple. Three different EMA's are shown in figure 4.2: EMA of length 12 in purple, EMA of length 24 in green, and EMA of length 36 in orange; which is equal to a length of 1, 2 and 3 minutes respectively.
For the leg reactions, an EMA of length 24 is used to refine their time series; which is equal to the time it takes for one preload sub-cycle as marked in figure 4.2 by the dotted lines. The difference in the maximum value between the original sample and its 24 EMA is in this case less than a percent. Therefore the refined data represents the actual data very well but without the risk of an individual outlying measurement compromising the analysis.
All following parts of the research use the refined 24 EMA leg reaction time series, instead of the original measurements.

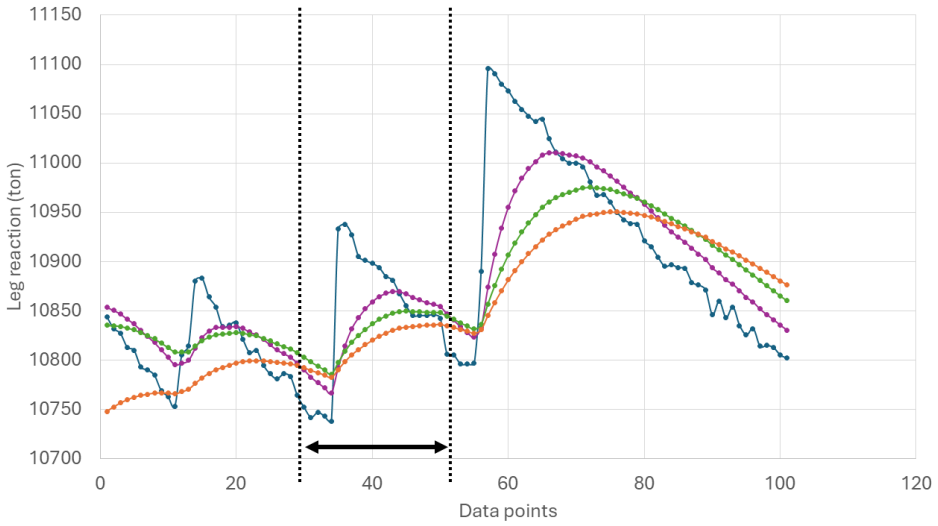

Figure 4.2: Leg reaction EMA's of length 12, 24 and 36

Filtering

Once the needed data is gathered and refined, it is filtered to exclude jacking operations with bad or inaccurate data; which could otherwise compromise the analysis as well. Bad measurement data in one of the parameters of interest can occur due to different reasons, like the malfunctioning of a measuring instrument or software errors leading to the disappearance of data. Luckily, the gathered data is overall of good quality, and only a few jacking operations are excluded; which are mentioned in chapter 6.
A jacking operation is filtered out if one of the following criteria is met:

- one of the four leg reactions has a maximum load of less than 2000 ton
- the crane load is never larger than fifty ton and the crane slewing angle does not increase more than five degrees

Although the limits in these criteria are relatively mild, they filter out very accurately because bad measurements are very obvious. For instance, an operation with a measurement error in the crane load will often result in empty data cells for the crane load.

4.1.2. Leg reactions

Actual leg reactions

From the processed data, the maximum leg reactions during preloading and lifting operations are determined for each of the four legs for each viable jacking location. To model this in Python, a clear distinction should be made in the data between the preloading phase and the operation phase. Since every jacking operation is of different duration and preloading does not always start and end at the same point in the time series, the distinction can not be time-based. For this reason the obtained crane load and crane slewing angle are used. Only one of these two parameters is enough for the analysis, but for some locations one or the other was not correctly presented in the measurement sheets. This is why for both parameters a method is created to split the leg reactions into the desired phases.

Heavy crane lifting operations will not take place if the complete preloading phase is not done yet. Therefore the data can be split into a preloading and operational phase, based on when the crane load starts to be large for the first time. By observing multiple operations, the limit to identify a heavier crane operation is set at fifty ton. This still leaves some room for minor crane operations, which might sometimes take place while the preloading phase is still coming to an end.
An example of this method is presented in figure 4.3, where one of the four leg reactions of a certain operation is shown in blue and the corresponding crane load in purple. The point where the crane load is larger than 50 ton for the first time is marked by the dotted line. Indicating the preloading phase and some minor operational activities on the left and the heavy lifting operations on the right. In both these phases the maximum leg reaction is then obtained for each leg. The maximum leg reaction in the first phase is the preload, and the maximum leg reaction in the second phase is the maximum operational leg reaction. These are marked in orange and green respectively in figure 4.3 for that jacking leg.

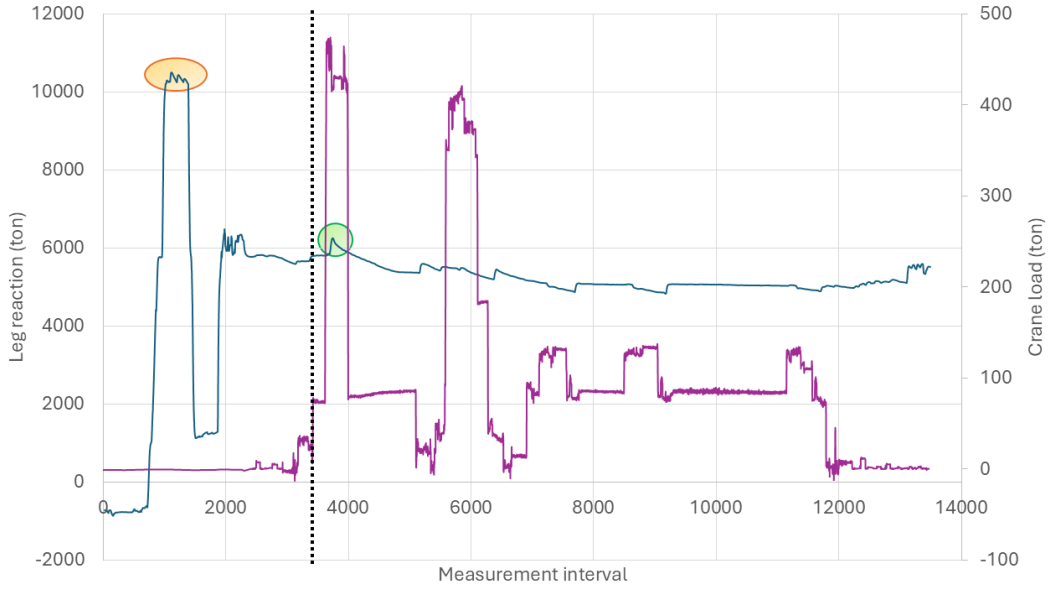

Figure 4.3: Leg reaction phases based on crane load

If the crane load is never larger than 50 ton, it is considered unsuitable and the second method is used, based on the slewing angle of the crane. This method works very similar as the first one and is based on the idea that when a wind turbine component is installed, the slewing angle of the crane can not be the same as it was in resting position; since the installation happens next to the vessel. Therefore, the first time when the slewing angle of the crane is different than its starting angle for 400 consecutive data points, a large lifting operation is about to take place and the preload phase should be finished. The limit of 400 data points is validated with multiple jacking operations and equals a time frame of 80 minutes after the first change in the slewing angle.
An example of this method can be seen in figure 4.4, which is the same jacking operation as for the previous method in figure 4.3. In this figure, the leg reaction is again shown in blue and the slewing angle is shown in red. As can be seen, the measurement of the slewing angle sometimes jumps between 360 degrees and 0 degrees; which does not interrupt the analysis. The 400 data points where the slewing angle is different than its starting angle are marked in grey, and the last point is marked by a dotted line which indicates the start of the operational phase. This method then also obtains the maximum leg reaction in both phases for each leg. These are shown in orange and green in figure 4.4, marking the preload and maximum operational leg reaction respectively.

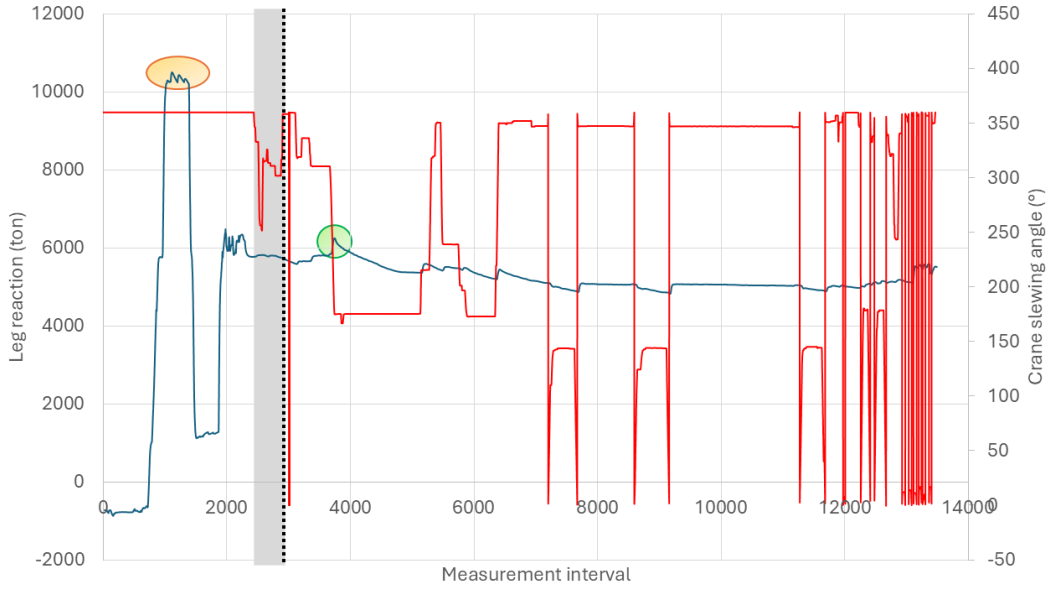

Figure 4.4: Leg reaction phases based on crane slewing angle

For this particular jacking operation shown in figure 4.3 and figure 4.4, both parameters are viable and therefore the first method is used to distinguish both phases. Although both methods do not mark the phase change at the exact same data point they do deliver the same outcome.

After the actual preload and actual (maximum) operational leg reaction of each leg is determined with one of these methods. Both values of the leg with the highest actual operational leg reaction are selected since this is the critical point of the operation. Which is done for each location and repeated for each wind farm site. For each site, an output sheet is then generated containing the actual operational leg reaction for the heaviest loaded leg and the corresponding actual applied preload of that leg, for each jacking location.

Estimated leg reactions

In order to complete the required data for the first research sub-question, the prescribed preload and operational leg reaction as estimated in the SSA should be acquired as well, for each location at each site.
As discussed in section 3.1, the heavy lifting operation assessment considers both operational environ-

mental loads and the loads caused by lifting and installing the heaviest wind turbine component. When a component is moved by the crane, the centre of gravity of the vessel will shift, resulting in an unequal distribution of the loads over the legs [35]. The assessment will analyse the point in the lifting operation where the maximum leg reaction occurs in one of the legs at the footings. Which is done for both the heavy hull condition and the light hull condition.
For each loading condition at each soil category, the required preload at the footing has then been optimised by maximising the preload and foundation bearing capacity checks based on ISO 19905-1 as discussed in section 2.2.

Both parameters are obtained from the SSA's and converted to the respective values at hull level, since the measured data is also obtained at hull level. This is done by excluding the buoyant leg and spudcan weight from the values at the footing, as seen in equation (4.2). In this equation F_{hull} represents the leg reaction hull level in tons, F_{foot} the reaction at the footing level, $B_{legs,spudcan}$ the buoyancy of the submerged leg and spudcan and W_{leg} the weight of the leg equal to 1276 ton. If the sum of the leg penetration p and the water depth d is larger than 7.975 meters the buoyancy can be obtained by equation (4.3) [24]. In this equation, the buoyancy of the spudcan and the lowest part of the leg is estimated at 344.4 ton by Jan De Nul, and the 15.54 equals the amount of buoyancy in ton per meter submerged leg. The leg penetration and water depth are both found in the SSA's.

$$F_{hull} = F_{foot} + B_{leg,spudcan} - W_{leg} \tag{4.2}$$

$$B_{legs,spudcan} = 344.4 + (p + d - 7.975) \cdot 15.54 \qquad \text{for } p + d > 7.975 \tag{4.3}$$

Categorizing
When leg reactions are compared, as per the first research sub-question, a distinction should be made between jacking operations in low-risk soil and high-risk soil. Because in high-risk soils, more preload is often applied relative to the operational loads than in low-risk soils. Which might be done to provoke rapid leg settlements or punch-through in a controlled manner during preloading [28].
For each location, the risk category is determined based on the soil profiles from the SSA's as described in section 3.1. For Kriegers Flak, the locations with a category 1 soil profile are labelled as low-risk, and the locations with a category 2 or 3 soil profile are labelled as high-risk. At Saint Nazaire, the pre-cut seabed locations are considered low-risk, and the channel deposit locations as high-risk. At Vesterhav, all locations are considered low-risk profiles apart from a few exceptions.

The acquired and processed data can be summarized as follows. For each of the three offshore wind farm sites, the jacking locations are categorized into low-risk or high-risk locations, totalling 6 different scenarios. For each location, four maximum leg reactions are obtained: the estimated operational leg reaction, the prescribed preload, the actual measured operational leg reaction, and the actual applied preload.

4.2. Reliability study

The processed data is further analysed through a reliability study, aimed at addressing the first and second research sub-questions. This is achieved using a Monte Carlo Simulation, which utilizes the defined leg reaction distributions and the established limit states to assess the probability of preload exceedance for each scenario of the case study.

4.2.1. Distributions

In order to answer the first research sub-question, two ratios are calculated for each location: actual operational leg reaction versus estimated operational leg reaction, and actual applied preload versus estimated preload. These ratios show how well the actual conditions are estimated and should ideally be close to one. However, it is to be expected that actual load conditions of complex jack-up operations are difficult to estimate precisely and that these ratios could therefore likely deviate slightly from one.
In addition, a third ratio is calculated for each location as well, namely the utilization, which is the actual operational leg reaction versus the actual applied preload. As discussed in section 4.1 both of

these parameters are obtained at their maximum value during the operation in the heaviest loaded leg. Therefore, this utilization quantifies the critical point in the operation where the experienced leg reaction got the closest to the applied preload, which will later on be used for the second research sub-question.

For a proper analysis, a histogram is made for each ratio containing the obtained values of each location for each of the six scenarios. These histograms show the frequency of the assessed ratios for each determined bin; which is a range of values into which the data points are grouped. These frequencies are then converted into probabilities by dividing them by the total amount of data points. The histograms then display how the probabilities are distributed, indicating the likelihood that the assessed ratio falls within each specific bin, as seen in figure 4.5.
The bin width affects the appearance of the histogram; if it is too large, it oversimplifies the data, and if it is too small it can make the histogram over-detailed. A bin size of 0.02 was found to give the desired level of detail for the analysis of the data.

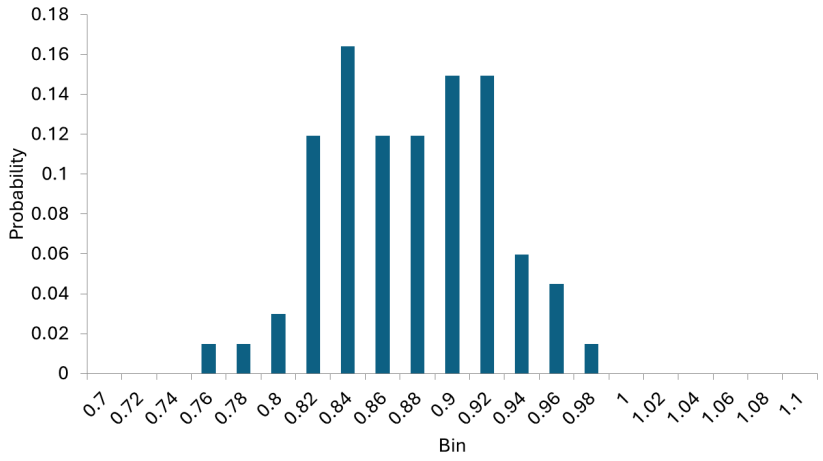

Figure 4.5: Example histogram

In some histograms, an outlier was observed; in which case the original measurement sheet for the corresponding location was consulted to find an explanation for this behaviour. Every outlier originates from a faulty measurement of the leg reactions during preloading. Which could remain undetected by the earlier filtering process, because after the preloading phase the leg reactions are measured correctly. An example of such a faulty measurement is shown in figure 4.6. In total, three such outliers are observed and their corresponding locations are excluded from the data.

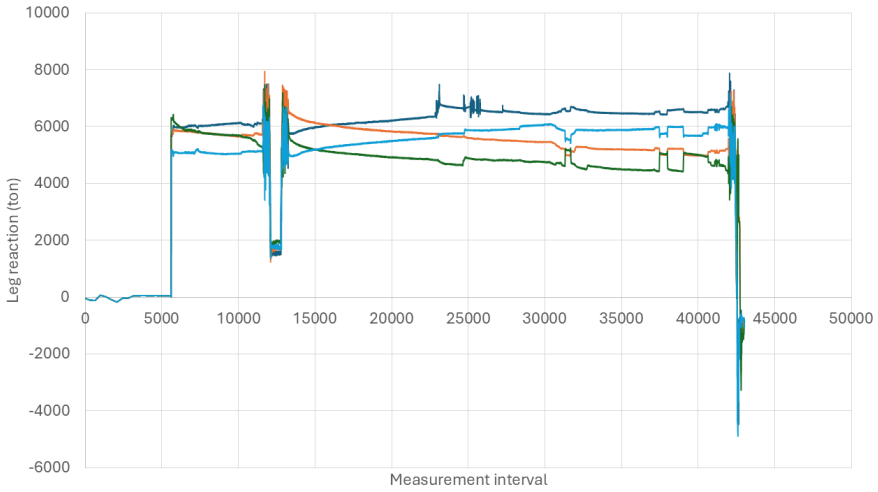

Figure 4.6: Faulty leg reaction measurements

The distribution of the actual operational leg reaction versus the estimated operational leg reaction represents the operational uncertainty $M_{operation}$, quantified by its standard deviation. In the same way, the distribution of the actual applied preload versus estimated preload illustrates the preload uncertainty $M_{preload}$ by its standard deviation. Because both these distributions do not have a mean value of one with a very small standard deviation, it can be concluded that the actual leg reactions during the operations and preload do not correspond with the estimated values from the SSA.

Lastly, the third distribution gives an indication of the applied preload conservatism. Its mean value represents how much of the preload was needed on average to support the maximum operational loads for the assessed scenario. The closer this value is to zero the more conservative the preload is, and the opposite is true the closer it is to one. But, in order to have a proper framework to answer the first research question, the preload conservatism should mainly be analysed at the extreme of the distributions and not so much at its average.

4.2.2. Limit state function

To further answer the first research question, a method should be designed which can quantify the conservatism at the upper limit of the maximum operational leg reaction versus the applied preload distribution.
Stochastic methods are ideal for analysing these extremes, because of their ability to model the randomness of rare events effectively. In contrast to deterministic approaches, they can also be used to simulate the likelihood of extreme events playing out over many jacking operations, by focusing on the tail behaviour of the distributions, which helps to capture the extreme outcomes of smaller datasets. In addition, these methods are flexible enough to deal with distributions where the extreme values deviate significantly from their mean; which can be the case for non-Gaussian distributions [38].
Developing such a stochastic or reliability method will help in answering the second research subquestion.

A reliability analysis will evaluate the probability of a failure by assessing if a certain limit state is exceeded. An actual failure event during a jacking operation would lead to severe rapid leg settlements, which could cause a structural collapse of the vessel. Such a scenario should be analysed at the soil level beneath the spudcans; by performing foundation capacity and sliding checks with non-linear springs as mentioned in the foundation integrity assessment in section 2.2. Since the available data does not contain the response of the bearing capacity of the soil to the applied loads, failure will be determined by the preload check.
As discussed in more detail in section 2.2, the preload check can be applied if the horizontal load on the leg is no greater than the limiting horizontal capacity of the bearing capacity envelope for the assessed soil type and embedment. Since only the operational conditions will be assessed, during which the horizontal loads from environmental loads will be relatively small compared to storm conditions [24], it is assumed that this condition is met.

The general preload check states that for a pinned support, the maximum gross vertical force $F_{V\,spudcan}$ acting on the soil beneath the spudcan due to the assessment load case should comply with the limits presented in equation (4.4). Because the obtained leg reactions are at the hull level instead of the spudcan level, the buoyancy of the soil below the spudcan B_S can be excluded from the equation as well as the weight of the backflow and infill $W_{BF,o}$. The preload check can therefore be adjusted and reformatted as seen in equation (4.5), with F_V the vertical maximum operational leg reaction and V_L the applied vertical preload, both at hull level. The preload resistance factor or safety factor is represented by $\gamma_{R,PRE}$, which is the inverse of the utilization U, per the definition in section 2.2. A failure can therefore be described by a situation where the actual maximum operational leg reaction would exceed the actual applied preload.
Because this is the first and most conservative integrity check the foundation should definitely be acceptable if the limits are not exceeded.

$$F_{V\,spudcan} \leq \frac{V_{Lo}}{\gamma_{R,PRE}} + W_{BF,o} - B_S \tag{4.4}$$

$$U = \frac{1}{\gamma_{R,PRE}} = \frac{F_V}{V_L} \tag{4.5}$$

For each of the scenarios from the case study, the utilization can be represented by the distribution of the actual operational leg reaction versus the actual applied preload; which is defined in the previous section. The reliability method then describes the limit state by a limit state function, which uses random variables from the actual utilization distributions as input. The limit state in this case is the preload check, and its limit state function is formulated as in equation (4.6). If a random variable from the assessed distribution leads to g being equal to or smaller than zero, a failure will occur.

$$g = 1 - U_{actual} \tag{4.6}$$

The second research sub-question asks to consider both the estimated or theoretical utilization values and actual utilization values in the reliability assessment. The above-discussed limit state function can only be used to assess the actual utilization values. Simply using equation (4.7), where $U_{theoretical}$ is equal to the inverse of the used resistance factor in the SSA won't work. Because, if the limit is exceeded here, this does not result in the defined actual failure on an operational level, since the estimated values from the SSA and actual values from the measurement are not the same. Which is discussed in the previous section by the operational and preload uncertainties.

$$g = 1 - U_{theoretical} \tag{4.7}$$

Therefore, a second limit state function with $U_{theoretical}$ is derived from the first one, as seen in equation (4.8). Here, the theoretical utilization values are combined with the earlier defined distributions for operational uncertainty and preload uncertainty.
In this function, $U_{theoretical}$ can be a distribution if a different foundation safety factor was used for each location in the assessed scenario or simply a mean value if the same foundation safety factor was used for each location in the scenario.

$$\begin{aligned} g &= 1 - U_{actual} \\ &= 1 - \frac{F_{actual}}{V_{actual}} \\ &= 1 - \frac{F_{estimated} \cdot \dfrac{F_{actual}}{F_{estimated}}}{V_{estimated} \cdot \dfrac{V_{actual}}{V_{estimated}}} \\ &= 1 - U_{theoretical} \cdot \frac{M_{operation}}{M_{preload}} \end{aligned} \tag{4.8}$$

Since one of the limit state functions is derived from the other they will both provide the same results if the obtained data is applied. But, these two limit states make it possible to separately adjust the theoretical mean utilization and actual mean utilization; which will be used in chapter 5 to find an optimal value for both of them. The results of the actual limit state function are also used to validate the results of the theoretical limit state; which is the main point of interest.

4.2.3. Sampling

To analyse the obtained distributions for each scenario with the limit state functions a Monte Carlo Simulation (MCS) is developed using a Python model. This sampling method is used since it can effectively fill the gaps in the obtained data and scale it up to a much larger dataset for a more accurate analysis and is convenient to use. An MCS samples a random value from each distribution and puts them in the limit state function to calculate a value for g; this is then repeated many times to generate the full distribution of the limit state function as seen in figure 4.7.

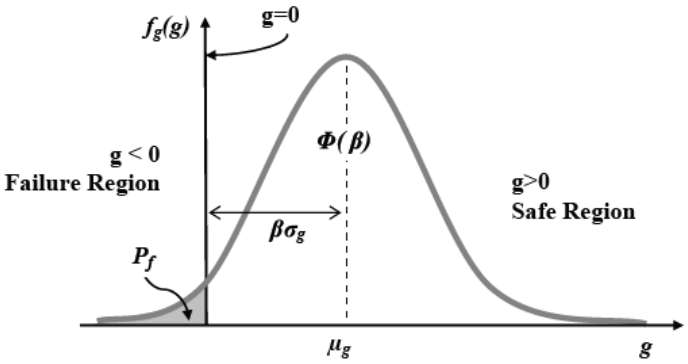

Figure 4.7: Probability Density for Limit state g(.) [5]

Although the dataset contains many jacking operations, it is still too small to effectively analyse the values at the extremes of the distributions. Therefore, each distribution obtained from the data is represented by a fitting probability density function (PDF). Which theoretically contains the values at the very extremes of the distribution as well. This function should represent the probability distribution from the data as well as possible. A PDF can be defined by three parameters: the type of distribution, the mean value, and the standard deviation. Failure rates are best described by a lognormal distribution [5]. By plotting a normal and a lognormal distribution over the distributions from the data, it is indeed observed that the lognormal distribution delivers the best fit at the extremes around one. This can be seen in figure 4.8 marked in purple, where the respective histograms of both distributions are shown alongside the histogram from the data. The complete data set behind each histogram is now represented by the mean and standard deviation of a single PDF, making it easier to calculate. The mean and standard deviation will be rounded up to three decimal places, which provides the same accuracy as the accuracy range of the measuring instruments on the vessel, as described in appendix A.

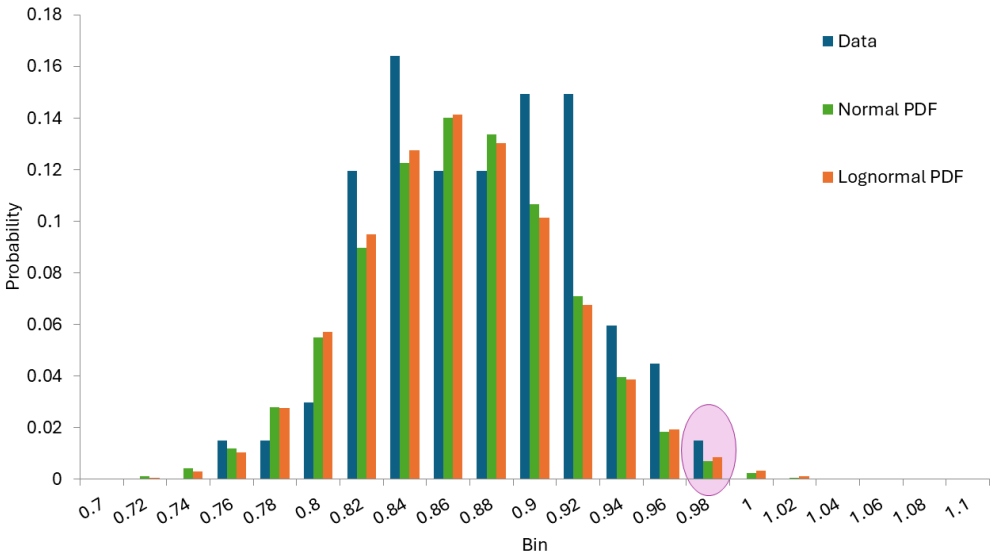

Figure 4.8: Comparing normal and lognormal distributions with original data

To use a lognormal function, the mean and standard deviation of the data distributions are transformed into lognormal parameters with equations equation (4.9), equation (4.10), and equation (4.11). In these equations, μ_X and σ_X are the mean and standard deviation of the data distribution and μ_Y and σ_Y the lognormal mean and lognormal standard deviation of the respective lognormal PDF. The PDF can be described by equation (4.12); which uses the lognormal parameters [5].

$$\phi = \sqrt{\mu_X^2 + \sigma_X^2} \tag{4.9}$$

$$\mu_Y = \ln \frac{\mu_X^2}{\phi} \tag{4.10}$$

$$\sigma_Y = \sqrt{\ln \frac{\phi^2}{\mu_X^2}} \tag{4.11}$$

$$f_X(x) = \frac{1}{\sqrt{2\pi} x \sigma_Y} \exp\left[-\frac{1}{2}\left(\frac{\ln x - \mu_Y}{\sigma_Y}\right)^2\right], 0 \leq x < \infty \tag{4.12}$$

Python then samples from the assessed distribution with the function np.random.lognormal(μ_Y, σ_Y, N). Which uses equation (4.12) to generate a PDF of the input parameters μ_Y and σ_Y as in figure 4.8, the amount of drawn samples is indicated by N.
The more samples are drawn the more accurately they will represent the PDF, especially at the tails, but the longer it will take for the Python code to run. 100 million samples are found to provide a good balance between accuracy and run time, this is further validated in the next section.

4.2.4. Annual probability of preload exceedance

When all samples are drawn from the assessed distributions and implemented in the limit state function a histogram is generated for the limit state function as in figure 4.9. Since both limit state functions are derived from one another they lead to an almost identical histogram of the limit state. Therefore, only the limit state function with the actual utilization is assessed to define the probability of failure for each original scenario, since it is the most simple one of the two. Later on, in chapter 5 both limit state functions are used to find an optimal value for both the actual and theoretical preload safety factor.

As per definition, all sampled values from the limit state function below or equal to zero are defined as failures. By zooming in on figure 4.9 around the failure region, a better understanding of the tail of

the distribution in the failure region is achieved as in figure 4.10.
The probability of failure of a single event $P_{f,event}$ is then obtained as the number of failures divided by the total amount of samples [5]. Where failure is in this case defined as preload exceedance, and a single event is a single jacking operation.

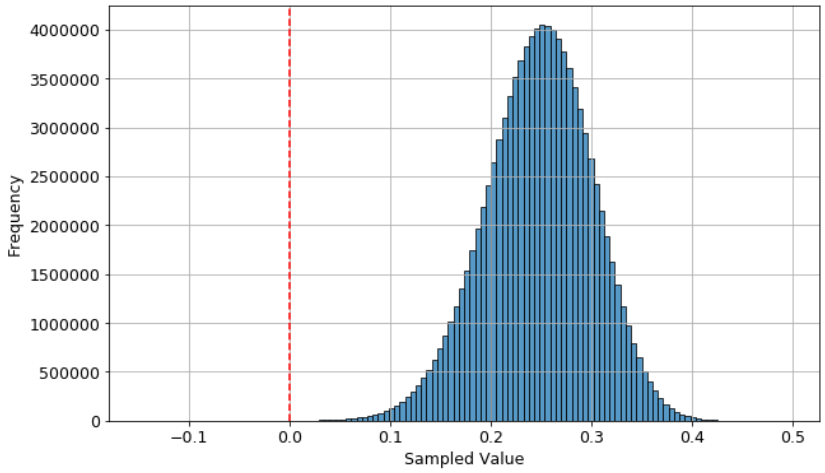

Figure 4.9: Example histogram of sampled limit state function

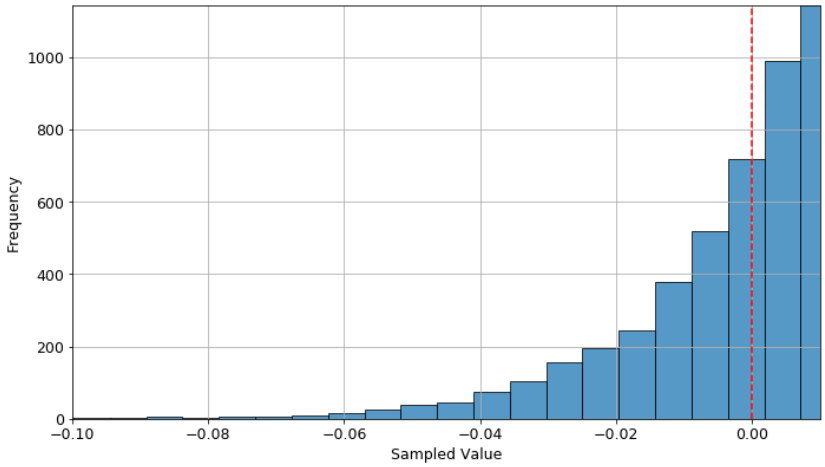

Figure 4.10: Detailed histogram at the tail

As discussed earlier, the total amount of samples for each MCS in this research is equal to 100 million samples, as it provides a good balance between the accuracy and run time of the simulation. To further confirm this, the convergence of the probability of failure ϵ is checked, which can be obtained as in equation (4.13) [5]. This equation calculates the rate of change of the probability of failure between the current and previous samples. When this rate of change is less than 0.001, the simulation has converged, meaning that increasing the number of samples will not provide much more accuracy to the obtained value for the probability of failure [5].

For the same example as the histograms the convergence of the probability of failure is checked after every million samples up to 200 million as presented in figure 4.11. From this example, it can be observed that the probability of failure converges around 100 million samples since ϵ ranges between 0.001 and -0.001, as shown by the green dotted lines.

$$\epsilon = \frac{P_{f,k} - P_{f,k-1}}{P_{f,k-1}} \tag{4.13}$$

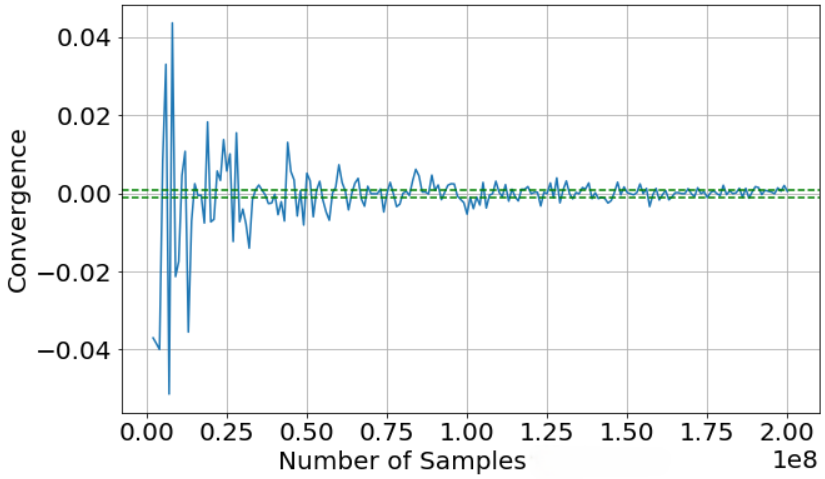

Figure 4.11: Convergence of probability of failure

The probability of failure, or probability of preload exceedance for this research, is commonly analysed at an annual level, as discussed in section 5.1. The obtained probability of preload exceedance for a single event at the assessed scenario can be extrapolated by equation (4.14) to get the annual probability of preload exceedance $P_{f,annual}$.
In consultation with Jan De Nul, an estimate of 100 jacking operations per year is determined. To calculate the annual probability of preload exceedance, it is assumed that 100 jacking operations are performed at each offshore wind farm site per year. The number of jacking operations associated with each risk profile at the site is then determined as in equation (4.15) by multiplying the total number of operations by r, the ratio of measured locations at a given risk profile to the total number of measured locations at that site. This accounts for the probability of encountering a certain risk profile.
For example, if in total 20 locations are measured at a site, with 15 classified as low-risk and 5 as high-risk, the ratio r for the low-risk profile would be 0.75. Which then results in a total of 75 events per year at low-risk profiles.

$$P_{f,annual} = 1 - (1 - P_{f,event})^{events/year} \tag{4.14}$$

$$\frac{\text{events}}{\text{year}} = \frac{\text{total jacking operations}}{\text{year}} \cdot r \tag{4.15}$$

The amount of risk of preload exceedance is now quantified by its annual probability, and different sites and risk profiles can therefore be compared to each other. To check its conservatism it should be compared to established targets for the annual probability of failure, which is done in the next chapter.

5

Optimal preload safety factor

This chapter will provide an approach to define targets for the annual probability of preload exceedance, based on the consequences of failure in section 5.1. By comparing these targets to the obtained reliability, the conservatism of past operations can be assessed; which should provide an answer to the third research sub-question. In section 5.2 a method is described to find the ideal actual preload safety factor and ideal theoretical preload safety factor leading to the target reliability; which should answer the second research question.

5.1. Target reliability

To fully answer the first research question, the conservatism of the obtained annual probabilities of preload exceedance is verified for each assessed scenario. This is done by comparing the obtained probabilities to a target probability, as per the third research sub-question.
As earlier discussed in section 2.4, reliability requirements can be derived from the consequences of the respective failure. Which can be categorized into consequence classes based on multiple socioeconomic aspects as earlier presented in table 2.2. The consequence of failure for each consequence class should be reflected by the appropriate target reliability level; which is expressed as the annual probability of failure.
This research uses a method based on monetary optimisation to establish a target reliability, which has been formulated by the International Organisation of Standardisation [11]. This gives a target annual probability of failure for each structural consequence class depending on the relative cost of the risk reduction measure; as seen in table 5.1.

Table 5.1: Tentative target reliabilities based on monetary optimization from [11]

Relative cost of safety measure	**Consequences of failure (classes from table 2.2)**		
	Class 2	**Class 3**	**Class 4**
Large	$\beta = 3.1\,(P_f \approx 10^{-3})$	$\beta = 3.3\,(P_f \approx 5 \times 10^{-4})$	$\beta = 3.7\,(P_f \approx 10^{-4})$
Medium	$\beta = 3.7\,(P_f \approx 10^{-4})$	$\beta = 4.2\,(P_f \approx 10^{-5})$	$\beta = 4.4\,(P_f \approx 5 \times 10^{-6})$
Small	$\beta = 4.2\,(P_f \approx 10^{-5})$	$\beta = 4.4\,(P_f \approx 5 \times 10^{-6})$	$\beta = 4.7\,(P_f \approx 10^{-6})$

In this research, already two different risk categories are identified for the soil profiles at the jacking locations. The consequences of preload exceedance in a high-risk soil, which is prone to punch-through, are higher than for a low-risk soil. Therefore both identified risk categories should fit in a different consequence class.
The description of expected consequences and example structures for each consequence class from section 2.4.1 do not exactly include a jack-up vessel. Therefore, the consequences for a worst-case scenario when preload exceedance occurs are used to identify the consequence class.

When preload is exceeded in a low-risk soil profile the leg will settle further into the soil until a new equilibrium is found between the applied loads and the bearing capacity under the spudcan [37]. Causing only insignificant material damages; which fits the description of consequence class 1. However, since many more people are present on the jack-up vessel compared to the example structures of consequence class 1, the consequence class is increased to class 2. The expected worst consequences for preload exceedance in low-risk soil will cause no societal impact, and the number of fatalities should definitely be fewer than five, which indeed fits the description of consequence class 2.
The worst-case scenario for a preload exceedance in a high-risk soil is severe punch-through. Where rapid leg settlements and severe additional leg penetration could cause structural failure of a jack-up leg. The consequences of such a failure and example structures fit the description of consequence class 3 or 4.

Other guidelines for offshore structures recommend an annual probability of failure target of 10^{-4} for scenarios prone to punch through [34]. This, in combination with the described consequences in high-risk soils, is equal to the result for a consequence class 4 with a relative large cost of safety measure in table 5.1. Using the same large relative cost of safety measure for low-risk soil profiles with a consequence class 2, leads to a target annual probability of preload exceedance of 10^{-3} for low-risk soil profiles. Both these targets are also approved by Jan De Nul.
The probability of preload exceedance for multiple years is shown in figure 5.1, based on both annual targets. For low-risk soils, the annual target will lead to a probability of failure of 0.0250 after 25 years. For high-risk soils, the probability of failure after 25 years is equal to 0.0025.

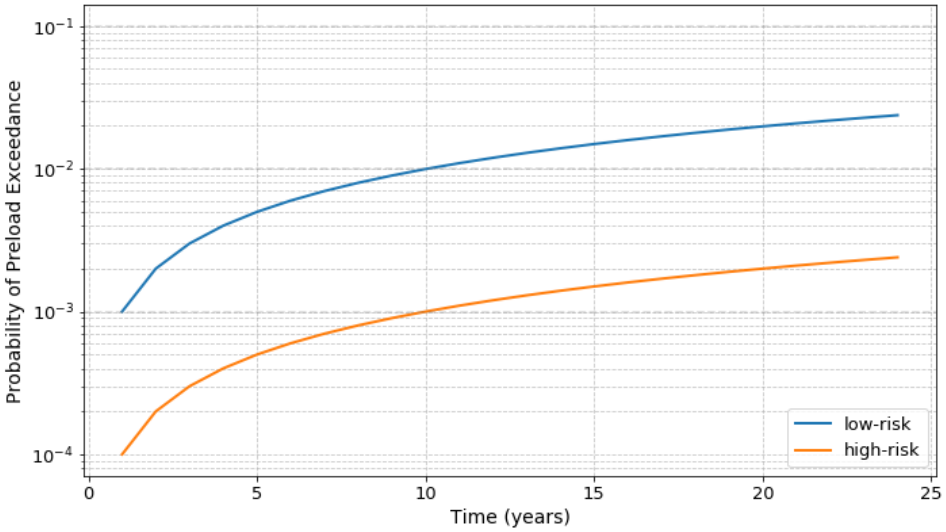

Figure 5.1: Probability of preload exceedance for different return periods

For each scenario from the case study, the obtained annual probability of preload exceedance from the MCS can therefore be compared to the appropriate target to assess its conservatism. Which completely answers the first research question.

5.2. Ideal safety factor

If an ideal target exists for the annual probability of preload exceedance, it would be interesting to know what the respective improved preload safety factor would be to achieve this target for operational conditions. This leads to the second research question.

Two different preload safety factors are of interest: the actual safety factor and the theoretical safety factor, which can be described by equation (5.1) and equation (5.2). Where U_{actual} and $U_{theoretical}$ are the utilization distributions obtained as in section 4.2.

The actual safety factor is the ratio between the applied preload and experienced leg reactions, that eventually lead to the experienced probability of preload exceedance. But, because estimated and applied values are not the same, the theoretical safety factor is defined as well. Which is the safety factor that can be applied to the estimated maximum operational leg loads and leads to the applied actual preload by applying the uncertainties for preload $M_{preload}$ and operation $M_{operation}$. It is the ideal theoretical safety factor that could ultimately be used as an alternative or improved version of the currently used operational preload safety factor in industry practices.

$$SF_{actual} = \frac{1}{U_{actual}} \tag{5.1}$$

$$SF_{theoretical} = \frac{1}{U_{theoretical}} \tag{5.2}$$

In the previous chapter, an annual probability of preload exceedance is calculated with a Monte Carlo Simulation for the assessed scenarios of the case study. Two different limit state functions could be used in this MCS; which would both lead to the same outcome as one is derived from the other. Both limit state functions are summarised here as well in equation (5.3) and equation (5.4), for clarity. Each of the variables in these functions represents their respective distribution, each of which is defined by its mean and standard deviation.

$$g = 1 - U_{actual} \tag{5.3}$$

$$g = 1 - U_{theoretical} \cdot \frac{M_{operation}}{M_{preload}} \tag{5.4}$$

By using the same MCS as before, for each limit state function, but as a function of the mean value for U instead. The annual probability of preload exceedance can be obtained for a range of mean U values and therefore of their corresponding safety factor, as shown in figure 5.2 and figure 5.3. The annual probability of preload exceedance on the y-axis is plotted on a logarithmic scale to better highlight the results for lower values and improve clarity in their representation. Apart from the mean U values, all other parameters are still defined as before for each scenario, since the obtained uncertainties from the data remain the same as before.

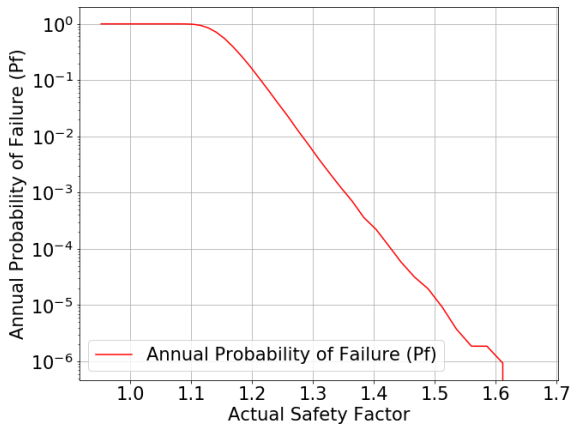

Figure 5.2: Example annual probability of preload exceedance as a function of actual safety factor

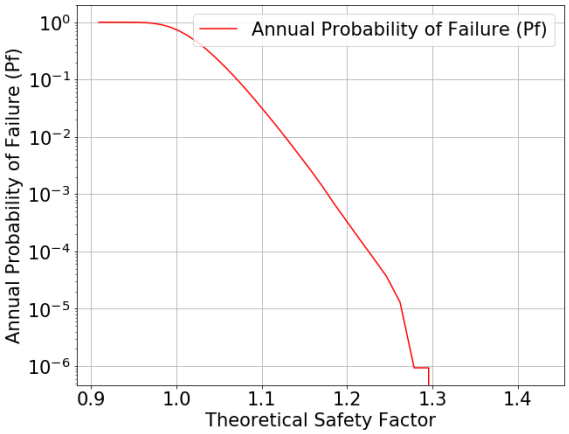

Figure 5.3: Example annual probability of preload exceedance as a function of theoretical safety factor

As the safety factor increases, it makes sense that the probability of preload exceedance decreases. In both figure 5.2 and figure 5.3 it can be seen that the plot gets unstable at very low probabilities of failure. This happens because for higher safety factors only the very end of the tail of the limit state functions gets in the failure zone, which can be slightly different for each simulation.

The ideal safety factor is then determined by interpolating the safety factor value that corresponds to the desired target annual probability of preload exceedance from section 5.1 on the obtained graph, as marked by the dotted lines in figure 5.4 and figure 5.5. This leads to an answer to the second research question.

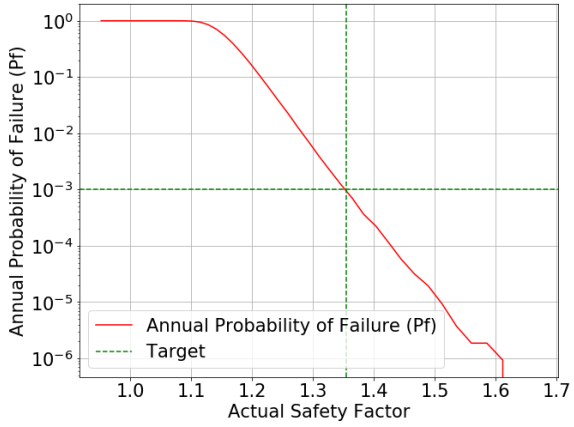

Figure 5.4: Example target annual probability of preload exceedance leading to the actual ideal safety factor

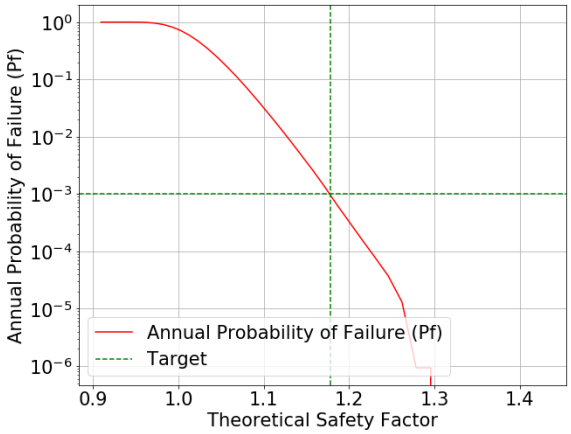

Figure 5.5: Example target annual probability of preload exceedance leading to the theoretical ideal safety factor

The fourth and last research sub-question can be answered by comparing the obtained ideal actual and theoretical preload safety factors with their respective applied values of past jacking operations, at each scenario. These values can be found by taking the mean of the distributions for U_{actual} and $U_{theoretical}$; and inserting these mean values into equation (5.1) and equation (5.2). This comparison indicates how the currently used preload safety factor from the industry guidelines might be improved for heavy crane operations.

6

Case study results

This chapter presents the results for each of the three assessed offshore wind farm sites from the case study. The three sites are treated separately in section 6.1, section 6.2, and section 6.3. For each site, the obtained results are presented for the main research phases; namely data processing, reliability study, and ideal preload safety factors. In section 6.4, the results are summarised with different comparisons. A comparison is made between the originally applied safety factors and the obtained ideal safety factors across all scenarios. In addition, the theoretical safety factor and actual safety factor from each scenario are compared to each other as well.
The execution of the research method might slightly differ for each site and is adjusted to their specific conditions and data.

6.1. Danish Kriegers Flak

On the Danish Kriegers Flak (DKF) a total of 72 wind turbines are installed by jacking operations. Of these, 22 locations have a low-risk soil profile, and 50 locations have a high-risk soil profile. Resulting in overall challenging ground conditions for jacking operations.

6.1.1. Data processing

The data processing of the acquired measurements is executed in two phases: firstly, the data gathering, refining and filtering, and then identifying and categorizing the maximum actual leg reactions and maximum estimated leg reactions. Section 4.1 offers a detailed explanation of the methods used for the data processing.

Data gathering, refining and filtering

After the needed data is gathered and refined the jacking operations containing bad or inaccurate data are filtered out. Of the available 72 jacking operations, 12 are filtered out. Therefore, 60 viable locations remained for the rest of the analysis.

An example of one of the excluded jacking operations can be seen in figure 6.1. This figure presents the smooth leg reactions of location DKF 75. As can be seen in the figure, the leg reactions are not measured correctly, all four leg reaction measurements remain the same and stay around zero ton for the main part of the measurements.

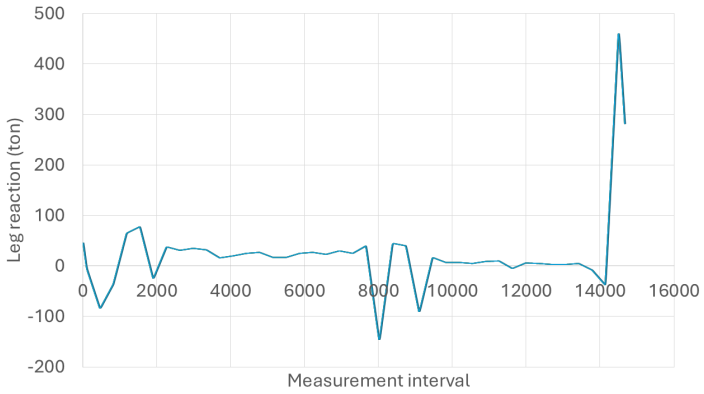

Figure 6.1: Leg reactions of DKF 75

Actual leg reactions

For the remaining jacking locations, the actual preload and actual (maximum) operational leg reaction of each leg is determined, based on the operational phases indicated by the crane load or crane slewing angle, as explained in section 4.1. Both values of the leg with the highest actual operational leg reaction are then selected for each location, as seen in table 6.1 for leg 3 for DKF 3. Resulting in the values for the actual operational leg reaction and the corresponding actual applied preload for each jacking location.

Table 6.1: Actual preload and actual (maximum) operational leg reaction of DKF 3

	Leg 1	Leg 2	**Leg 3**	Leg 4
Preload (ton)	11959	11553	**11336**	11623
Operational leg reaction (ton)	5913	6344	**7156**	6270

Estimated leg reactions

In the Site Specific Assessment for Kriegers Flak, a maximum operational leg reaction is estimated. Which calculates the leg loads in each leg caused by operational loads and environmental loads. For Kriegers Flak, the estimated maximum operational leg reaction at hull level is equal to 8613 ton for each jacking location.
From the estimated operational leg reaction and soil conditions, a preload was estimated for each location as well, based on ISO 19905-1. These estimated preloads at foot level are then converted to their respective values at hull level, as discussed in section 4.1 with equation (4.2) and equation (4.3). For all the assessed locations, the range of the prescribed preloads at hull level is summarized in table 6.2, for each soil category.

Table 6.2: Optimised preload ranges at Kriegers Flak from the SSA

	Category 1	**Category 2 and 3**
Optimised preload at footing (ton)	9623-10316	9745-12110
Optimised preload at hull level (ton)	9037-9600	9152-11468

Categorizing

A distinction is then made between jacking operations in low-risk soil and high-risk soil. For each location, the risk category is determined based on the soil profiles from the SSA's as described in section 3.1. For Kriegers Flak, the locations with a category 1 soil profile are labelled as low-risk, and the locations with a category 2 or 3 soil profile are labelled as high-risk.
Of the viable jacking operations at Kriegers Flak 18 are categorized as low-risk and 42 as high-risk.

6.1.2. Reliability study

This section presents the results of the preload reliability study for both soil risk profiles; which is analysed in two phases. First, the distributions for preload uncertainty, operational uncertainty, and actual utilization are derived from the measured and estimated preloads, as well as the measured and estimated operational leg reactions. Next, the annual probability of preload exceedance is calculated using a Monte Carlo Simulation by implementing the obtained distributions into the defined limit state function. Which is compared to a target annual probability of failure to assess its conservatism.
Detailed descriptions of these methods and their reasoning are provided in section 4.2 and the defined target probabilities in section 5.1.

Leg reaction distributions

For both the low-risk and high-risk categories at Kriegers Flak, three probability distributions are obtained from the leg reactions at each location: the operational uncertainty $M_{operation}$, preload uncertainty $M_{preload}$ and actual utilization U_{actual}.
At the high-risk locations, one outlier was observed in the distributions. Since this outlier is caused by a faulty measurement, the jacking operation is excluded from the distributions, as explained in section 4.2. This leaves a total of 41 high-risk locations and still 18 low-risk locations where no outliers are observed.
Each probability distribution is then fitted with a corresponding lognormal probability density function as described in section 4.2 and presented in figure 6.2, figure 6.3, and figure 6.4 for the low-risk category and in figure 6.5, figure 6.6, and figure 6.7 for the high-risk category.
The preload uncertainty distribution for Kriegers Flak high-risk needed a modified PDF to better represent the probability distribution. As can be seen in figure 6.6, the distribution clearly shows two peaks. Just plotting a lognormal PDF based on the mean value and standard deviation of the distribution would result in the PDF shown in green; which does not represent the data correctly. Therefore, a modified lognormal PDF was determined by combining the two PDF's for both peaks in the distribution, which results in the PDF shown in orange. The combined PDF is obtained with equation (6.1), as the weighted sum of both distributions [5]. The weights w_X and w_Y represent the ratio of the samples in each separate distribution over the total amount of samples.

$$f_{XY}(x) = f_X(x) \cdot w_X + f_Y(x) \cdot w_Y \tag{6.1}$$

The mean and standard deviation of the obtained lognormal PDF's are summarized in table 6.3 and table 6.4 for Kriegers Flak low-risk and Kriegers Flak high-risk respectively. Not the same theoretical utilization was used for each location in the SSA; which results in a lognormal distribution for this parameter as well. The mean and standard deviation of $U_{theoretical}$ are therefore also included in the mentioned tables.

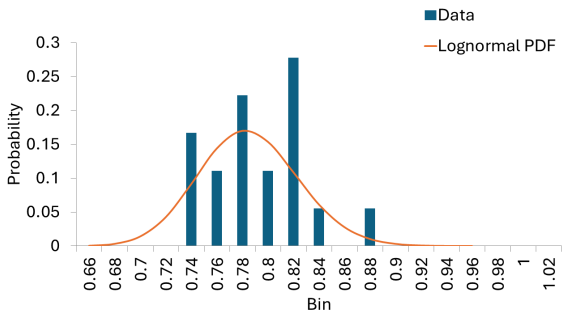

Figure 6.2: Data probability distribution of $M_{operation}$ and corresponding lognormal probability density function for DKF low-risk

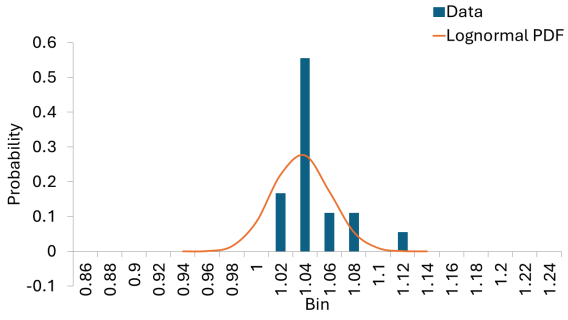

Figure 6.3: Data probability distribution of $M_{preload}$ and corresponding lognormal probability density function for DKF low-risk

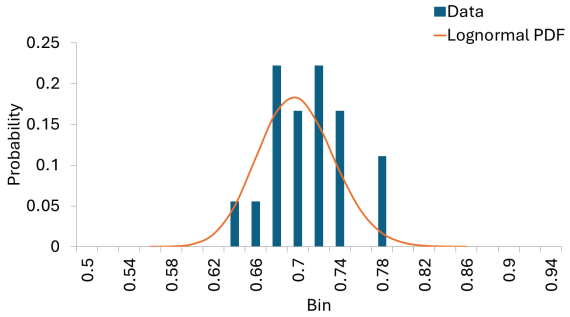

Figure 6.4: Data probability distribution of U_{actual} and corresponding lognormal probability density function for DKF low-risk

Table 6.3: Distributions parameter summary for DKF low-risk

	μ	σ
$M_{operation}$	0.785	0.039
$M_{preload}$	1.037	0.024
U_{actual}	0.699	0.036
$U_{theoretical}$	0.923	0.012

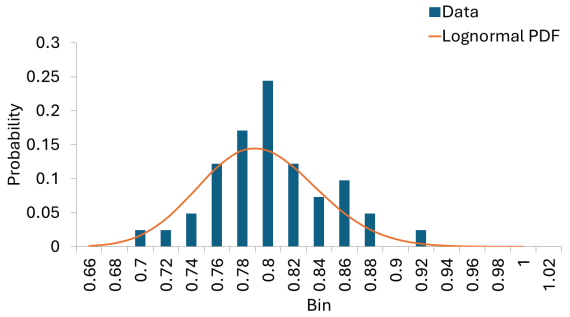

Figure 6.5: Data probability distribution of $M_{operation}$ and corresponding lognormal probability density function for DKF high-risk

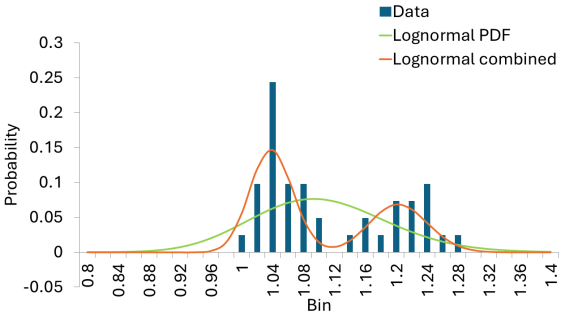

Figure 6.6: Data probability distribution of $M_{preload}$ and corresponding single lognormal and combined lognormal probability density function for DKF high-risk

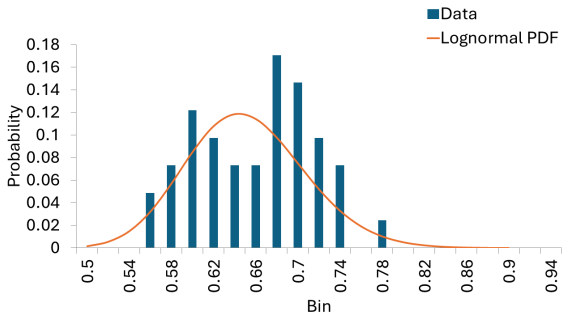

Figure 6.7: Data probability distribution of U_{actual} and corresponding lognormal probability density function for DKF high-risk

Table 6.4: Distributions parameter summary for DKF high-risk

	μ	σ
$M_{operation}$	0.794	0.046
$M_{preload}$	1.103	0.087
U_{actual}	0.651	0.057
$U_{theoretical}$	0.901	0.038

Annual probability of preload exceedance

The 100 million sampled values of U_{actual} from the Monte Carlo Simulation are then inserted in the corresponding limit state function to obtain the histogram of the limit state function. The histogram of the sampled limit state function around the failure zone for Kriegers Flak low-risk and high-risk are presented in figure 6.8 and figure 6.9 respectively. From the number of samples in the failure region a probability of failure is determined and converted to an annual probability of actual preload exceedance as explained in section 4.2.

For the low-risk profiles, an annual probability of preload exceedance of 0.000000 is obtained. As can be observed in figure 6.8, the limit state function does indeed not enter the failure zone by quite some margin. This indicates that the applied preload safety factor is too conservative, and can be lowered to meet the target probability of failure.

The high-risk profiles barely enter the failure zone, as seen in figure 6.9. Leading to an annual proba-

bility of preload exceedance of 0.000017; which is also lower than the defined targets.

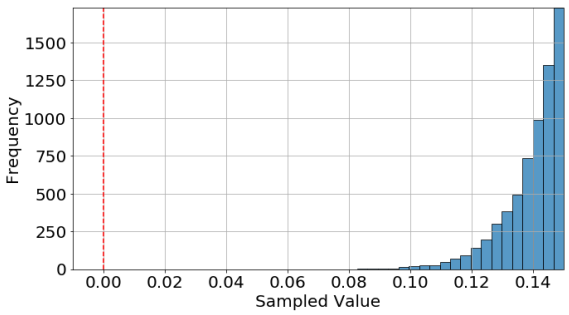

Figure 6.8: Detailed histogram at the failure zone of the sampled limit state function for DKF low-risk

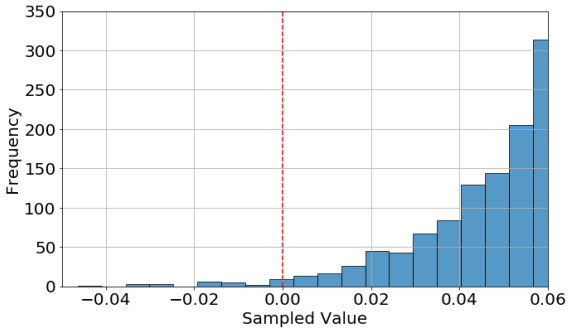

Figure 6.9: Detailed histogram at the failure zone of the sampled limit state function for DKF high-risk

6.1.3. Ideal preload safety factors

Since a target annual probability of failure is defined in section 5.1, an ideal preload safety factor can be obtained which leads to this target reliability. This is done for two preload safety factors, namely the theoretical safety factor and the actual safety factor. The theoretical preload safety factor represents the ratio of the prescribed preload versus the estimated maximum operational leg reaction, and the actual preload safety factor represents the ratio of the applied preload versus the experienced maximum operational leg reaction. A comprehensive explanation of the methods used to obtain both ideal safety factors is given in section 5.2.

The annual probability of preload exceedance for a range of actual and theoretical safety factors is presented in figure 6.10 and figure 6.11 respectively for Kriegers Flak low-risk. By applying the target annual probability of failure for low-risk soils of 0.001, an ideal value for both preload safety factors is obtained. For Kriegers Flak low-risk, an ideal actual preload safety factor would be 1.186, and an ideal theoretical preload safety factor would be 0.946.

For Kriegers Flak high-risk the annual probability of preload exceedance for a range of actual and theoretical safety factors is shown in figure 6.12 and figure 6.13. By applying the target annual probability of failure for high-risk soils of 0.0001, an ideal value for both preload safety factors is obtained. For Kriegers Flak high-risk, an ideal actual preload safety factor would be 1.481, and an ideal theoretical preload safety factor would be 1.081.

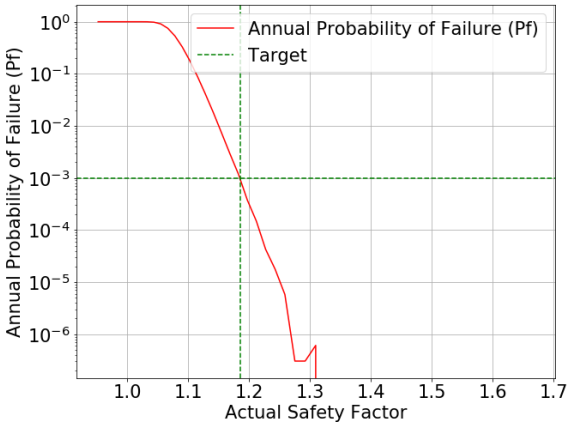

Figure 6.10: Annual probability of preload exceedance as a function of actual safety factor. With the target annual probability of preload exceedance leading to the actual ideal safety factor. For Kriegers Flak low-risk soil.

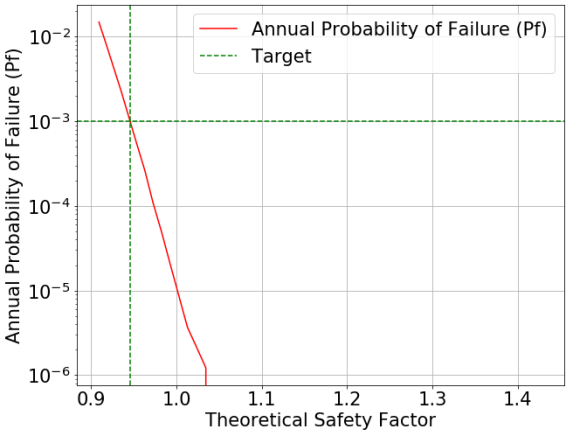

Figure 6.11: Annual probability of preload exceedance as a function of theoretical safety factor. With the target annual probability of preload exceedance leading to the theoretical ideal safety factor. For Kriegers Flak low-risk soil.

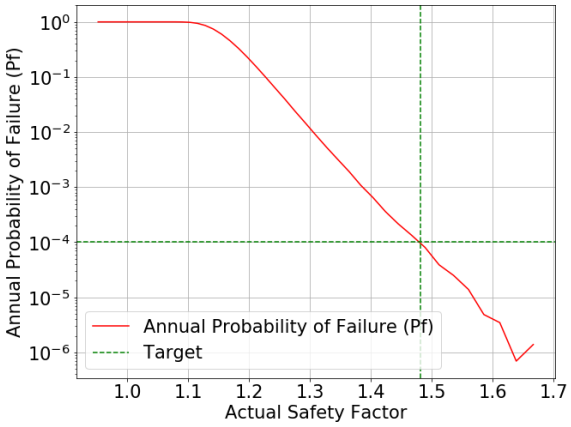

Figure 6.12: Annual probability of preload exceedance as a function of actual safety factor. With the target annual probability of preload exceedance leading to the actual ideal safety factor. For Kriegers Flak high-risk soil.

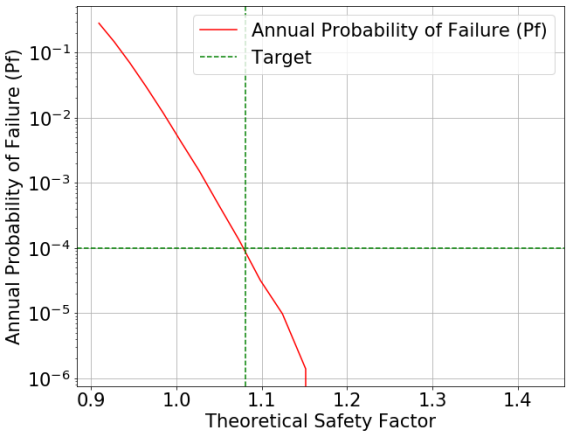

Figure 6.13: Annual probability of preload exceedance as a function of theoretical safety factor. With the target annual probability of preload exceedance leading to the theoretical ideal safety factor. For Kriegers Flak high-risk soil.

6.2. Saint Nazaire

The Saint Nazaire offshore wind farm site is located in the Bay of Biscay and contains 80 installed wind turbines. The soil of 75 locations is pre-cut to create a gravel bed; which results in a low-risk soil profile. The other five locations comprise of dense sand overlaying clay, which is categorized as a high-risk soil.

6.2.1. Data processing

The data processing of the acquired measurements is executed in two phases: firstly, the data gathering, refining and filtering, and then identifying and categorizing the maximum actual leg reactions and maximum estimated leg reactions. Section 4.1 offers a detailed explanation of the methods used for the data processing.

Data gathering, refining and filtering

After the needed data is gathered and refined the jacking operations containing bad or inaccurate data are filtered out. Of the available 80 jacking operations, eight are filtered out. Therefore, 72 viable locations remained for the rest of the analysis.

An example of one of the excluded jacking operations can be seen in figure 6.14. This figure presents the crane slewing angle of location Saint Nazaire 18. Although the leg reactions are measured correctly, no crane load was measured, and for the first 3700 measurements no crane slewing angle was measured as well, as can be seen in the figure. Due to the lack of a viable crane load or crane slewing angle, the phases in the leg reactions for this operation could not be analysed. Hence, this jacking operation is excluded.

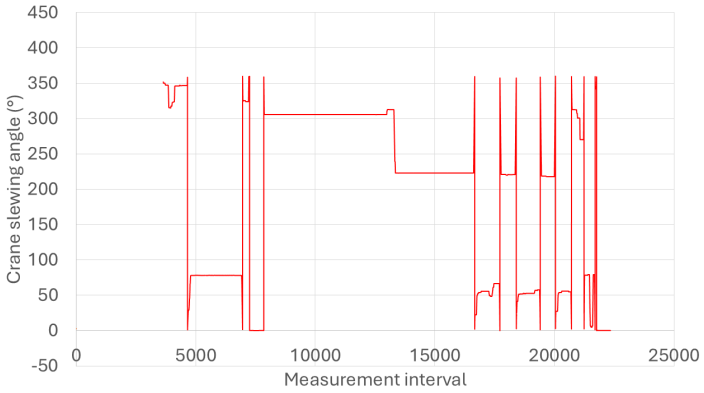

Figure 6.14: Crane slewing angle of Saint Nazaire 18

Actual leg reactions

For the remaining jacking locations, the actual preload and actual (maximum) operational leg reaction of each leg is determined based on the operational phases indicated by the crane load or crane slewing angle, as explained in section 4.1. Both values of the leg with the highest actual operational leg reaction are then selected for each location, as seen in table 6.5 for leg 3 for Saint Nazaire 1. Resulting in the values for the actual operational leg reaction and the corresponding actual applied preload for each jacking location.

Table 6.5: Actual preload and actual (maximum) operational leg reaction of Saint Nazaire 1

	Leg 1	Leg 2	**Leg 3**	Leg 4
Preload (ton)	9212	8763	**8757**	8829
Operational leg reaction (ton)	6393	5536	**6555**	5657

Estimated leg reactions

In the Site Specific Assessment for Saint Nazaire, a maximum operational leg reaction is estimated. Which calculates the leg loads in each leg caused by operational loads and environmental loads. For Saint Nazaire, the estimated maximum operational leg reaction at hull level is equal to 7845 ton for the pre-cut seabed locations and 7787 ton for the locations with channel deposits.
From the estimated operational leg reaction and soil conditions, a preload was estimated for each location as well, based on ISO 19905-1. The prescribed preload at hull level at pre-cut seabed locations and locations with channel deposits are summarized in table 6.6.

Table 6.6: Optimised preloads at Saint Nazaire from the SSA

	Pre-cut seabed	**Channel deposit**
Optimised preload at footing (ton)	9388	9509
Optimised preload at hull level (ton)	8794	9159

Categorizing

A distinction is then made between jacking operations in low-risk and high-risk soil. For each location, the risk category is determined based on the soil profiles from the SSA's as described in section 3.1. For Saint Nazaire, the locations with a pre-cut seabed are labelled as low-risk, and the locations with channel deposits are labelled as high-risk.

Of the viable jacking operations at Saint Nazaire, 67 are categorized as low-risk and five as high-risk.

6.2.2. Reliability study

This section presents the results of the preload reliability study for the low-risk soil profiles, which are analysed in two phases. First, the distributions for preload uncertainty, operational uncertainty, and actual utilization are derived from the measured and estimated preloads, as well as the measured and estimated operational leg reactions. Next, the annual probability of preload exceedance is calculated using a Monte Carlo Simulation, by implementing the obtained distributions into the defined limit state function. Which is compared to a target annual probability of failure to assess its conservatism.
Detailed descriptions of these methods and the reasoning behind them are provided in section 4.2 and the defined target probabilities in section 5.1.

Leg reaction distributions

For both the low-risk and high-risk categories at Saint Nazaire, three probability distributions are obtained from the leg reactions at each location: the operational uncertainty $M_{operation}$, preload uncertainty $M_{preload}$ and actual utilization U_{actual}.
At the low-risk locations, one outlier was observed in the distributions. Since this outlier is caused by a faulty measurement the jacking operation is excluded from the distributions, as explained in section 4.2. This leaves a total of 66 low-risk locations and still 5 high-risk locations where no outliers are observed. Each probability distribution is then fitted with a corresponding lognormal probability density function as described in section 4.2 and presented in figure 6.15, figure 6.16, and figure 6.17 for the low-risk category and in figure 6.18, figure 6.19, and figure 6.20 for the high-risk category.

Since the high-risk category is only represented by five locations, an analysis of this category will not be further executed as the available data is insufficient. This can also clearly be seen in the obtained PDF's.

The mean and standard deviation of the obtained lognormal PDF's are summarized in table 6.7 and table 6.7 for Saint Nazaire low-risk and Saint Nazaire high-risk respectively. This table includes the mean value for the used theoretical utilization as well, with a standard deviation of zero because the same value is used for each operation in the SSA.

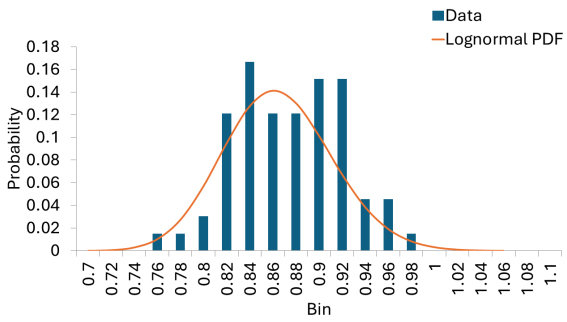

Figure 6.15: Data probability distribution of $M_{operation}$ and corresponding lognormal probability density function for Saint Nazaire low-risk

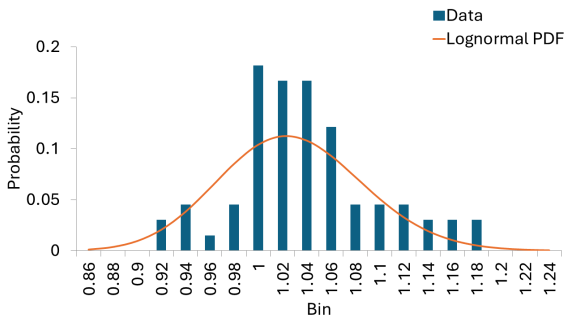

Figure 6.16: Data probability distribution of $M_{preload}$ and corresponding lognormal probability density function for Saint Nazaire low-risk

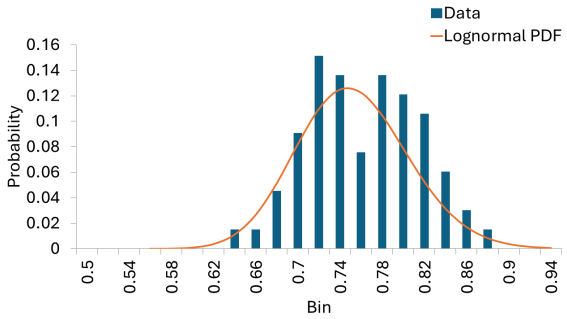

Figure 6.17: Data probability distribution of U_{actual} and corresponding lognormal probability density function for Saint Nazaire low-risk

Table 6.7: Distributions parameter summary for Saint Nazaire low-risk

	μ	σ
$M_{operation}$	0.865	0.047
$M_{preload}$	1.028	0.059
U_{actual}	0.753	0.053
$U_{theoretical}$	0.892	0.000

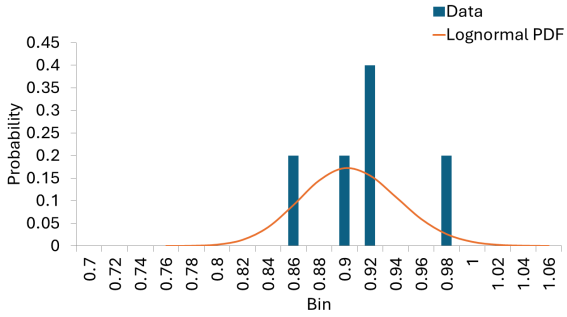

Figure 6.18: Data probability distribution of $M_{operation}$ and corresponding lognormal probability density function for Saint Nazaire high-risk

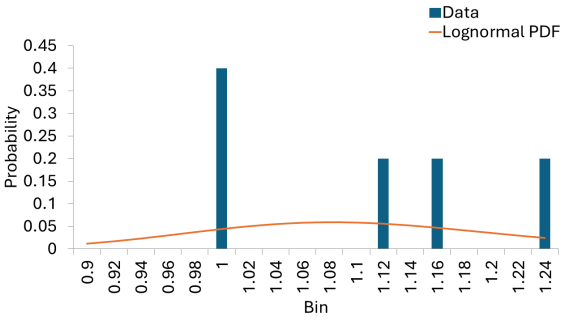

Figure 6.19: Data probability distribution of $M_{preload}$ and corresponding lognormal probability density function for Saint Nazaire high-risk

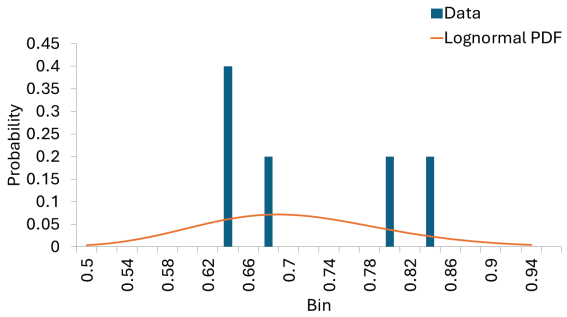

Figure 6.20: Data probability distribution of U_{actual} and corresponding lognormal probability density function for Saint Nazaire high-risk

Table 6.8: Distributions parameter summary for Saint Nazaire high-risk

	μ	σ
$M_{operation}$	0.905	0.038
$M_{preload}$	1.099	0.113
U_{actual}	0.707	0.094
$U_{theoretical}$	0.850	0.000

Annual probability of preload exceedance

The 100 million sampled values of U_{actual} from the Monte Carlo Simulation are then inserted in the corresponding limit state function to obtain the histogram of the limit state function. The histogram of the sampled limit state function around the failure zone for Saint Nazaire low-risk is presented in figure 6.21. From the number of samples in the failure region a probability of failure is determined and converted to an annual probability of actual preload exceedance as explained in section 4.2.
For this scenario, an annual probability of preload exceedance of 0.002060 is obtained, which is higher than the defined target of 0.001. As can be observed in the histogram, the limit state function enters the failure zone by quite some margin. This indicates that the applied preload safety factor is too low, and should be increased to meet the target probability of failure.

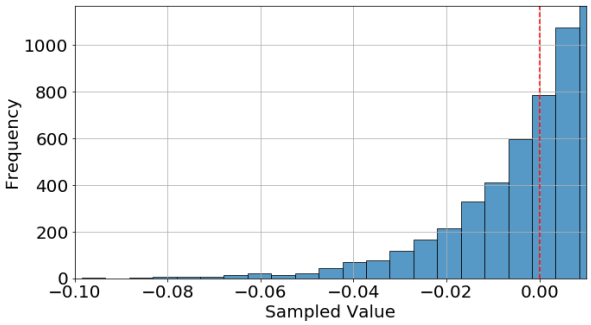

Figure 6.21: Detailed histogram at the failure zone of the sampled limit state function for Saint Nazaire low-risk

6.2.3. Ideal preload safety factors

Since a target annual probability of failure is defined in section 5.1, an ideal preload safety factor can be obtained which leads to this target reliability. This is done for two preload safety factors, namely the theoretical safety factor and the actual safety factor. The theoretical preload safety factor represents the ratio of the prescribed preload versus the estimated maximum operational leg reaction, and the actual preload safety factor represents the ratio of the applied preload versus the experienced maximum operational leg reaction. A comprehensive explanation of the used method to obtain both ideal safety factors is given in section 5.2.

The annual probability of preload exceedance for a range of actual and theoretical safety factors is presented in figure 6.22 and figure 6.23 respectively for Saint Nazaire low-risk. By applying the target annual probability of failure for low-risk soils of 0.001, an ideal value for both preload safety factors is obtained. For Saint Nazaire low-risk, an ideal actual preload safety factor would be 1.354, and an ideal theoretical preload safety factor would be 1.179.

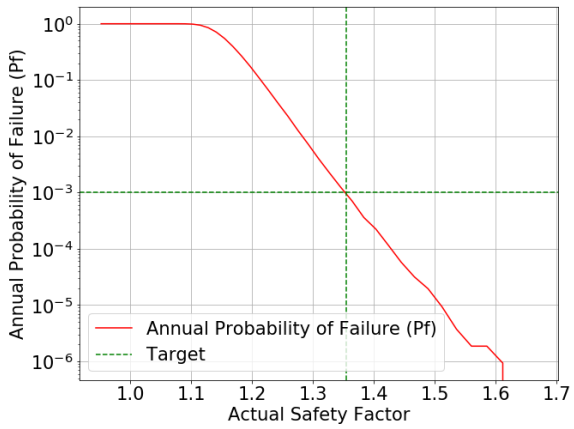

Figure 6.22: Annual probability of preload exceedance as a function of actual safety factor. With the target annual probability of preload exceedance leading to the actual ideal safety factor. For Saint Nazaire low-risk soil.

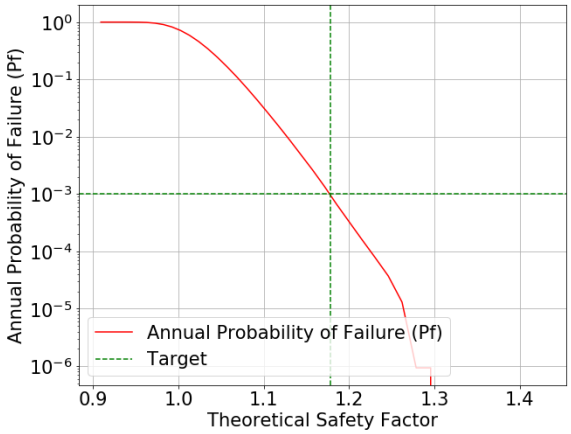

Figure 6.23: Annual probability of preload exceedance as a function of theoretical safety factor. With the target annual probability of preload exceedance leading to the theoretical ideal safety factor. For Saint Nazaire low-risk soil.

6.3. Vesterhav

The third site is the Vesterhav Nord and Syd offshore wind farm in the Danish waters of the North Sea. Which consists of 41 wind turbines where medium dense to dense sands dominate the soil, resulting in an overall low-risk site.

6.3.1. Data processing

The data processing of the acquired measurements is executed in two phases: firstly, the data gathering, refining and filtering, and then identifying and categorizing the maximum actual leg reactions and maximum estimated leg reactions. Section 4.1 offers a detailed explanation of the methods used for the data processing.

Data gathering, refining and filtering

After the needed data is gathered and refined the jacking operations containing bad or inaccurate data are filtered out. Of the available 41 jacking operations, nine are filtered out. Therefore, 32 viable locations remained for the rest of the analysis.

One of the excluded operations is location Vesterhav 5. For this jacking operation, only the leg reactions during preloading were obtained but not during the rest of the operation, as seen in figure 6.24 where the measurements stop at interval 2500. Which is a duration of around 3.5 hours. In addition also no crane load and crane slewing angle were measured, making the data for this location not useful.

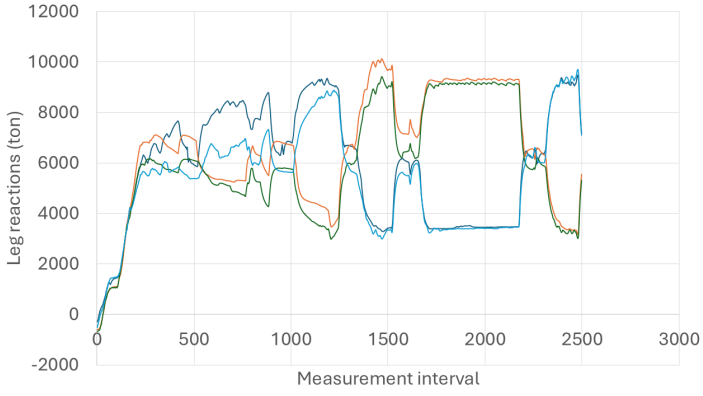

Figure 6.24: Leg reactions of Vesterhav 5

Actual leg reactions

For the remaining jacking locations, the actual preload and actual (maximum) operational leg reaction of each leg is determined based on the operational phases indicated by the crane load or crane slew-

ing angle, as explained in section 4.1. Both values of the leg with the highest actual operational leg reaction are then selected for each location, as seen in table 6.9 for leg 2 for Vesterhav 1. Resulting in the values for the actual operational leg reaction and the corresponding actual applied preload for each jacking location.

Table 6.9: Actual preload and actual (maximum) operational leg reaction of Vesterhav 1

	Leg 1	**Leg 2**	Leg 3	Leg 4
Preload (ton)	9820	**9308**	9755	9384
Operational leg reaction (ton)	6728	**6994**	6363	6268

Estimated leg reactions

In the Site Specific Assessment for Vesterhav, a maximum operational leg reaction is estimated. Which calculates the leg loads in each leg caused by operational loads and environmental loads. For Vesterhav, the estimated maximum operational leg reaction at hull level is equal to 8220 ton for each location. From the estimated operational leg reaction and soil conditions, a preload was estimated for each location as well, based on ISO 19905-1. The prescribed preload at hull level for locations with a soil category 1 and 2, and locations with a soil category 3 are summarized in table 6.10.

Table 6.10: Optimised preloads at Vesterhav from the SSA

	Category 1 and 2	**Category 3**
Optimised preload at footing (ton)	9480	9480
Optimised preload at hull level (ton)	9036	9021

Categorizing

A distinction is then made between jacking operations in low-risk soil and high-risk soil. For each location, the risk category is determined based on the soil profiles from the SSA's as described in section 3.1. For Vesterhav all locations are considered low-risk profiles apart from a few exceptions.
Therefore, all 32 viable jacking operations at Vesterhav are categorized as low-risk, and no high-risk category will be analysed for this site.

6.3.2. Reliability study

This section presents the results of the preload reliability study for the low-risk soil profiles, which is analysed in two phases. First, the distributions for preload uncertainty, operational uncertainty, and actual utilization are derived from the measured and estimated preloads, as well as the measured and estimated operational leg reactions. Next, the annual probability of preload exceedance is calculated using a Monte Carlo Simulation, by implementing the obtained distributions into the defined limit state function. Which is compared to a target annual probability of failure to assess its conservatism.
Detailed descriptions of these methods and the reasoning behind them are provided in section 4.2 and the defined target probabilities in section 5.1.

Leg reaction distributions

For the low-risk profiles at Vesterhav, three probability distributions are obtained from the leg reactions at each location: the operational uncertainty $M_{operation}$, preload uncertainty $M_{preload}$ and actual utilization U_{actual}.
One outlier was observed in the distributions. Since this outlier is caused by a faulty measurement, the jacking operation is excluded from the distributions, as explained in section 4.2. Which leaves a total of 31 low-risk locations.
Each probability distribution is then fitted with a corresponding lognormal probability density function

as described in section 4.2 and presented in figure 6.25, figure 6.26, and figure 6.27.

The mean and standard deviation of the obtained lognormal PDF's are summarized in table 6.11 for Vesterhav. This table includes the mean value for the used theoretical utilization as well, with a standard deviation of zero because the same value is used for each operation in the SSA.

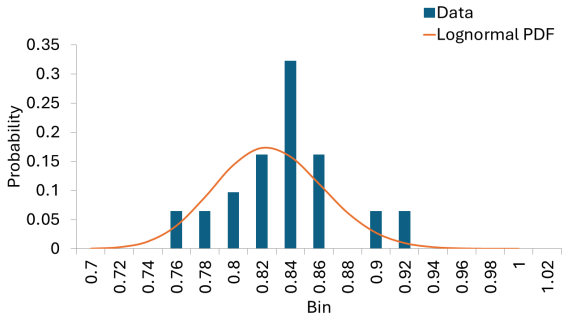

Figure 6.25: Data probability distribution of $M_{operation}$ and corresponding lognormal probability density function for Vesterhav low-risk

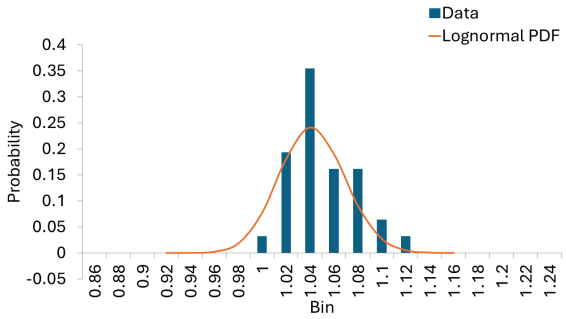

Figure 6.26: Data probability distribution of $M_{preload}$ and corresponding lognormal probability density function for Vesterhav low-risk

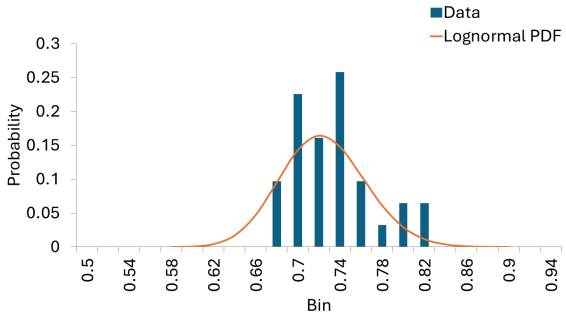

Figure 6.27: Data probability distribution of U_{actual} and corresponding lognormal probability density function for Vesterhav low-risk

Table 6.11: Distributions parameter summary for Vesterhav low-risk

	μ	σ
$M_{operation}$	0.826	0.038
$M_{preload}$	1.042	0.028
U_{actual}	0.724	0.041
$U_{theoretical}$	0.913	0.000

Annual probability of preload exceedance

The 100 million sampled values of U_{actual} from the Monte Carlo Simulation are then inserted in the corresponding limit state function to obtain the histogram of the limit state function. The histogram of the sampled limit state function around the failure zone for Vesterhav low-risk is presented in figure 6.28. From the number of samples in the failure region a probability of failure is determined and converted to an annual probability of actual preload exceedance as explained in section 4.2.
For this scenario, an annual probability of preload exceedance of 0.000000 is obtained. As can be observed in figure 6.28, the limit state function does indeed not enter the failure zone. This indicates that the applied preload safety factor is too conservative, and can be lowered to meet the target probability of failure.

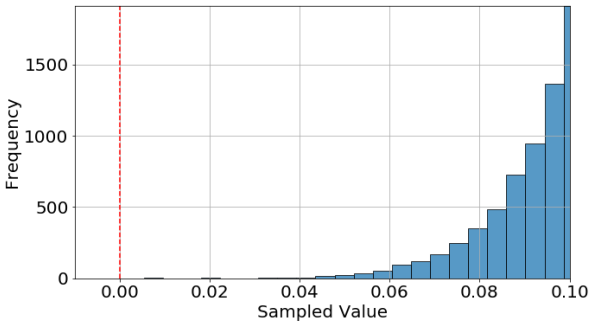

Figure 6.28: Detailed histogram at the failure zone of the sampled limit state function for Vesterhav low-risk

6.3.3. Ideal preload safety factors

Since a target annual probability of failure is defined in section 5.1, an ideal preload safety factor can be obtained which leads to this target reliability. This is done for two preload safety factors, namely the theoretical safety factor and the actual safety factor. The theoretical preload safety factor represents the ratio of the prescribed preload versus the estimated maximum operational leg reaction, and the actual preload safety factor represents the ratio of the applied preload versus the experienced maximum operational leg reaction. A comprehensive explanation of the used method to obtain both ideal safety factors is given in section 5.2.

The annual probability of preload exceedance for a range of actual and theoretical safety factors is presented in figure 6.29 and figure 6.30 respectively for Vesterhav low-risk. By applying the target annual probability of failure for low-risk soils of 0.001, an ideal value for both preload safety factors is obtained. For Vesterhav low-risk, an ideal actual preload safety factor would be 1.242, and an ideal theoretical preload safety factor would be 0.994.

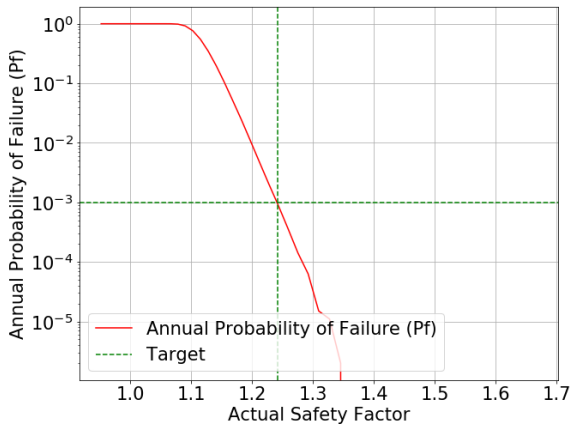

Figure 6.29: Annual probability of preload exceedance as a function of actual safety factor. With the target annual probability of preload exceedance leading to the actual ideal safety factor. For Vesterhav low-risk soil.

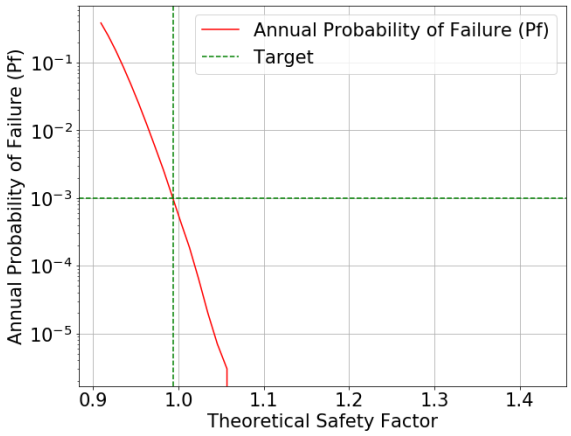

Figure 6.30: Annual probability of preload exceedance as a function of theoretical safety factor. With the target annual probability of preload exceedance leading to the theoretical ideal safety factor. For Vesterhav low-risk soil.

6.4. Results Comparison

This section summarises the obtained results by comparing them in different ways to answer the last research sub-question. First, the ideal actual and theoretical preload safety factors are compared to the originally applied values at each offshore wind farm site. Next, the applied theoretical preload safety factors are compared to the applied actual preload safety factors.

6.4.1. Applied safety factor vs ideal safety factor

The applied actual and theoretical safety factors can be obtained by taking the inverse of the mean actual utilization and mean theoretical utilization for each assessed scenario. These mean values are acquired from table 6.3, table 6.4, table 6.7, and table 6.11.

Applied actual safety factor vs ideal actual safety factor

For each scenario, the applied actual safety factor and ideal actual safety factor are presented in table 6.12. From this table, it can be observed that for Kriegers Flak low-risk and high-risk, and for Vesterhav low-risk the ideal actual safety factor is lower than the applied one. For Saint Nazaire the ideal actual safety factor is higher than the applied actual safety factor.

The ideal actual safety factor is on average also lower than the applied actual safety factor, both for the low-risk profiles and high-risk profiles. This means that on average the applied preload is too conservative. Apart from Saint Nazaire, where the actual conditions are less reliable than estimated.

These values and conclusions can be used to verify the results of the theoretical safety factor, which is the main point of interest.

Table 6.12: Applied actual preload safety factor and ideal actual preload safety factor for each assessed scenario and the average for each risk profile

Site	Risk profile	Applied SF_{actual}	Ideal SF_{actual}
Kriegers Flak	low	1.431	1.186
Kriegers Flak	high	1.536	1.481
Saint Nazaire	low	1.328	1.354
Vesterhav	low	1.381	1.242
Average	low	1.38	1.261
Average	high	1.536	1.481

Applied theoretical safety factor vs ideal theoretical safety factor

For each scenario, the applied theoretical safety factor and ideal theoretical safety factor are presented in table 6.13. The results for the theoretical safety factor align with the results for the actual safety factor. Namely, on average the ideal theoretical safety factor is lower than the applied theoretical safety factor for both low-risk and high-risk soils, apart from Saint Nazaire.
Therefore, given the current operational and preload uncertainties, the theoretical safety factor could be lowered to achieve the ideal target annual reliability and as a result improve the currently used theoretical preload safety factor.

An additional observation can be made: the average applied theoretical safety factor is equal to the prescribed preload safety factor of 1.1 by the ISO. For high-risk soils, the applied theoretical safety factor is a bit higher, which also makes sense.

Table 6.13: Applied theoretical preload safety factor and ideal theoretical preload safety factor for each assessed scenario and the average for each risk profile

Site	Risk profile	Applied $SF_{theoretical}$	Ideal $SF_{theoretical}$
Kriegers Flak	low	1.083	0.946
Kriegers Flak	high	1.110	1.081
Saint Nazaire	low	1.121	1.179
Vesterhav	low	1.095	0.994
Average	low	1.100	1.040
Average	high	1.110	1.081

6.4.2. Theoretical safety factor vs actual safety factor

Ideally, the applied actual preload safety factor should match the applied theoretical preload safety factor. This would imply that the experienced maximum leg reactions are correctly estimated in the site specific assessment and that the prescribed preload is correctly estimated and applied during the jacking operation.
Table 6.14 presents both the applied actual preload safety factor and the applied theoretical preload safety factor for each assessed scenario. It is observed that for each scenario, the actual values are higher than the theoretical values by quite some margin, which is not ideal.

Table 6.14: Applied actual preload safety factor and applied theoretical preload safety factor for each assessed scenario

Site	Risk profile	Applied SF_{actual}	Applied $SF_{theoretical}$
Kriegers Flak	low	1.431	1.083
Kriegers Flak	high	1.536	1.110
Saint Nazaire	low	1.328	1.121
Vesterhav	low	1.381	1.095

This difference can be caused by one or both parts of the safety factor equation: the maximum operational leg reaction and/or the preload. For both values, a distribution has already been obtained to display the uncertainty between what is estimated and what is measured. Namely, the operational uncertainty $M_{operation}$ and preload uncertainty $M_{preload}$, of which the mean values of each scenario are repeated in table 6.15.

Table 6.15: Mean values of operational uncertainty and preload uncertainty for each scenario

Site	Risk profile	$M_{operation}$	$M_{preload}$
Kriegers Flak	low	0.785	1.037
Kriegers Flak	high	0.794	1.103
Saint Nazaire	low	0.865	1.028
Vesterhav	low	0.826	1.042

From these operational and preload uncertainties, the following two general observations are made:

$$\text{measured maximum operational leg reaction} < \text{estimated maximum operational leg reaction}$$

$$\text{measured preload} > \text{prescribed preload}$$

In an ideal scenario, both parameters would be equal to one. However, it is to be expected that actual load conditions of complex jack-up operations are difficult to estimate precisely and that these ratios could therefore likely deviate slightly from one. Instead, on average, the operational uncertainty is 18.3 percent lower and the preload uncertainty 5.3 percent higher than one. The preload uncertainty being a bit larger than one could be explained by the operator not exactly applying the prescribed preload. The exact reason for this small deviation could be verified with the operator. For example, additional preload could be applied if the soil conditions on site appear to be more unstable than predicted.
In contrast to the small deviation in preload uncertainty, the operational uncertainty has a much larger deviation from one. The estimated leg reactions seem way too conservative compared to what is measured. Also, unlike the applied preload, the experienced leg loads should be estimated pretty accurately by the performed simulations and calculations since the exact parameters for the lifting operations are known very accurately.

To try to answer the large difference between estimated maximum operational leg reactions and measured maximum operational leg reactions, additional research was conducted. Which is thoroughly explained in appendix B, where the elevated hull weight is studied in detail.

7

Conclusion

This chapter rounds up the thesis report by presenting the final conclusions, a discussion, and recommendations. In section 7.1 the conclusions on the research questions and sub-questions are formulated. Thereafter, a discussion on the research and the obtained results is provided in section 7.2. Finally, recommendations for future research and jacking operations are given in section 7.3.

7.1. Research conclusions

The main objective of this research was to develop a robust method for analysing the applied preload in past jack-up crane operations conducted by the vessel Vole au vent. This analysis aims to provide a better understanding of the effectiveness of traditional offshore jack-up guidelines within the rapidly growing offshore wind industry, where heavy crane operations are now performed on a daily basis. Such understanding is crucial, as these guidelines were not originally intended for the advanced state of the current offshore wind sector and are not specifically calibrated for its unique demands. The findings of this research may indicate an urgent need to evaluate and improve these standards to better align with the evolving requirements of the industry.

To satisfy this objective, a method was designed to assess the preload safety factors of past jacking operations and determine their optimal value for heavy lifting operations. The developed models were then applied to a case study using measuring data from jacking operations of the Vole au vent to validate their effectiveness.

7.1.1. Conclusions to the research questions

Multiple research questions with sub-questions were composed to solve this engineering problem systematically. This section answers these questions based on the case study results and the designed methods. The first research question answered by this thesis is:

Research question 1: *How can a framework be developed to assess preload conservatism of past offshore wind jack-up vessel lifting operations?*

This research question can be answered by formulating an answer to the first three research sub-questions. Each of these sub-questions has been answered by subjecting the defined research framework to a real-life case study, and are summarised as follows:

RQ 1.1: *How do the estimated leg reactions compare to observed leg reactions during past operations, specifically at maximum preload and maximum operational load?*

At both maximum operational leg reaction and preload, a probability distribution is obtained for the operational uncertainty and the preload uncertainty. The operational uncertainty is equal to the ratio

of the measured maximum operational leg reaction over the estimated maximum operational leg reaction. The preload uncertainty gives the ratio of the applied preload versus the prescribed preload. By determining these probability distributions for each viable scenario of the case study, the following conclusions can be drawn.

In an ideal scenario, both parameters would be equal to one. However, it is to be expected that actual load conditions of complex jack-up operations are difficult to estimate precisely and that these ratios could therefore likely deviate slightly from one. Instead, for all scenarios, the mean value of the operational uncertainty is smaller than one, and the mean value of the preload uncertainty is larger than one. Therefore, the estimated maximum operational leg reaction is way too conservative compared to the measured maximum operational leg reaction. On average, the estimation is 18.3 percent higher than the measured value.
The applied preload is on average a bit higher than prescribed, namely 5.3 percent. Which could be caused by the operator on the jack-up vessel exceeding the prescribed preload.
Both probability distributions have on average a standard deviation between 4 and 5 percent, which reflects a fairly large amount of uncertainty.

In contrast to the small deviation in preload uncertainty, the operational uncertainty has a much larger deviation from one. The estimated leg reactions seem way too conservative compared to what is measured. Also, unlike the applied preload, the experienced leg loads should be estimated accurately by the simulations and calculations since the exact parameters for the lifting operations are accurately known. The large deviation in operational uncertainty is further researched in appendix B, which is covered in detail in section 7.2 and section 7.3.

RQ 1.2: *How can the probability of preload failure be evaluated in relation to operational loads, considering both estimated and applied preload values?*

To evaluate the preload in relation to the operational loads, considering both estimated and applied preload values, a couple of ratios are firstly determined for each jacking operation. These include the actual utilization, which is equal to the measured maximum operational leg reaction versus the measured applied preload. Both of these parameters are obtained at their maximum value during the operation in the heaviest loaded leg. Therefore, the utilization quantifies the critical point in the operation where the experienced leg reaction got the closest to the applied preload. Additionally, the defined ratios include the theoretical utilization, which is the ratio of the estimated maximum operational leg reaction over the prescribed preload, the operational uncertainty, and the preload uncertainty, which are described in previous sub-question. For each soil risk profile at each wind farm site, a probability distribution can then be obtained for each of these ratio with the values from each assessed jacking operation.

A reliability analysis evaluates the probability of a failure of a system under defined conditions by assessing whether a certain limit state is exceeded. Failure in this case, is determined by the preload check from ISO 19905-1 and is defined as the operational leg reactions becoming larger than the preload. This failure criterion is described by a limit state function, defined for both the estimated and applied preload as a function of the earlier defined ratios. If the outcome of this function is smaller than zero, failure is detected.

A Monte Carlo Simulation is then used to obtain the annual probability of preload exceedance for the given limit state functions with the defined leg reaction probability distributions. It does so by sampling values for each ratio based on their probability distribution and applying them to the limit state function. This is then done many times to generate a probability distribution of the limit state function, from which the probability of failure can be defined as the ratio of the number of values below zero over the total amount of samples.

For each scenario from the case study, the obtained annual probability of preload exceedance gives an indication of how reliable the preload is in relation to the operational loads. Since the limit state functions for the estimated and applied values are derived from one another, their MCS should deliver the same outcome. This was indeed observed, validating both methods.

RQ 1.3: *What is an acceptable threshold for the annual probability of preload exceedance in offshore wind jack-up vessel operations?*

This last sub-question answers the conservatism aspect of the first research question by giving a target to compare the obtained reliabilities from the previous sub-question with. An acceptable reliability target can be defined based on the consequences of failure, in this case preload exceedance. For the jack-up vessel operations, two consequence classes are established: operations in low-risk soil profiles and operations in high-risk soil profiles.

When preload is exceeded in a low-risk soil profile the leg will settle further into the soil until a new equilibrium is found between the applied loads and the bearing capacity under the spudcan. Causing only insignificant material damages and no severe casualties, matching the description of a consequence class 2. The worst-case scenario for a preload exceedance in high-risk soil is severe punch-through. Where rapid leg settlements and severe additional leg penetration could cause structural failure of a jack-up leg. The consequences of such a failure fit the description of consequence class 3 or 4.
The worst-case consequences of failure in high-risk soil are larger than in low-risk soil, which is reflected in their respective reliability targets. Based on the consequence classes for both soil profiles, an acceptable threshold for the annual probability of preload exceedance is defined as 10^-3 for low-risk soil and 10^-4 for high-risk soil. These targets provide a balance between the efficiency and safety of the jacking operations.

The results of the case study reveal that the majority of both low-risk and high-risk operations are designed too conservatively. For each scenario, apart from Saint Nazaire low-risk, the obtained annual probability of preload from the MCS is lower than the defined targets.

Once the conservatism of past offshore jack-up operations is established, the next step is to find out how the acceptable reliability targets could be achieved by improving the preload safety factor, which leads to the second research question. The second research question is answered by itself, and the last research sub-question serves as an additional level of depth to the second research question.

Research question 2: *What is the optimal preload safety factor relative to the acceptable annual probability of preload exceedance?*

Since the estimated values and observed values for the preload and leg reactions do not match, two ideal preload safety factors are determined. First, the ideal actual preload safety factor is determined, which provides the ideal ratio between the applied preload and experienced leg reactions that leads to the desired reliability target. Second, the ideal theoretical preload safety factor is obtained. This safety factor gives the ideal ratio between the prescribed preload and estimated maximum operational leg reactions, which will lead to the actual ideal safety factor through the operational and preload uncertainty and, therefore to the desired reliability as well.

These ideal values are obtained by the same Monte Carlo Simulations as before, but, for a range of actual and theoretical utilizations instead. By doing so, the annual probability of failure is obtained as a function of the actual and theoretical preload safety factor. By then applying the defined targets for the annual probability of failure, an ideal value can be obtained for both the actual and theoretical preload safety factors.

Based on the case study, the following optimal preload safety factors are obtained:
On average, the determined ideal theoretical preload safety factor for low-risk soil profiles is equal to 1.04. Through the defined uncertainties, this theoretical value will lead to an ideal actual preload safety factor of 1.26, providing the target annual probability of preload exceedance of 10^-3 during operations. The ideal theoretical preload safety factor for high-risk soil profiles equals 1.08 on average. During jack-up operations, this will lead to the ideal actual preload safety factor of 1.48, resulting in an annual probability of preload exceedance of 10^-4.

RQ 2.1: *How does the determined optimal safety factor compare to values applied in previous operations?*

Currently, the applied theoretical preload safety factor value is based on the recommendations by ISO 19905-1. For low-risk soil profiles, on average, a theoretical preload safety factor of 1.10 is used; for high-risk soil profiles, this safety factor should be a bit higher; on average, this was observed to be 1.11.

It is observed that for Kriegers Flak low-risk and high-risk, and Vesterhav low-risk, the ideal theoretical safety factor is lower than the applied one. For Saint Nazaire, the ideal theoretical safety factor is higher than the applied actual safety factor.

By comparing the average ideal theoretical preload safety factors, as described in research question 2, to the average applied theoretical preload safety factors, it can be concluded that, in general, the ideal theoretical safety factor is lower than the applied actual safety factor, both for the low-risk profiles and high-risk profiles. This means that on average the applied preload is too conservative. Apart from Saint Nazaire, where the actual conditions are less reliable than estimated.

By lowering the applied theoretical preload safety factor by 5.5 percent for low-risk locations and 2.6 percent for high-risk locations. The optimal amount of actual preload would be achieved during the jacking operations, with current industry practices and uncertainties leading to the desired reliability targets.

7.1.2. Final conclusions

Reliability methods based on the failure description of the preload integrity check from ISO 19905-1 and the measured and estimated leg reactions from offshore jacking operations were used to develop a robust method to analyse the applied preload for past jack-up crane operations by the Vole au vent. With these methods, it was shown that the currently used preload safety factor from traditional offshore jack-up guidelines is not yet correctly calibrated for heavy crane operations on jack-up vessels. To achieve an optimal balance between operational efficiency and safety, the applied preload, with respect to the experienced loads from heavy crane operations, should be slightly lowered compared to what is currently applied.
In addition, through this research, it was observed that the measured conditions during jack-up operations are not correctly estimated. Leading to operational and preload uncertainties.

7.2. Discussion

This part of the conclusion will discuss the results of the main research and additional research from appendix B. This additional research was conducted because the obtained operational and preload uncertainties were not equal to one. Indicating that the measured maximum operational preload is on average lower than the estimated maximum operational leg reactions and that more preload is in reality applied than originally prescribed. In the additional research, certain hypotheses were tested to validate the deviations in uncertainty, through studying the elevated hull weight.

7.2.1. Research discussion

For the limit state functions, the first and most conservative foundation integrity check is used. Therefore, the obtained ideal preload safety factor could probably be lowered even further.

It is important that the soil risk category is estimated correctly since this will determine the ideal target for the theoretical preload safety factor. In this case study, Saint Nazaire low-risk is the only scenario where the ideal safety factor is higher than the applied safety factor. Therefore it could be concluded that this was perhaps not truly a low-risk soil profile.
This could lead to the recommendation of adding a third risk category for the medium-risk profiles. For these risk profiles, an average of the low-risk and high-risk ideal theoretical safety factors could be

used, which is equal to 1.06.
By excluding Saint Nazaire from the low-risk category, the average ideal theoretical preload safety factor for low-risk soil profiles would become lower than one. Which is not allowed since, by definition, a safety factor should be larger than one. This also points to problems with current operational and preload uncertainties, which should definitely be addressed to maintain the reliability of future assessments.

7.2.2. Additional research discussion

The additional research concluded that the operational uncertainty might be caused by load dissipation via friction between the leg and leg shaft and perhaps because ballast water is dumped after preloading, which is not accounted for in the assessments. If both of these factors would be accounted for in the assessments and measurements of future operations, this could solve the operational uncertainty, but make the preload uncertainty larger than it currently is.
Therefore, by fixing current inaccuracies, it should come to light that the preload is applied way too conservatively compared to what is prescribed.

7.3. Recommendations

Based on the results and conclusions, some recommendations can be made. Including recommendations for future research and recommendations concerning procedures for jacking operations.

7.3.1. Future research

By lowering the standard deviation of the preload uncertainty, the outcomes of the jacking operations could become more predictable. A study could be performed on the compliance of the operator with the prescribed preload during the operation. This feedback can bring further insights into the actual conditions during jacking operations, which could then be used to formulate additional guidelines or procedures to make the process more reliable.

The reliability targets are an important parameter to define the ideal preload safety factor. In this research, those targets are estimated based on general consequence classes. If a study could be done to exactly determine what the most optimal value would be for the target annual probability of preload exceedance in different soil profiles, the ideal safety factors could become even more reliable.

From the results of the case study, it was observed that the actual preload safety factor does not match the respective theoretical preload safety factor. This is mainly caused by the operational uncertainty, where the estimated maximum operational leg reactions are very conservative compared to what is measured during the operations. This observation is studied more in detail in appendix B and verifies two things. The elevated hull weight of the jack-up vessel is estimated too conservatively, and the elevated hull weight is undervalued by the measurements, possibly due to load dissipation through friction.
Based on this additional research, the following recommendations can be made for future research.

An investigation could be conducted into why the estimated elevated hull weight is too conservative compared to the real elevated hull weight. For example, because ballast water is dumped after preloading, which is not accounted for in the calculations.

More research should be done to confirm that friction really occurs between the leg and leg shaft. If this is actually the case, it could be further estimated how much of the loads are exactly dissipated via friction. This research could then be performed again but with higher actual leg reactions, accounting for friction. Leading to an even more reliable preload safety factor.

7.3.2. Procedures

By making a comprehensive analysis after each jacking operation, the applied models can be refined and calibrated based on actual data. After many operations this will also lead to a dataset of analysed operations, which provides a solid basis for data-driven decision-making. The assessed parameters from appendix B give a good indication of what kind of information should be logged and collected by the operator. These include the real elevated hull weight, estimated elevated hull weight, and measured elevated hull weight before and after the first lifting operation.

Measurements are currently not always viable, so improving the systems to correctly measure and save the data would improve such data analysis.

References

[1] 4C Offshore. *Offshore wind farm map*. Oct. 2024.

[2] "Application of Reliability Methods in Design and Analysis of Offshore Platforms". In: *Journal of Structural Engineering* 109.10 (Oct. 1983).

[3] Gregory B. Baecher, M. Elisabeth Paté, and Richard De Neufville. "Risk of dam failure in benefit□cost analysis". In: *Water Resources Research* 16.3 (1980), pp. 449–456. issn: 19447973. doi: 10.1029/WR016i003p00449.

[4] Mehmet Bilgili and Hakan Alphan. "Global Growth in Offshore Wind Turbine Technology". In: (2022). doi: 10.21203/rs.3.rs-1202466/v1.

[5] Choi Seung-Kyum, Grandhi Ramana, and Canfield Robert. *Reliability-based Structural Design*. London: Springer, 2007.

[6] Mohammad Daghigh. *Structural system reliability analysis of jack-up platforms under extreme environmental conditions*. Delft University of Technology, Faculty of Mechanical Engineering and Marine Technology], 1997. isbn: 9037001556.

[7] E.T.R. Dean et al. "Numerical Modelling of Three-Leg Jackup Behaviour Subject to Horizontal Load". In: *Soils and Foundations* 37.2 (June 1997), pp. 17–26. issn: 0038-0806. doi: 10.3208/SANDF.37.2{_}17.

[8] Dean E et al. "Centrifuge Modelling of 3-Leg Jackups with Non-skirted and skirted spuds on Partially Drained Sand". In: *27th Offshore Technology Conference*. Houston: OTC 7839, 1995.

[9] Adrian. Dier et al. *Guidelines for jack-up rigs with particular reference to foundation integrity*. HSE Books, 2004, p. 83. isbn: 0717629260.

[10] DNV-OS-F201. *Dynamic Risers*. Tech. rep. Det Norske Veritas, Jan. 2018.

[11] "Draft BS ISO 2394 General principles on reliability for structures". In: (2013). url: http://standardsdevelopment.bsigroup.com.

[12] Ian C Giddings. *QUALITY ASSURANCE SESSION IMO Guidelines for Vessels with Dynamic Positioning Systems y g*. Tech. rep.

[13] *GUIDELINES FOR LOAD-OUTS*. Tech. rep. 2015. url: http://www.dnvgl.com/.

[14] *Guidelines for the Selection and Operation of Jack-ups in the Marine Renewable Energy Industry Issue 2: 2013 www.RenewableUK.com*. Tech. rep. url: www.RenewableUK.com.

[15] Hunt Rupert and Marsh Philip. "Opportunities to improve the operational and technical management of jack-up deployments". In: *Marine Structures* 17.3-4 (May 2004), pp. 261–273.

[16] Osias Julie. *The new SG 8.0-167 DD Greater rotor for greater benefit*. Tech. rep.

[17] Kuen Kok and Beng Lee. *Investigation of Potential Spudcan Punch-Through Failure on Sand Overlying Clay Soils*. Tech. rep.

[18] landerson. *Noble Denton Report format*. Tech. rep. url: www.gl-nobledenton.com.

[19] Min Jy Lee and Yun Wook Choo. "Penetration Behavior of Jack-up Leg with Spudcan for Offshore Wind Turbine to Multi-layered Soils Using Centrifuge Tests". In: *Journal of Ocean Engineering and Technology* 38.1 (Feb. 2024), pp. 30–42. issn: 22876715. doi: 10.26748/KSOE.2023.039.

[20] Zhongqiang Liu et al. "Reliability of API and ISO Guidelines for Bearing Capacity of Offshore Shallow Foundations". In: (2015). doi: 10.3233/978-1-61499-580-7-821.

[21] Mohammed A. Al-Maadheedi and Marijn J. Dekker. "Numerical modelling of sand plug formation during punch-through of a spudcan footing". In: *Ocean Engineering* 284 (Sept. 2023), p. 115198. issn: 0029-8018. doi: 10.1016/J.OCEANENG.2023.115198.

[22] Miftahuddi Nur, Priyanta Dwi, and Hari Prastowo. “124205291-Calculation-of-Displacement-LWT-and-DWT”. In: *Electrical Systems and Engine Room* ().

[23] *NOBLE DENTON MARINE SERVICES Disclaimer*. Tech. rep. url: https://mww.dnvgl.com/Document/Get?projectId=2022&docName=DNVGL-ST-N00....

[24] Det Norske Veritas. *OFFSHORE STANDARD DESIGN OF OFFSHORE WIND TURBINE STRUCTURES*. Tech. rep. 2007, pp. 2009–2020. url: http://webshop.dnv.com/global/,.

[25] *Offshore Wind Farm Saint-Nazaire, France*. Oct. 2024.

[26] Mohamad H.B. Osman and Richard Willden. “Added mass and damping forces of a floating tidal turbine undergoing pendulum motion”. In: *Ocean Engineering* 283 (Sept. 2023), p. 115014. issn: 0029-8018. doi: 10.1016/J.OCEANENG.2023.115014.

[27] *Petroleum and natural gas industries-Site-specific assessment of mobile offshore units-Part 1: Jack-ups COPYRIGHT PROTECTED DOCUMENT*. 2016. url: www.iso.org.

[28] Mark Randolph and Gourvenec Susan. *Offshore geotechnical engineering*. Taylor & Francis Group, 2011.

[29] *Rules for planning and execution of marine operations*. Tech. rep. Saint-Petersburg: Russian maritime register of shipping, 2017.

[30] *Simple vs. exponential moving averages*. url: https://www.steema.com/docs/financialFunctionsRef/expMovingAverageFunction.htm.

[31] Nadja Skopljak. *Vattenfall Picks EDS HV for Danish Offshore Wind Work*. July 2020.

[32] Wouter Sonnema et al. “Preloading of four-legged jack-ups in clay: Geotechnical time effects and fulfilment of preloading criteria”. In: *Ocean Engineering* 278 (June 2023). issn: 00298018. doi: 10.1016/j.oceaneng.2023.114425.

[33] R D J M Steenbergen, Á Rózsás, and A C W M Vrouwenvelder. *Target reliability of new and existing structures-A general framework for code making*. Tech. rep. 3. 2018.

[34] *Structural reliability analysis of marine structures*. Tech. rep. Det Norske Veritas, July 1992, pp. 1–51.

[35] *T & R Guidelines for Site Specific Assessment of Mobile Jack-Up Units*. Tech. rep. 2008.

[36] Templeton J. “Jackup Foundation Performance in Clay”. In: *38th Offshore Technology Conference*. Houston: OTC 18367, June 2006.

[37] Arnold Verruijt. *SOIL MECHANICS*. Tech. rep. url: http://geo.citg.tudelft.nl/..

[38] Vijay P. Singh. “Stochastic and statistical methods in hydrology and environmental engineering ”. In: *Water science and technology library* 3 (1994).

[39] *VOLE au VENT-Self Elevating Wind Turbine Installation Unit OPERATING MANUAL SELF ELEVATING WIND TURBINE INSTALLATION UNIT OPERATING MANUAL Vessel Name VOLE au VENT IMO N O 9655315 NOTHING CONTAINED IN THIS MANUAL SHALL RELIEVE THE OWNER, OPERATOR, MASTER AND CREW OF THE SHIP THEIR RESPONSIBILITY FOR EXERCISING SOUND JUDGEMENT BASED ON EDUCATION, TRAINING AND EXPERIENCE*. Tech. rep.

[40] Wong P and Murff J. “Dynamic Analysis of jack-up rigs Using Advanced Foundation Models”. In: *OMAE*. Houston, 1994, pp. 94–1315.

[41] Tien H. Wu et al. “Reliability Of Offshore Foundations—State Of The Art”. In: *Journal of Geotechnical Engineering* 115.2 (1989), pp. 157–178. issn: 0733-9410. doi: 10.1061/(ASCE)0733-9410(1989)115:2(157).

[42] Jitao Yao, Hui Gu, and Liuzhuo Chen. “Probability analysis of crane load and load combination actions”. In: *Mathematical Problems in Engineering* 2018 (2018). issn: 15635147. doi: 10.1155/2018/6527307.

A

Sensor uncertainty

The jack-up vessel's leg loads are measured by the pressure in the hydraulic holding system and then converted to tons. To account for the inaccuracies of these measuring sensors, the defined limit state functions originally included a component for the sensor uncertainty as well. After quantifying these uncertainties it became clear that the sensors in the hydraulic systems are very accurate. Since such a sensor uncertainty would not impact the results of the limit state function but only increase its complexity, it was left out.
Nevertheless, quantifying the sensor accuracy through the measured leg reactions might provide value. Therefore, it is briefly discussed here.

Sensor uncertainty can be quantified by the coefficient of variation (COV) of the leg reactions during a period when no change occurs in the applied loads [42]. This can be expressed as a normal distribution with a mean value of 1 since certain sensor deviations can happen equally in both directions. From the acquired unrefined data, the only way of verifying that the applied loads during a certain time frame are constant is by the crane load and crane slewing angle. For all jacking operations at Saint Nazaire, a window of 500 consecutive leg loads is obtained where the crane load and crane slewing angle remain constant, indicating no change in applied loads, apart from minor changes in the environmental loads during this window. This is done by designing a Python code to execute these requirements.

From each obtained viable time frame of the leg loads, the COV is obtained as in equation (A.1), where σ and μ are the standard deviation and mean of the leg reactions. Hereafter, the average COV is calculated for all assessed jacking operations, leading to the standard deviation of the normalised distribution of the sensor uncertainty. This normalised standard deviation is equal to 0.0032 or 0.32 percent.

$$\delta = \frac{\sigma}{\mu} \tag{A.1}$$

Guidelines can indicate the allowable sensor sensitivity for certain operational scenarios. For crane load measurements, typically an upper limit of 2 to 5 percent is given to ensure operational safety and reliability [24]. Comparing these targets with the obtained 0.32 percent for the leg reaction measurements also confirms how low the sensor uncertainty for the leg reactions is.

B

Additional research: elevated hull weight

From the results of the assessed case study in the main research, it is concluded that the estimated maximum operational leg reactions are much higher than what is measured during the operations. This appendix provides additional research into what this large difference could be caused by.
The engineers at Jan De Nul had a few hypotheses for the obtained behaviour. Since these additional questions are outside the scope of this thesis, only the provided hypotheses that could be answered by the already acquired data are further researched.

B.1. Hypotheses

A very low ratio of measured leg reaction versus estimated leg reaction can be caused by one or both parts of the ratio. Namely, the measured leg reaction does not correctly measure all the applied loads on the hydraulic system causing the measured leg reactions to be lower than the actual experienced leg reactions. The second factor could be that the estimated leg loads are too conservative by accounting for weights that are not present on the vessel during certain jack-up operations.
These two causes are formulated into the following hypotheses:

Conservative weight estimation

In the SSA, the maximum leg reactions during operation are estimated with a fully loaded vessel, containing the components of 4 wind turbines. During the actual operations, the vessel is not always fully loaded since it will install all 4 wind turbines before returning to the harbour. This would cause the vessel to be lighter than estimated after one or multiple turbines are installed. But, this installed weight is compensated by ballast water, in order to have the same amount of weight on the vessel to preload. Although, this ballast is not always dumped after preloading.
These combinations of factors lead to uncertainty about how much the vessel actually weighs during operations. If the vessel weight is estimated too conservatively this could answer why the maximum operational leg reactions are estimated too conservatively as well.

Load dissipation through friction

Leg reactions are measured in the hydraulic systems, which control the position of the legs. Such a hydraulic system is located inside the leg shaft where the leg passes through. If the horizontal displacement of the leg would occur, then the leg could touch the leg shaft. Which would create friction between the leg and leg shaft when loading is applied. If a part of the loading between the hull and legs is transferred through this friction instead of the hydraulic system, then the measured leg reactions would not include all transferred loads. Causing the measured leg reactions to not accurately represent the actual leg reactions.

B.2. Research framework

Both hypotheses can be checked based on the elevated hull weight in the provided jacking logs and the refined time series of the leg reactions, which are already obtained for the main research. The flow of the input data for this additional research can be seen in figure 3.4 in section 3.2.
This section first describes the different types of elevated hull weight that are needed for this research and then explains the methods to obtain the maximum and minimum measured elevated hull weight during the jacking operation.

B.2.1. Elevated hull weight

The first hypothesis is checked by comparing the real maximum elevated hull weight with the estimated maximum elevated hull weight. Where the real maximum elevated hull weight is noted by the operator in the jacking logs and the estimated maximum elevated hull weight is the value obtained from the SSA.

The second hypothesis is verified by making two comparisons. The first one compares the measured maximum elevated hull weight with the real maximum elevated hull weight. If no friction would occur, then both these values would be very similar. Secondly, the measured maximum elevated hull weight before the first component is installed, is compared to the measured minimum elevated hull weight after this component is installed. If no friction would occur, then the difference between these two values should be equal to the weight of the installed component.

Real maximum

The operator notes certain parameters in the jacking logs during each jacking operation. One of these parameters is the hull weight based on the hull draught before the vessel is jacked up. From the draught, the vessel weight can be obtained with equation (B.1) [22] and the respective maximum elevated hull weight by equation (B.2).
In equation (B.1) the vessel weight Δ is calculated by multiplying the underwater volume of the vessel by the density of seawater. The underwater volume of the vessel is determined by the length of the water line Lwl, the breadth of the vessel B, the draught of the vessel T and the block coefficient Cb. These are all defined parameters based on the vessel draught. Therefore, the weight of the vessel can be determined by measuring its draught.
The maximum elevated hull weight is then obtained by subtracting the weight of the legs from the hull weight, as in equation (B.2). Where the weight of the legs can be obtained from the SSA and is equal to four times 1246 ton.

$$\Delta = \nabla \cdot \rho_{seawater} = Lwl \cdot B \cdot T \cdot Cb \cdot \rho_{seawater} \tag{B.1}$$

$$\Delta_{elevated} = \Delta - W_{legs} \tag{B.2}$$

This is a very robust method to obtain the maximum elevated hull weight; since it only depends on one variable, the draught, which can easily be determined on the vessel. Therefore this value of the maximum elevated hull weight is considered the real value.

Estimated maximum

The estimated maximum elevated hull weight is obtained from the site specific assessment. Where the vessel weight is determined based on the weights of all the components on the vessel and the maximum elevated hull weight with equation (B.2) as well.

Measured

By adding the leg reactions of each leg together, the measured elevated hull weight can be obtained at any point in the operation. Just as for the previous two values, the measured maximum elevated hull weight is obtained after the vessel has been jacked up and before any component is installed. Since the measured elevated hull weight can be obtained during any point of the operation, it is also determined after the first component is installed. In this research, this second value is called the measured

minimum elevated hull weight.

B.2.2. Measured maximum and minimum elevated hull weight

The measured maximum and minimum elevated hull weights are determined from the refined leg reaction time series. Similar to the main research, this is done by designing a Python code that can extract the leg loads at the two desired phases of the operation: before and after the first component is installed. This code uses the same input data as the main research as well: the refined leg reactions, crane load, and crane slewing angle. Two methods are used to identify the operational phases in the data. One is based on the crane load, and the other one on the crane slewing angle, because for some operations only one of both parameters was measured.

The crane load method is the most precise one of the two methods and is therefore initially used for each jacking location. If the measured crane loads are always less than 50 ton or the measured maximum elevated hull weight is lower than 20000 ton with this method, the crane slewing angle method is used instead. Similarly, if no crane slewing angle is detected in the data or the measured maximum elevated hull weight is lower than 20000 ton with this method, then the assessed location is marked as unusable and filtered out.

Crane load method

For each assessed jacking location, the refined time series of the leg reactions are first of all summed; to obtain the time series of the measured elevated hull weight. The maximum elevated hull weight is defined as the average elevated hull weight after preloading and before the first heavy lifting operation. The minimum elevated hull weight is defined as the average elevated hull weight right after the first component is installed. The first installed component is usually the tower of the wind turbine, which is also the heaviest component. The first lifting operation is therefore identified in the data by the maximum crane load, as marked in purple in figure B.1.

Just as in section 4.1, the crane load during a heavy lifting operation should be above 50 ton. The start and end of the first heavy lifting operation are therefore determined respectively as the first time the crane load is lower than 50 ton before the maximum crane load and after the maximum crane load. In the example in figure B.1, the start of the heavy lifting operation is marked with A and the end with B, by the described method. The maximum elevated hull weight is then obtained as the average sum of the leg reactions during the 200 measuring points before the start of the heavy lifting operation, as marked in orange. A robust method to consistently determine the minimum elevated hull weight is found to be the average of the 80 percent lowest sum of the leg reactions after the end of the heavy lifting operation, but excluding the last 20 percent of the measuring points. The reason to exclude the last 20 percent of the measurements is because at the end of the jacking operation the legs will be extracted, which might first lead to a small increase in summed leg reactions. The zone in the data to obtain the average of the minimum elevated hull weight is marked in green in the example.

If this method is viable for the assessed operation, both obtained values are exported to an output sheet and the Python code will analyse the next jacking operation.

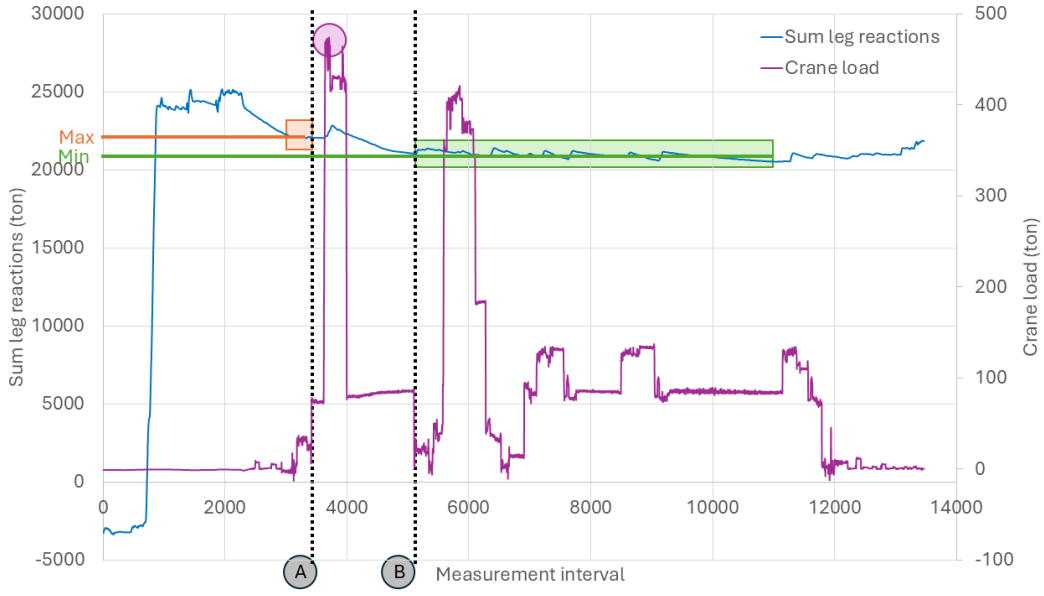

Figure B.1: Sum of leg reactions phases based on crane load

Slewing angle method

If the previous method is not viable, the slewing angle method is used to obtain both values. The slewing angle is not consistent in indicating when a heavy component is lifted, but it can accurately indicate when the preload phase is done. Just as in section 4.1, the end of the preload phase can be marked after 400 consecutive changes in the slewing angle, as marked by the grey zone in figure B.2.
By taking the average of the sum of the leg reactions for the 200 measurements after the end of the preload phase the maximum elevated hull weight can be obtained, as marked in orange in the example. No clear indication for the end of the first lifting operation is given by the crane slewing angle data. However, by taking the average of the 70 percent lowest values of the sum of the leg reactions after the zone for the maximum elevated hull weight and excluding the last 20 percent of the measurements, a minimum elevated hull weight can be obtained, which is consistent throughout the assessed jacking operations. In the example the minimum elevated hull weight is marked in green.
If this method is viable for the assessed operation, both obtained values are exported to an output sheet and the Python code will analyse the next jacking operation.

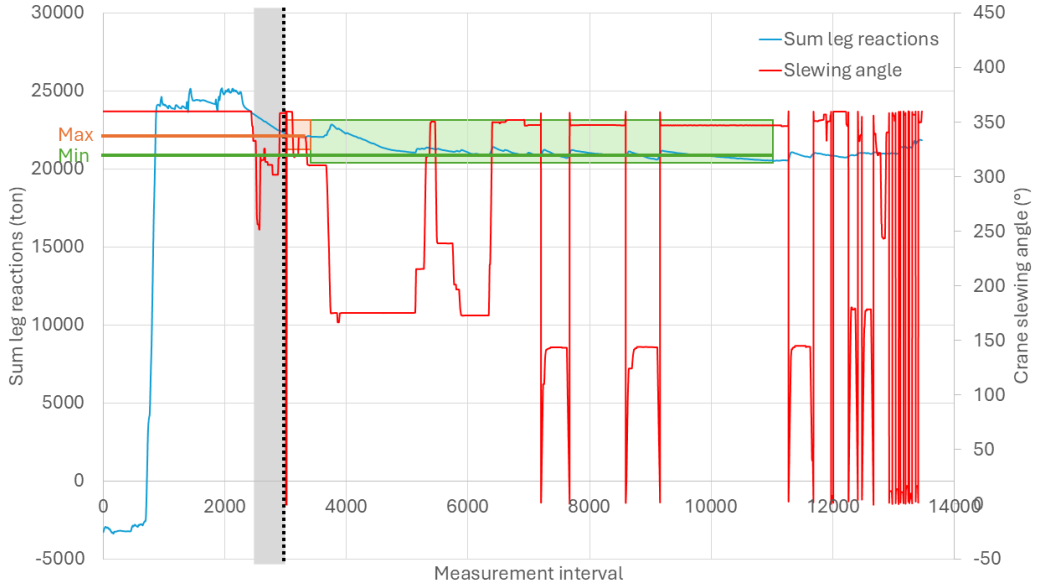

Figure B.2: Sum of leg reactions phases based on crane slewing angle

B.3. Results and conclusions

For each wind farm site in the case study, wind turbines are installed of approximately the same size. Because the elevated hull weight is further location-independent, all locations are assessed together. This means that in the results of this additional research, no distinction is made between wind farm sites and low-risk or high-risk soil profiles.

From the acquired data at each jacking location in the case study, the following three distributions are determined, as defined in appendix B.2:

- A distribution for the ratio of the real maximum elevated hull weight versus the estimated maximum elevated hull weight.
- A distribution for the ratio of the measured maximum elevated hull weight versus the real maximum elevated hull weight.
- A distribution for the difference between the measured maximum hull weight and the measured minimum elevated hull weight.

B.3.1. Distributions

For each distribution, the outliers are excluded; which are mostly due to a faulty measured elevated hull weight with the slewing angle method. For these locations, the applied method could not correctly interpret the data, resulting in a measured elevated hull weight that was too large or too small. From the remaining valid jacking locations the three distributions are obtained and presented in figure B.3, figure B.4, and figure B.5. The mean value μ and standard deviation σ of each distribution is summarised in table B.1.

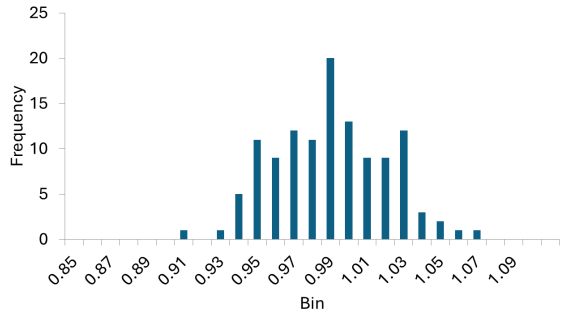

Figure B.3: Distribution of the real maximum elevated hull weight versus the estimated maximum elevated hull weight

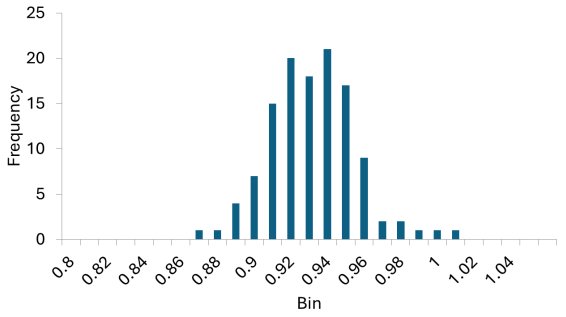

Figure B.4: Distribution of the measured maximum elevated hull weight versus the real maximum elevated hull weight

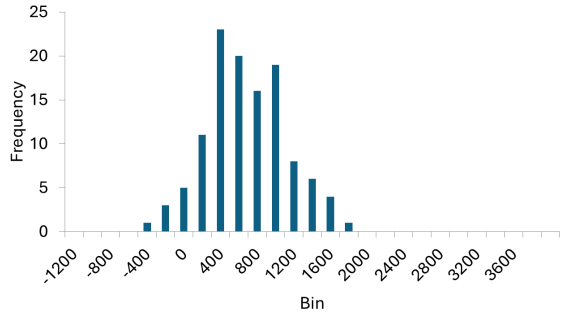

Figure B.5: Distribution of the difference between the measured maximum hull weight and the measured minimum elevated hull weight

Table B.1: Distributions parameter summary

	μ	σ
Real vs estimated	0.985	0.031
Measured vs real	0.927	0.023
Difference measured	584	441

Apart from the excluded outliers, the values in the distribution for the difference in elevated hull weight are spread across a wide range. Two jacking operations with extreme results will be discussed shortly.
The difference between the measured maximum hull weight and the measured minimum elevated hull weight is expected always to be larger than zero. However, as seen in the respective distribution, this is not always the case. One of the jacking operations with a negative difference is shown in figure B.6, where it can be verified that the minimum elevated hull weight is indeed larger than the maximum elevated hull weight. The data looks furthermore valid; the exact reason why the elevated hull weight increases during these few jacking operations should be researched in more detail.

A second observation is that many differences between maximum and minimum elevated hull weights are higher than 1000 ton; which is more than double the weight of the heaviest installed component. An example of such a jacking operation is shown in figure B.7; this is the same operation used to explain the designed methods in appendix B.2. Nothing about this data seems suspicious; the reason for such a large drop in weight should therefore also be further researched.

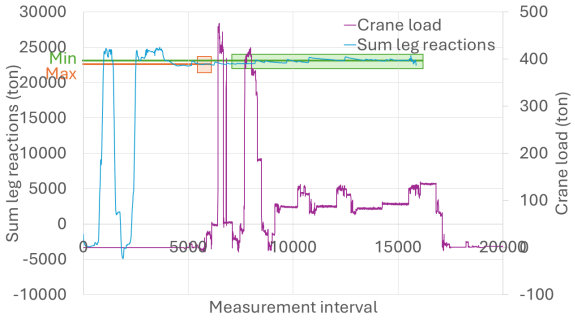

Figure B.6: Sum of leg reactions phases based on crane load for Danish Kriegers Flak 10

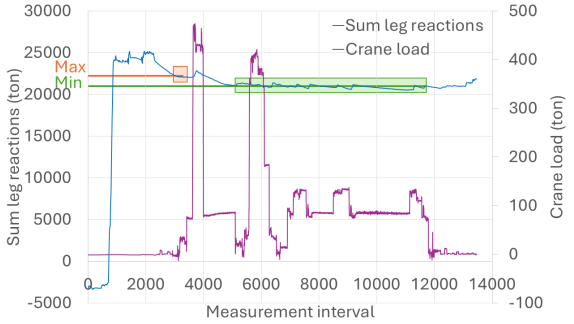

Figure B.7: Sum of leg reactions phases based on crane load for Danish Kriegers Flak 2

B.3.2. Conclusions

From the obtained results, the following conclusions can be drawn with respect to the formulated hypotheses in appendix B.1.

Conservative weight estimation

The mean value of the distribution for the real maximum elevated hull weight versus the estimated maximum elevated hull weight is slightly lower than one. This indicated that on average, the estimated hull weight is slightly overestimated.
Hereby, the first hypothesis can be confirmed.

Load dissipation through friction

The second hypothesis is verified by two distributions.
The mean value of the distribution for the measured maximum elevated hull weight versus the real maximum elevated hull weight equals 0.927. This shows that the measured elevated hull weight is reasonably lower than the real elevated hull weight from the jacking log, which could indicate friction, as discussed in the second hypothesis.

Secondly, the mean value of the distribution for the difference between the measured maximum hull weight and the measured minimum elevated hull weight equals 584 ton. In comparison, a tower should weigh around 465 ton, according to the SSA's. If friction occurs, it would rather be expected that the measured difference would be less than 465 ton.
Therefore, I would not use this distribution to draw conclusions about the load dissipation through friction. But, it raises questions about why the difference between the maximum and minimum elevated hull weight is so scattered over all these operations.
Nevertheless, the first conclusion is still valid, partly confirming the second hypothesis as well.

Summary

The goal of this additional research was to determine why the estimated maximum operational leg reactions are much higher than what is measured during the operations from the main research.
The final conclusion is that this is caused by two factors. Namely, the elevated hull weight is estimated too conservatively, leading to an over-conservative estimate of the maximum operational leg reactions. Which could be caused by the dumping of ballast water.
Also, the measured elevated hull weight is lower than the real elevated hull weight, leading to insufficient measurement of the maximum operational leg reactions. This could be caused by load dissipation through friction between the leg and leg shaft.